AD NUMBER

AD845620

LIMITATION CHANGES

TO:

Approved for public release; distribution is unlimited.

FROM:

Distribution authorized to U.S. Gov't. agencies and their contractors; Critical Technology; DEC 1968. Other requests shall be referred to Office of Naval Rsearch, Washington, DC 20360. This document contains export-controlled technical data.

AUTHORITY

onr, ltr, 28 jul 1977

SU-SEL-68-095

Mixed-Mode Oblique Ionograms: A Computer Ray-Tracing Interpretation

by

James Robert Barnum

December 1968

Technical Report No. 148

Prepared under
Office of Naval Research Contract
Nonr-225(64), NR 088 019, and
Advanced Research Projects Agency ARPA Order 196

RADIOSCIENCE LABORATORY

STANFORD ELECTRONICS LABORATORIES

STANFORD UNIVERSITY • STANFORD, CALIFORNIA

MIXED-MODE OBLIQUE IONOGRAMS: A COMPUTER RAY-TRACING INTERPRETATION

by

James Robert Barnum

December 1968

Technical Report No. 148

Prepared under

Office of Naval Research Contract
Nonr-225(64), NR 088 019, and
Advanced Research Projects Agency ARPA Order 196

Radioscience Laboratory
Stanford Electronics Laboratories
Stanford University Stanford, California

MISSING PAGE
NUMBERS ARE BLANK
AND WERE NOT
FILMED

ABSTRACT

Twenty-four high-resolution FMCW soundings taken over an east-west 1900-km forward-propagation path show unexpectedly complex mode structure near sunset. Because of the presence of 1- and 2-hop sporadic-E modes, it was suggested that multiple reflections from sporadic-E and F-layers--such as "M" and "N" modes--accounted for much of the unexplained structure.

This work represents an attempt to see how well these "mixed" modes can be understood by employing computer ray-tracing procedures developed by Dr. T. A. Croft at Stanford Electronics Laboratories.

A simple β-Chapman layer, with its parameters adjusted to give synthetic ionograms that matched the experimental 1- and 2-hop F-layer modes, proved to be an adequate model for the F-layer profile over the path. Reference to the calibrated experimental ionograms yielded values for the sporadic-E reflection heights for each time of day. Assuming no horizontal tilts in layer density and ignoring the earth's magnetic field, synthetic ionograms involving multiple F-layer and sporadic-E reflections were then computed.

The model-experiment comparisons show that surprisingly accurate estimations of both 1- and 2-hop and mixed modes are possible, using only relatively simple computational procedures. Although similar work has been done in this area, the present study is novel in its use of calibrated oblique ionograms for model derivation. The work should lead to a better understanding of both HF forward and backscatter propagation studies which are plagued with multiple, interlayer propagation modes.

A further extension of the modeling technique would include the insertion of additional electrons in the ionospheric profile--E-, F_1-, and F_2- layers--as becomes necessary. Horizontal tilts in electron density could also be modeled by use of a slowly-varying profile or by insertion of two or more different discrete models along the propagation path.

CONTENTS

TABLES

ILLUSTRATIONS

a	constant used in computing a discrete tilt
b	constant used in computing a discrete tilt
c	constant used in computing a discrete tilt
D_E	equivalent E_s-layer ground distance
D_F	equivalent F-layer ground distance
D'_F	a computer solution for ground distance
D_o	path length, 1881.27 km
f	frequency
$g(h)$	profile shape factor
h'_a	discrete F-layer virtual height at point "a"
h'_b	discrete F-layer virtual height at point "b"
h'_c	discrete F-layer virtual height at point "c"
h'_E	virtual height of sporadic-E layer
h'_F	virtual height of F-layer
h_m	height of maximum ionization
h	height
H_s	scale height that appears in β-Chapman equation for density
k	scaling factor of model's density function
k_1	constant used in computing a variable tilt
k_2	constant used in computing a variable tilt
K_f	frequency scaling factor, $\triangleq \sqrt{k}$
$N(h)$	electron density as function of height
N_o	maximum electron density
N'_o	revised maximum density, $= K_f{}^2 N_o$
P_1	specified constant used for calculating D_F
P_2	specified constant used for calculating D_F

P_3	specified constant used for calculating D_F
Q_1	specified constant used for calculating T_D
Q_2	specified constant used for calculating T_D
R	mean earth radius, 6370 km
T_D	group time delay
T_E	equivalent group time delay for a single hop to the F-layer
T_F	equivalent group time delay for a single hop to the E_s-layer
z	(height - h_m)/H_s
β	take-off (elevation) angle
θ	(actual range - starting range)/1881.27, variable used in modeling a variable tilt
μ	index of refraction of ionosphere
χ	solar zenith angle

ACKNOWLEDGMENTS

The author is grateful to Dr. T. A. Croft and Prof. O. G. Villard, Jr., for their suggestions and encouragement. Special thanks is due to R. Vincent, T. Dayharsh, and Bernadine Frank of Stanford Research Institute for the stimulating discussions regarding mode analysis. Some helpful suggestions were given by Prof. R. A. Helliwell during the early part of the work. Charles Shaffer aided in the early stages of data reduction.

I INTRODUCTION

A. Purpose

The purpose of the work reported here was to determine the origin of a set of unexplained modes appearing on a series of oblique sounding records of high-frequency (HF) radio signals taken over an E-W 1900-km path between Stanford University, California, and Lubbock, Texas. It was suggested that the mysterious modes were the result of interlayer propagation between sporadic-E (E_s) and F-layers. The author attempted to verify this suggestion by employing currently available computer ray-tracing techniques to aid in the modeling of several multiple-layer propagation modes, which were then compared with the experimental records.

B. Background

In the late 1950s, researchers began to consider seriously the different possible modes and corresponding angles of arrival that might occur when HF radio signals are transmitted over a given path.

In 1953, Wilkins and Kift [Ref. 1], working at the Department of Scientific and Industrial Research (DSIR) Radio Research Station in Slough, England, measured angles of elevation of incoming radiation from pulse and telegraph signals originating in Negombo, Ceylon, and Kirkee, India, and from telegraph signals originating in New Delhi. For frequencies between 15 and 19 MHz, energy was received most often and most strongly in the elevation range 7 ± 2 degrees. In the summer of 1954, signals from Kirkee showed a decrease in elevation at the receiver to 5 ± 2 degrees; this circumstance, correlated with backscatter observations at both Ceylon and Slough, suggests that the summer increase in E_s-layer ionization causes the decrease in received angles of elevation.

In October 1956, Silberstein [Ref. 2] at the National Bureau of Standards (NBS) in Boulder, Colorado, ran a long-distance pulse-propagation experiment at 20.1 MHz between Sterling, Virginia, and Maui, Hawaii. Simultaneous oblique ionograms were made along the path from Sterling to Boulder, and vertical incidence records were also obtained at Sterling. Silberstein's results showed mode structures that differed greatly from one day to the next, indicating that a long path is very sensitive to ionospheric conditions.

In 1959, Kift [Ref. 3] remarked that ". . . as early as 1938, Millington . . . pointed out that long-distance paths would consist of hops of unequal length, and that a knowledge of the distribution of ionization at every point along the route was desirable in solving the problem of how energy travels from one point on the earth's surface to another." Kift assumed that, in all thick layers, the distribution of electron density vs height followed a parabolic function, and that no lateral tilts of the layers were present. It was assumed that reflection from the E_s-layer was analogous to that from a mirror. Kift's treatment of the problem is based on the parabolic-layer transmission equations of Appleton and Beynon [Ref. 4], and uses ray theory throughout. He examined two long paths and found that, when the effect of tropical E_s ionization was included, he could predict time delays and angles of arrival for the various modes with some confidence. He used a fixed-frequency pulse sounder system, which yielded measurements of angles of arrival and propagation times for the various modes. He then compared the results with those predicted on the basis of a model assuming a parabolic layer.

Investigators at Stanford Research Institute (SRI), under the supervision of R. Vincent, did some extensive research titled "HF Communication Effects," which was finished by 1965; Ref. 5 gives a summary of their activity. Several oblique HF communication paths, including midlatitude and transauroral, were studied. A primary interest was given to what was termed the "Channel Scattering Function," with which the HF channel is characterized by a 3-dimensional plot of amplitude vs time delay and frequency. Individual modes (both simple and complex) are separated by their time of travel over the path, as well as by their characteristic doppler shift due to layer motion and changing density.

The phase-stable system used for these measurements is discussed in Ref. 6. The application of the phase-stable system to the measurement of frequency dispersion and doppler shift over both a transauroral and a midlatitude path is outlined in Refs. 7 and 8. Simultaneous phase-stable transmissions on 7.366 MHz, paralleled by step-frequency oblique incidence sounders, enabled the SRI workers to identify complex modes involving interlayer propagation between sporadic-E and F-layers--such as "M" and

"N" modes. The identification of more complicated modes was not attempted; because of ionospheric dispersion, it was difficult to identify and label the more complicated "in-between" ionogram mode traces. However, multiple hop E- and F-layer modes, as well as several off-path modes, were clearly identified. The doppler shifts for the two paths were nearly identical, but the frequency dispersion over the transauroral path was 10 times that over the midlatitude path.

In the same study, SRI workers, including T. Dayharsh and others [Ref. 9], studied the interrelationships of particular high-latitude phenomena, including E_s, magnetic storms, complex ray paths, and field-aligned ionization; included were HF oblique sounder observations from five paths for one year. The SRI investigators used their sounder data to plot $f_o E_s$ and percent occurrence; they found good agreement between observed oblique mode statistics on four paths and those predicted from the maps. As an extension of this (with particular interest to the present study), Dayharsh, working with Bernadine Frank of SRI, employed ray-tracing techniques (developed by T. Croft at Stanford University) [Ref. 10] to synthesize oblique ionograms containing complex modes involving E_s- and F-interlayer propagation. They derived the ionospheric profile models through analysis of vertical soundings made along the path; virtual height was transformed to real height through use of a computer program developed by Paul and Wright at the NBS [see Ref. 11]. Since some vertical sounders were located off-path, lateral tilts were estimated, and the computed profiles were suitably modified to approximate the true conditions over the propagation paths. Over some paths, two or three vertical soundings were available; thus the investigators were able to develop ionospheric models that exhibited a horizontal tilt over the oblique path.

In Ref. 12, Dayharsh discusses HF propagation in the complex auroral and polar environments. On an average of 20 to 40 percent of the time, depending on time of day and season, propagation was via E_s or complex, interlayer modes. Various different interlayer modes are analyzed, and a plot is shown that illustrates the relative placement of the various modes on an example oblique ionogram. (Several plots are then presented

that show "accumulated percentage by mode" plotted vs time of day, for several different paths and seasons.) It was found, for example, that the principal daytime modes, over a path from Palo Alto, California, to Thule, Greenland, for winter conditions, were in decreasing order of significance: the 2F, N, M, and 1F.

Quite recently (1967), P. L. George [Ref. 13], working at the Australian Department of Supply, conducted a series of HF radio wave experiments over a 1900-km path in Australia, located nearly along the Magnetic Meridian. He obtained both oblique soundings and vertical soundings at the midpoint of the path. He assumed a parabolic density model, which was determined from the midpoint records taken at fixed frequencies. His model contained a sporadic-E-layer, an E-layer, and an F_2-layer. He then synthesized an ionogram containing $1E_s$ (1-hop E_s), $2E_s$, $3E_s$, 1F, 2F, 3F, 4F, and E_s-F modes. The synthesized ionograms gave a good match to the corresponding experimental records for $1E_s$, $2E_s$, 1F, and 2F modes, as seen in the example below, which is reproduced from George's report. There also seems little doubt about the identification

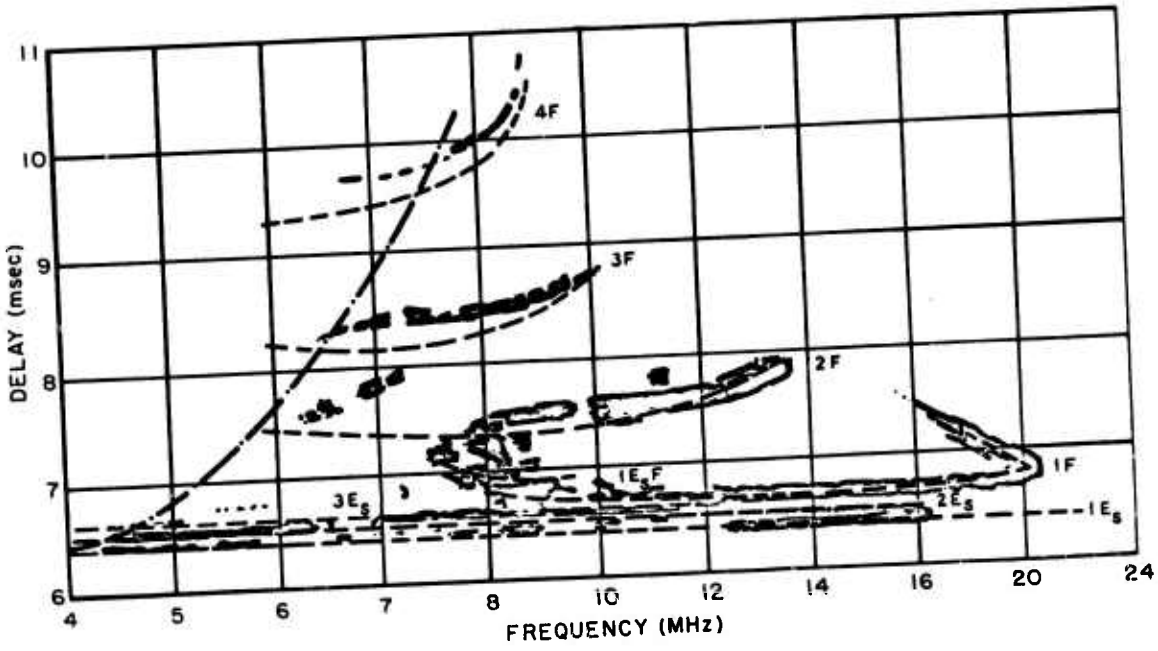

EXAMPLE OF A SYNTHESIZED OBLIQUE IONOGRAM SUPERIMPOSED ON AN EXPERIMENTAL RECORD TAKEN OVER A 1900-km PATH, BY P. L. GEORGE [REF. 13].

of the 3F and 4F modes, although there was a discrepancy of a few tenths of a millisecond between the experimental results and the predictions based on the model. It is difficult to predict the location of George's E_s-F mode, because the record was highly cluttered in the region between the 1F and 2F traces.

In summary, it appears that Dayharsh and George have made the greatest contributions toward explaining complex mode structure by use of computer synthesis procedures. Although the paths that Dayharsh studied were longer and more disturbed than was that studied by George, Dayharsh had access to more vertical soundings from which he could model a tilted ionosphere. Therefore, the reliability of the two techniques is probably comparable. The major problem in any analysis of this sort is that the ionospheric profile actually remains unknown, and a good guess is made on the basis of the behavior of HF propagation through the various "layers" of electron density. The density profile is therefore derived by an indirect method, over a specific point along, or near, the path, and is then assumed to vary smoothly (or perhaps stepwise) along the path.

E. M. Young, one of the SRI workers involved in the study discussed above, notes [Ref. 14, p. 16], ". . . a theory that would permit prediction of complex modes in satisfactory agreement with measured data has not yet been developed." Within the above context, the present work will provide still another contribution in the area of complex-mode synthesis by computer ray-tracing techniques. However, the primary differences in the present work are (a) no vertical soundings were available with which one could determine ionospheric structure along the path; therefore (b) a β-Chapman ionosphere is assumed for the F-layer. Thus, only a sequence of calibrated oblique ionograms is used in the present work to perform the complex-mode analysis; the ionospheric models are derived by making an educated guess at a first model, and then modifying parameters until a suitable final model is obtained. Tilts could be modeled only by examining model variation with time of day, because each model is obtained through matches to a sequence of 1F oblique modes.

C. Approach Used in the Present Work

The aforementioned oblique soundings taken over an E-W 1900-km path between Stanford University, California, and Lubbock, Texas, showed some complicated mode structure toward the latter part of the day. At the same time, a sporadic-E layer became evident, and it was conjectured that the "in-between" modes were those resulting from multiple, inter-layer propagation among the E_s- and F-layers. Midpoint vertical soundings were not available; however, the oblique ionograms were calibrated in time delay.

Fortunately, computer ray-tracing techniques had already been developed at Stanford by Dr. T. A. Croft. These techniques had been applied to the tracing of rays through model ionospheres. From these ray tracings, oblique ionograms could be constructed [Ref. 15]. The techniques had not been adapted for use in the construction of models of multiple layer mode ray sets; however, after a short inquiry, it was deemed feasible to attempt such a construction.

It was decided to apply ray-tracing techniques, assuming a β-Chapman layer [Ref. 16, p. 17] as a model for the F-layer, in order to:

(1) see whether by this procedure, a sufficiently accurate model could be obtained for the F-layer without having to include the effect of horizontal tilts in the electron density profile; and

(2) determine whether the various multi-hop modes could be sucessfully synthesized. If so, the result could explain the mysterious structure that gives rise to the unexplained modes appearing over the transmission path.

This report follows through the process by which the synthesized ionograms were obtained and compared with the experimentally obtained ionograms. The results are also compared with those derived on the basis of a simpler, mirror-analogy ionospheric model. The sources and magnitudes of errors are then estimated. The effect of tilts in electron density profiles (and how to model them) is discussed with regard to possible future work in mode prediction studies.

II THE EXPERIMENT

A series of FMCW oblique ionogram records--calibrated both in time delay and in frequency--was taken over a path between Stanford, California, and Lubbock, Texas, on Feb. 27, 1967; the path length was 1881.27 km; samples of these records are presented in Figs. 1-24, and will be discussed subsequently. Much greater clarity and larger signal-to-noise ratio were achieved on these records than was ever before possible--especially at the lower frequencies--using relatively low power. This improvement over previous ionogram records is attributable to the FMCW technique developed by Drs. R. B. Fenwick and G. H. Barry while working with some of the staff at the Radioscience Laboratory at Stanford University.

The equipment used has been described elsewhere [Refs. 17-20]. The time-delay calibration was achieved by carefully calibrating two Hewlett-Packard (HP) cesium-beam standards, one of which was subsequently flown to the field site in Lubbock. These standards yielded a time calibration of the system starting pulse and constituted the frequency standard from which each sweep system derived its calibrated input signal.

One hundred records were taken every hour, over a 24-hour period. A motion picture was made to show a running sequence of the records throughout the day. Time and frequency scales and notices of time of day were also included. This picture was run through a number of times; several interesting features in the ionograms that changed with time of day became apparent.

One- and two-hop F-layer returns were noted throughout the day into early nighttime. Vertical time-delay extensions on the 1F traces noted later in the evening can probably be attributed to multiple reflections from ionospheric irregularities (spread-F) [Ref. 7, p. 153]. Evidence of ground forward scatter--reflections from irregularities on the ground located at arbitrary points along the path--causing a severe vertical broadening of the 2F and 3F traces, was present throughout the day. Some interesting traveling ionospheric disturbances (TIDs) appeared several times in the record sequences; these have subsequently been investigated by Dr. T. A. Croft at Stanford.

The most notable feature of the records was the appearance of several "in-between" modes--modes appearing between 1F, 2F, and 3F traces--beginning in the later part of the day. As these modes became more pronounced, it was also noted that a sporadic-E-layer had formed, yielding 1- and 2-hop E_s modes--which may be identified from the time-delay vs frequency data as appearing as nearly straight lines with very high maximum usable frequencies (MUFs). The fact that the $1E_s$ trace did not extend into the lower frequencies earlier in the day suggests high D-layer absorption, coupled with low-gain, low-angle antenna patterns at low frequencies. Later in the evening, the $1E_s$ traces became much more pronounced, as one would expect.

To investigate the causes of these in-between modes, 24 records at various times throughout the day, with the majority at sunset, were selected (Figs. 1-24); these photographs were enlarged to approximately 8 by 10 inches, a convenient size for handling and scaling. Calibrated scale underlays on which the photos could be laid over a light box were constructed. The calibration was achieved by noting the time-delay tick marks on the photos and by deducing the frequency scale from the horizontal end-points of the records that contained the linear frequency sweep with known start and stop frequencies. The underlays were used to plot the various models derived as explained below.

Since the unexplained modes were not present when the E_s reflections were also absent--as Figs. 1-24 show when early and late times of the day are compared--it was suggested that the in-between modes were a result of multiple, alternate reflections from the E_s- and F-layers (as previously mentioned). There seems to be no indication of the presence of a normal E-layer, since the characteristic S-turn transition between the lower 1F and upper 1E traces was never evident. The S-turn may have occurred at some frequency lower than 4 MHz; it therefore would not be visible within the data taken. However, if this did occur, it is not likely that a layer of such low density would seriously perturb the mode structure, and it could therefore be ignored.

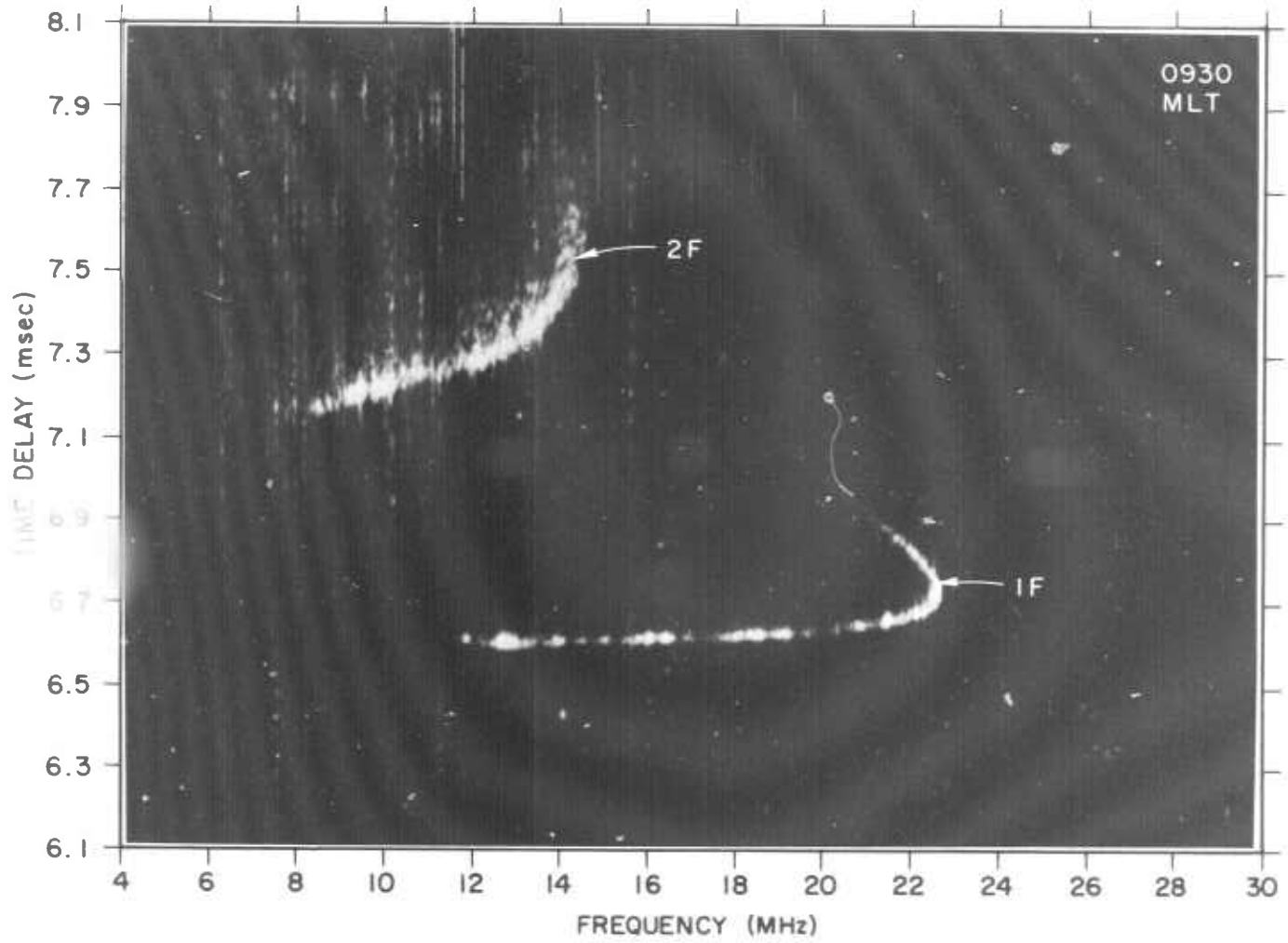

Fig. 1. EXPERIMENTAL CALIBRATED OBLIQUE IONOGRAM 1.
MLT = Midpath local time.

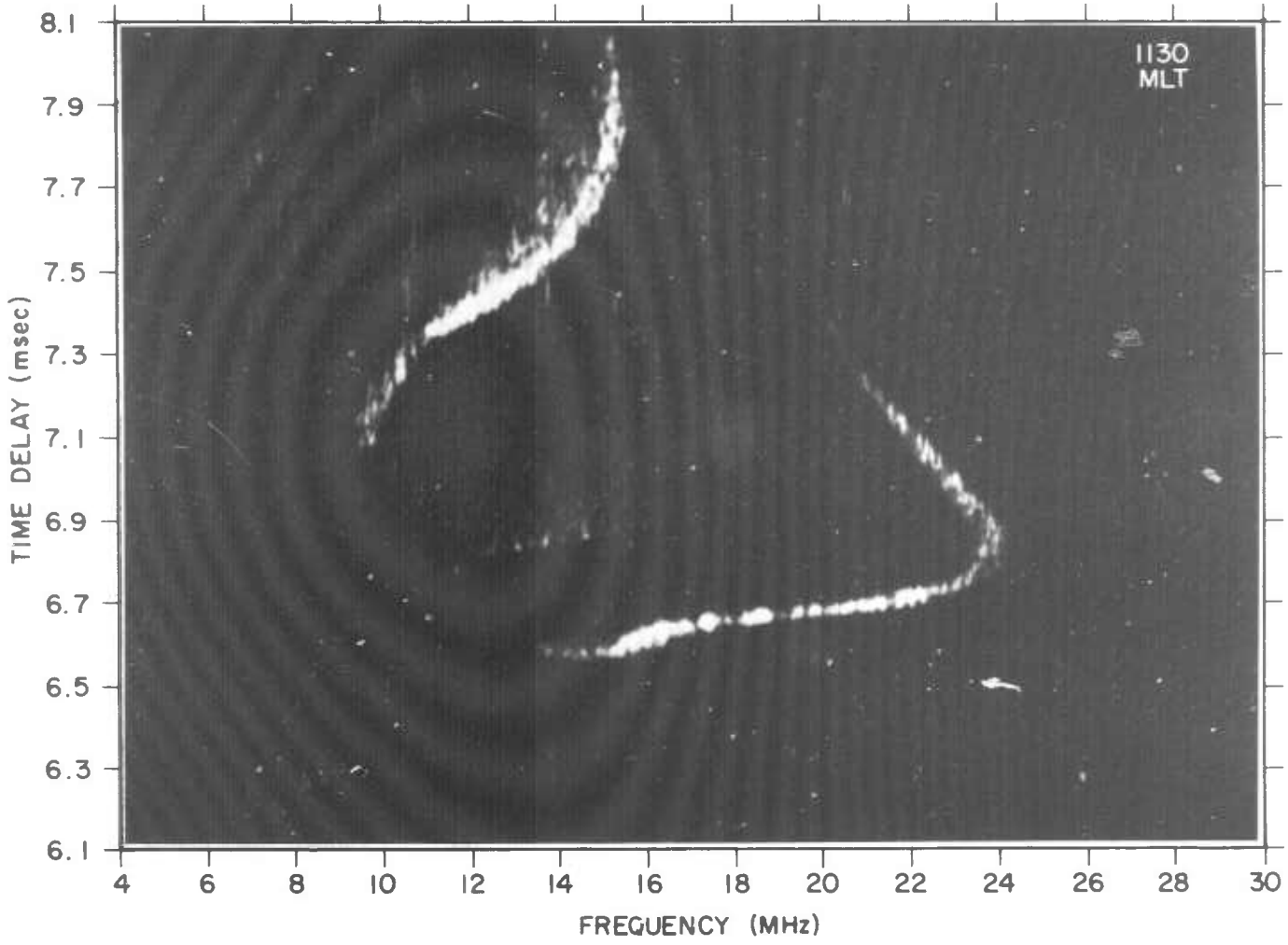

Fig. 2. EXPERIMENTAL CALIBRATED OBLIQUE IONOGRAM 2.

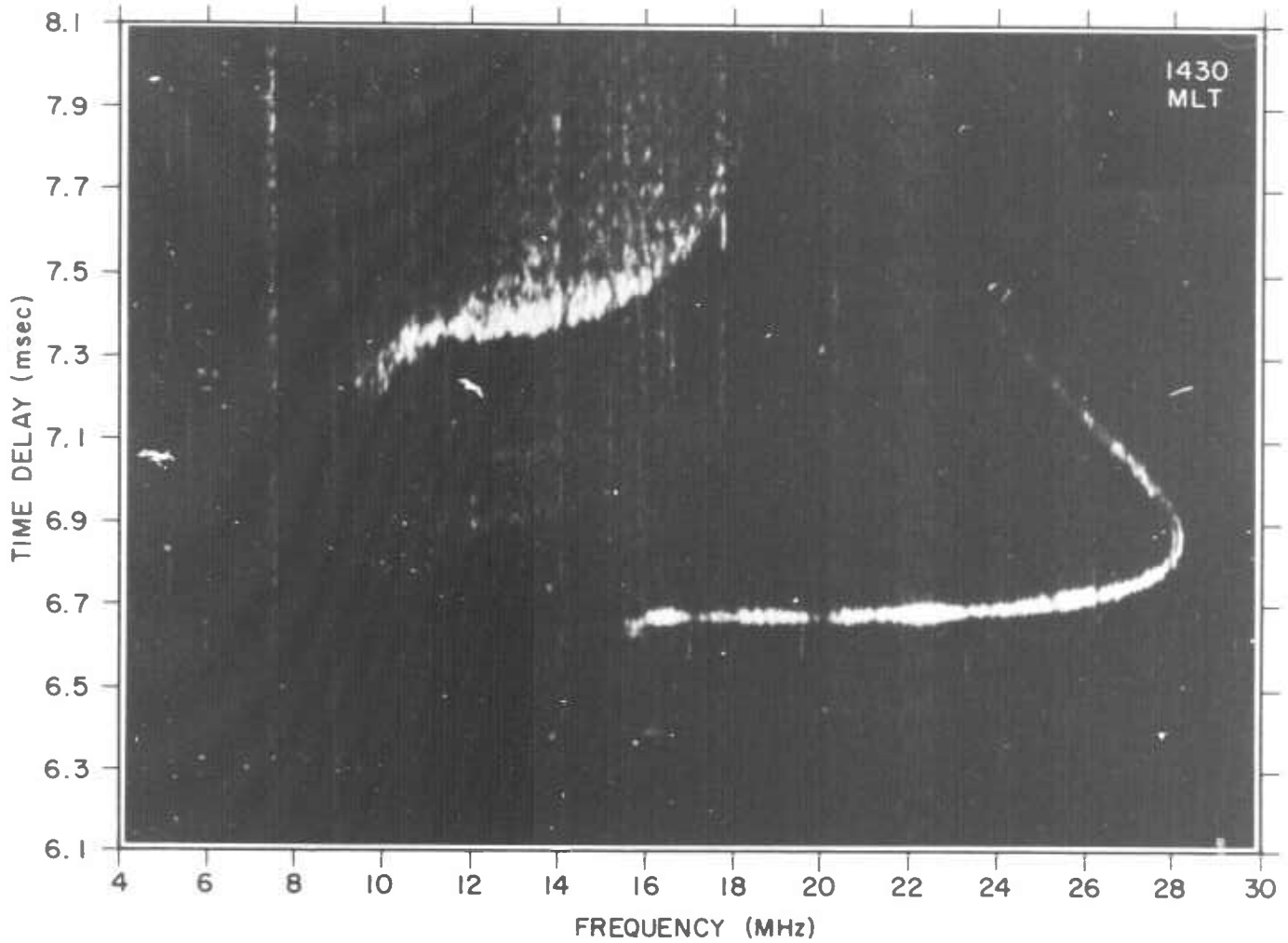

Fig. 3. EXPERIMENTAL CALIBRATED OBLIQUE IONOGRAM 3.

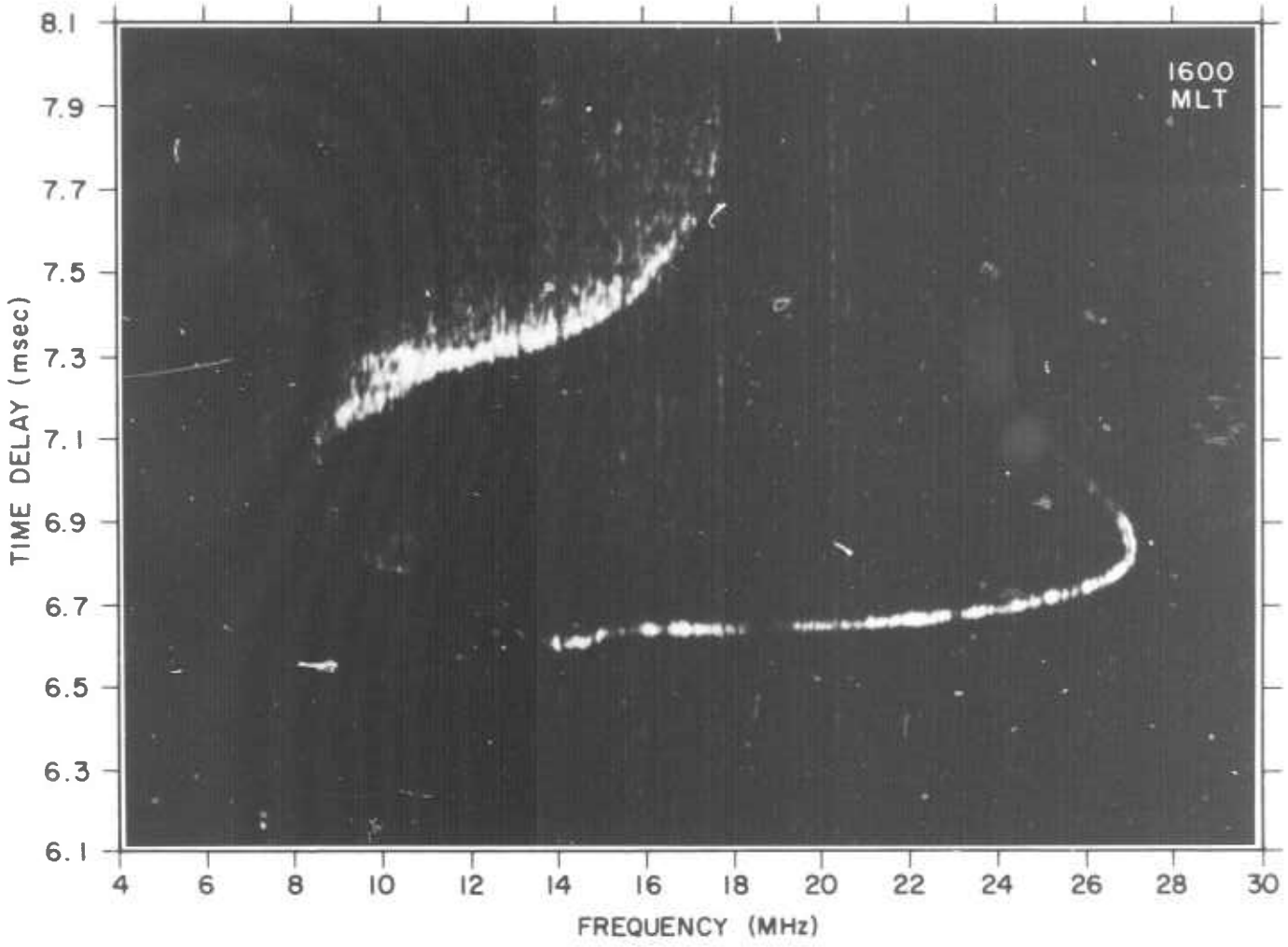

Fig. 4. EXPERIMENTAL CALIBRATED OBLIQUE IONOGRAM 4.

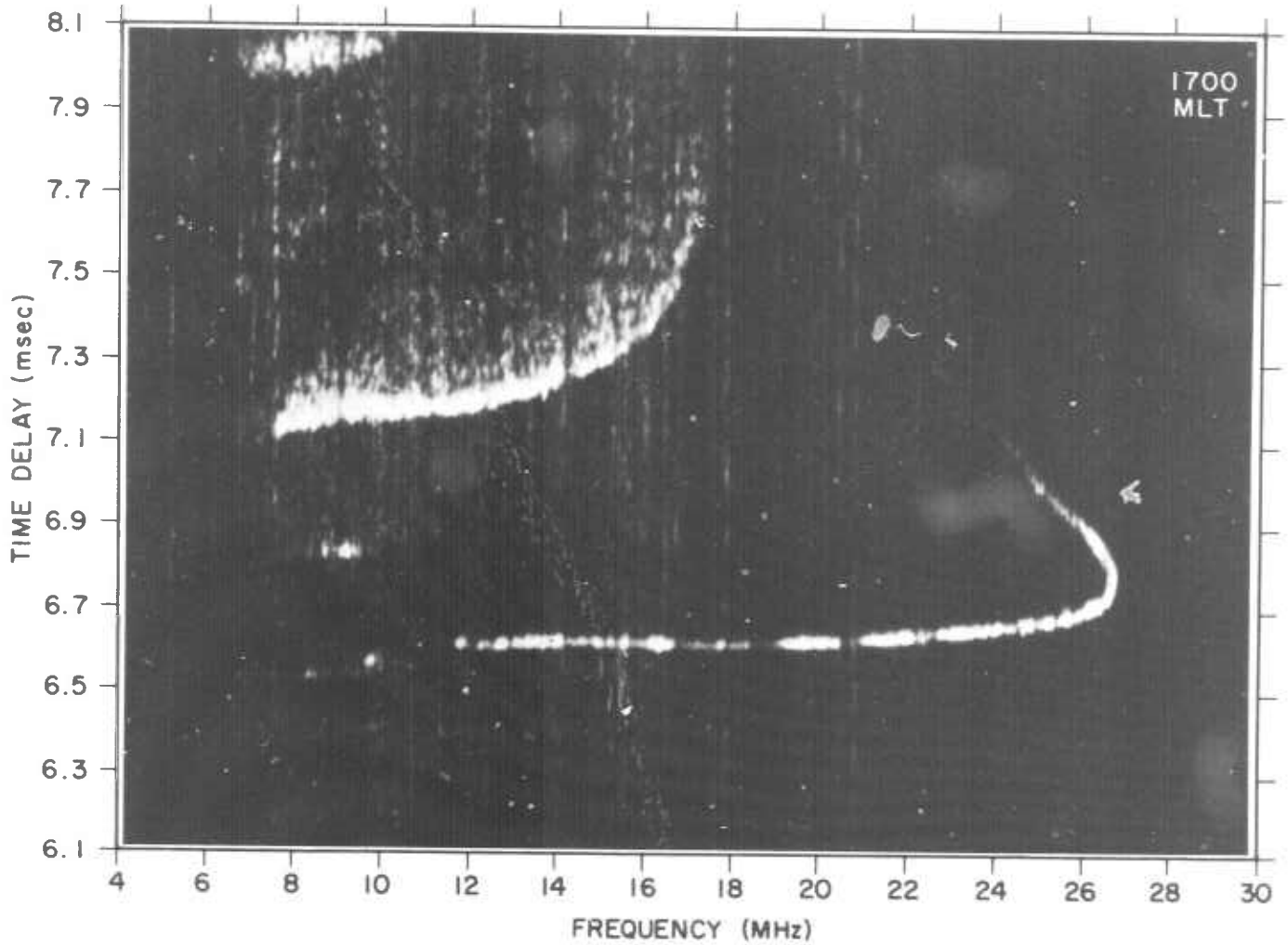

Fig. 5. EXPERIMENTAL CALIBRATED OBLIQUE IONOGRAM 5.

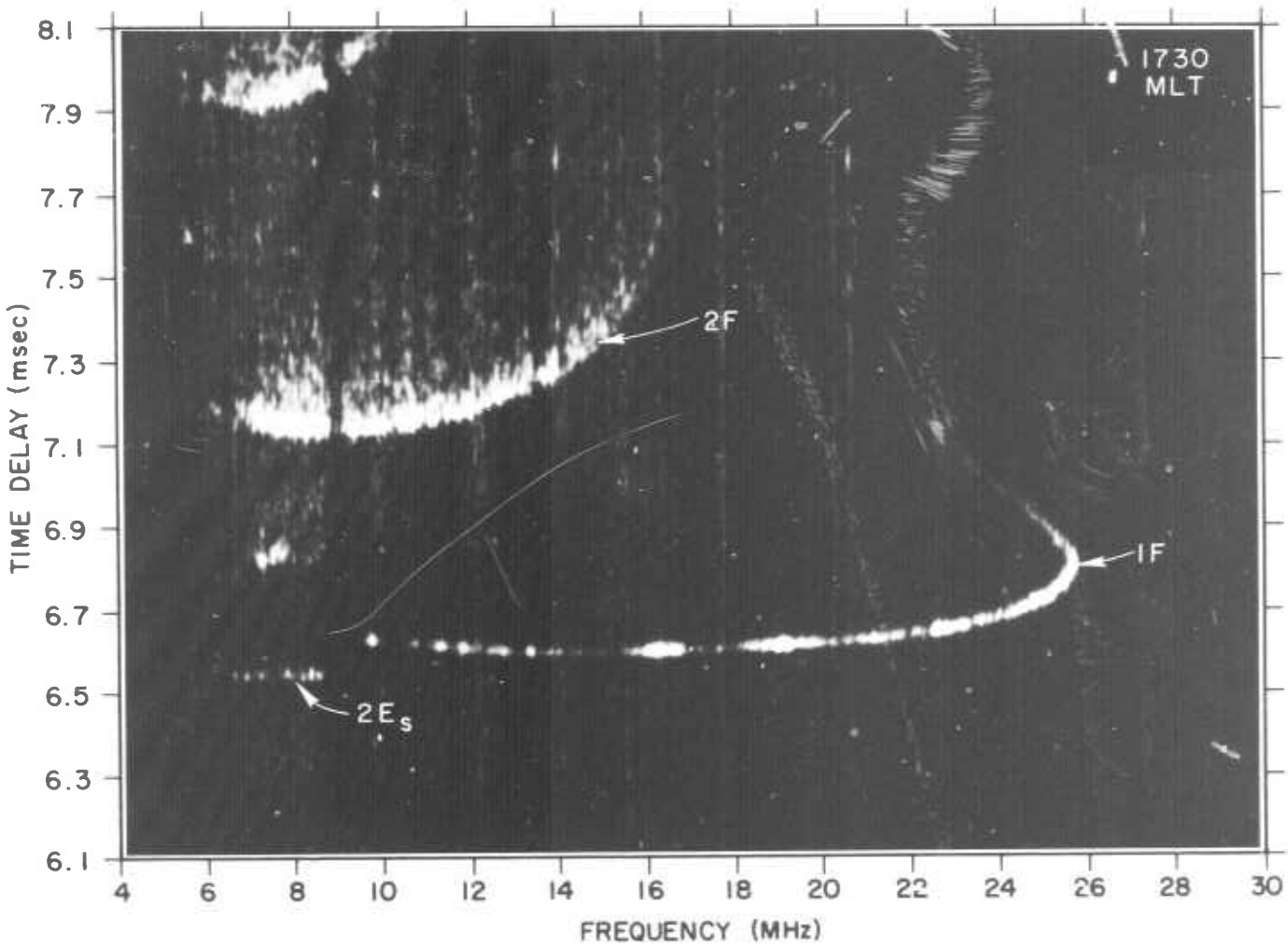

Fig. 6. EXPERIMENTAL CALIBRATED OBLIQUE IONOGRAM 6.

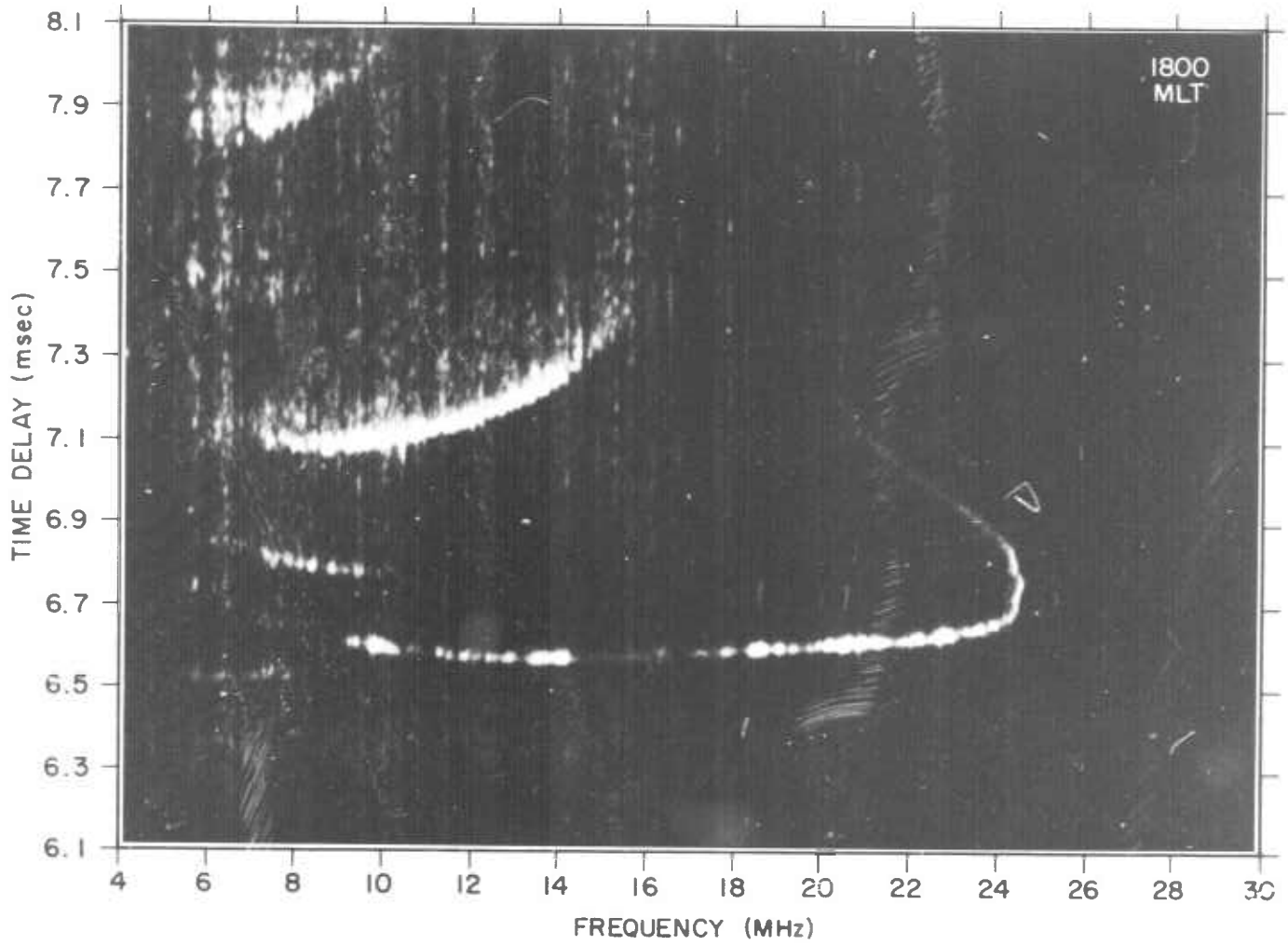

Fig. 7. EXPERIMENTAL CALIBRATED OBLIQUE IONOGRAM 7.

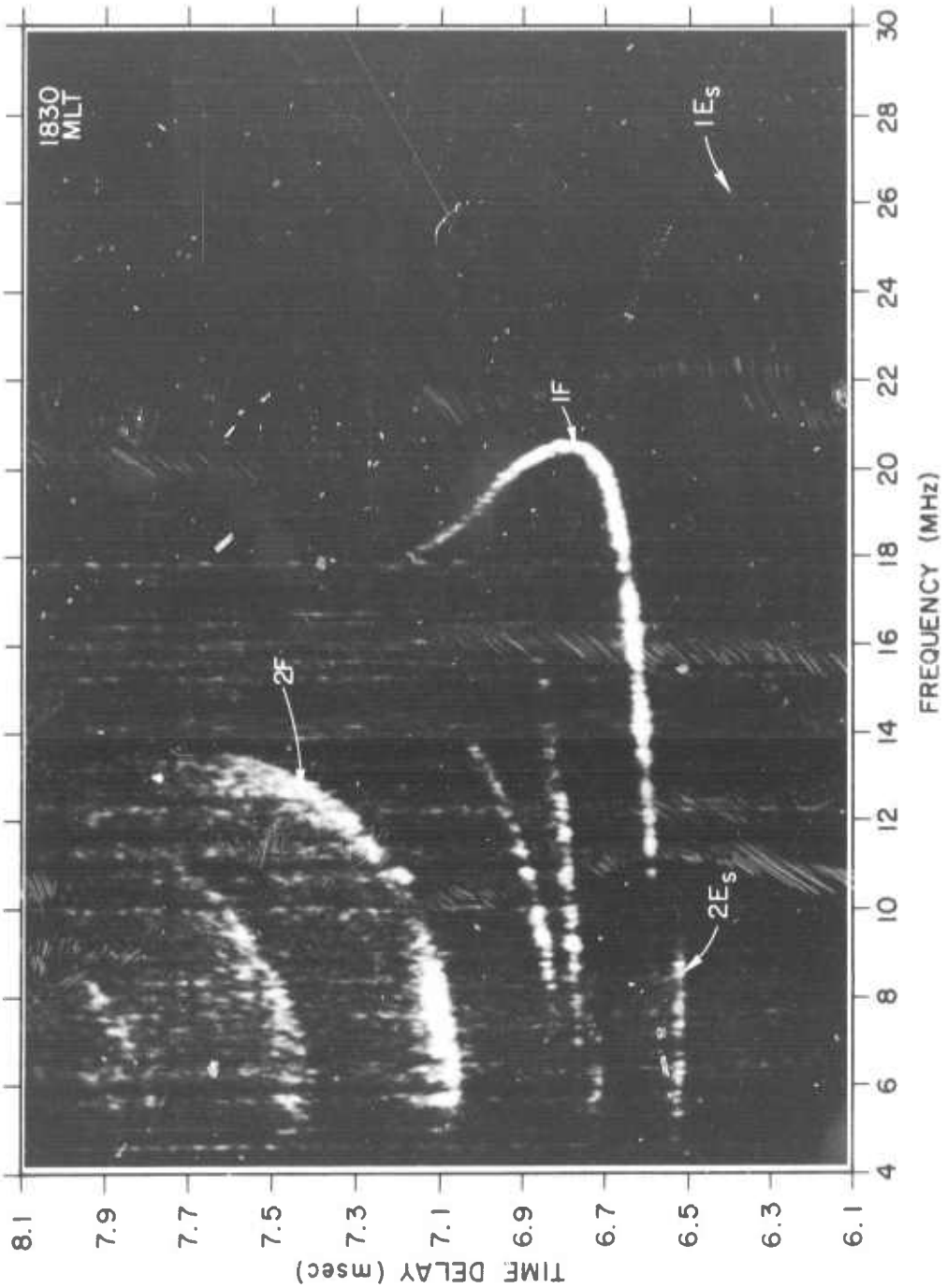

Fig. 8. EXPERIMENTAL CALIBRATED OBLIQUE IONOGRAM 8.

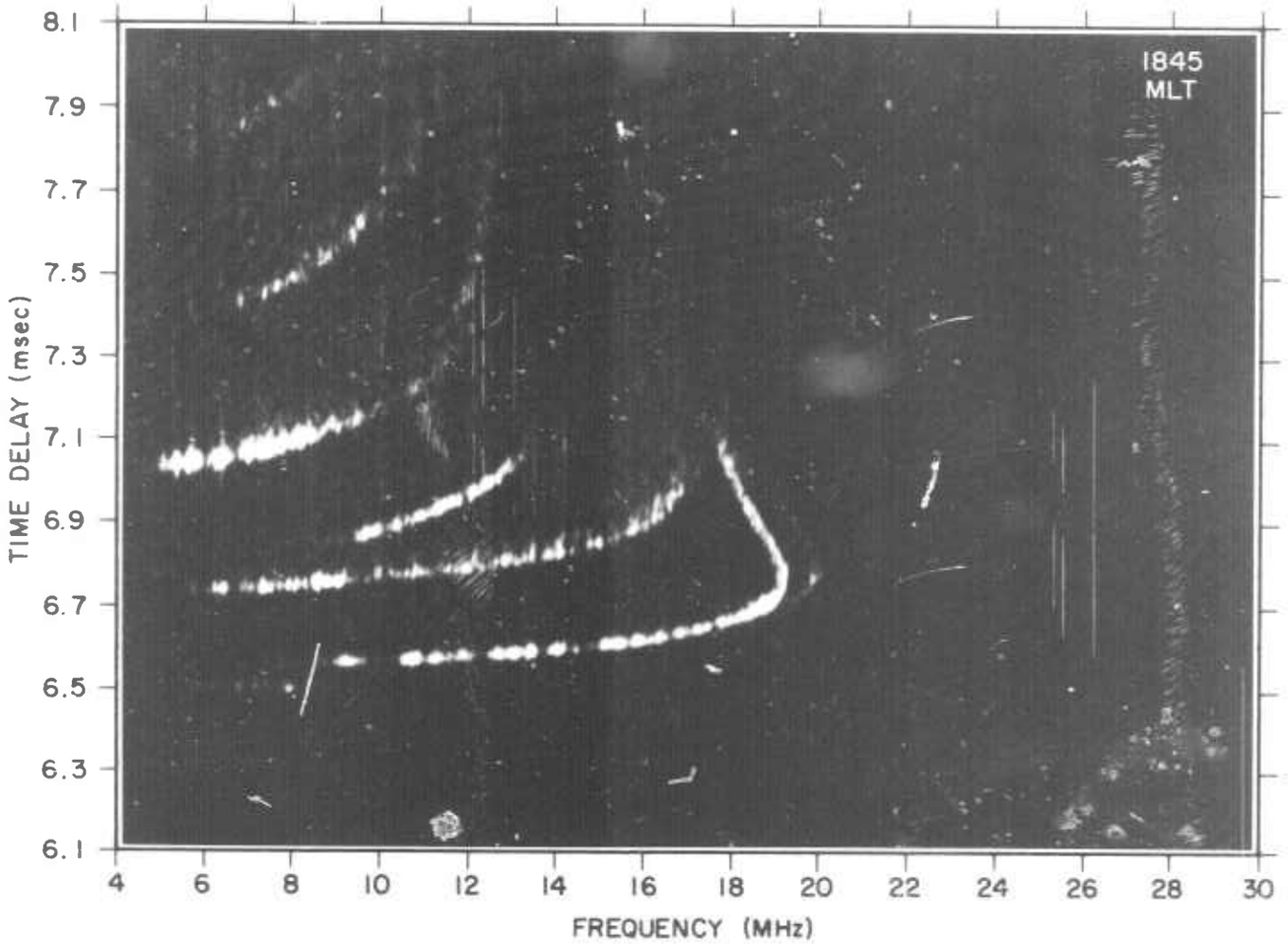

Fig. 9. EXPERIMENTAL CALIBRATED OBLIQUE IONOGRAM 9.

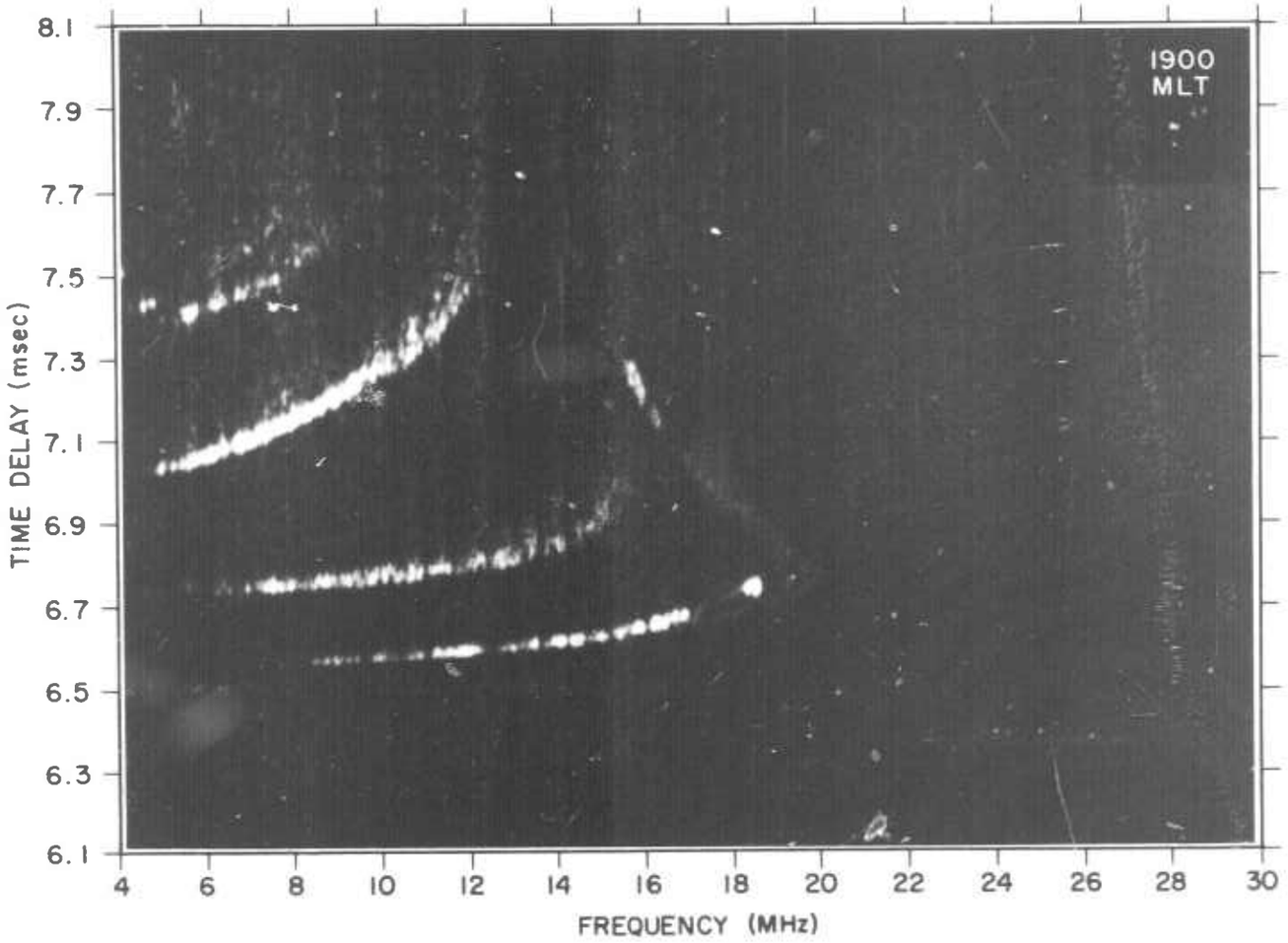

Fig. 10. EXPERIMENTAL CALIBRATED OBLIQUE IONOGRAM 10.

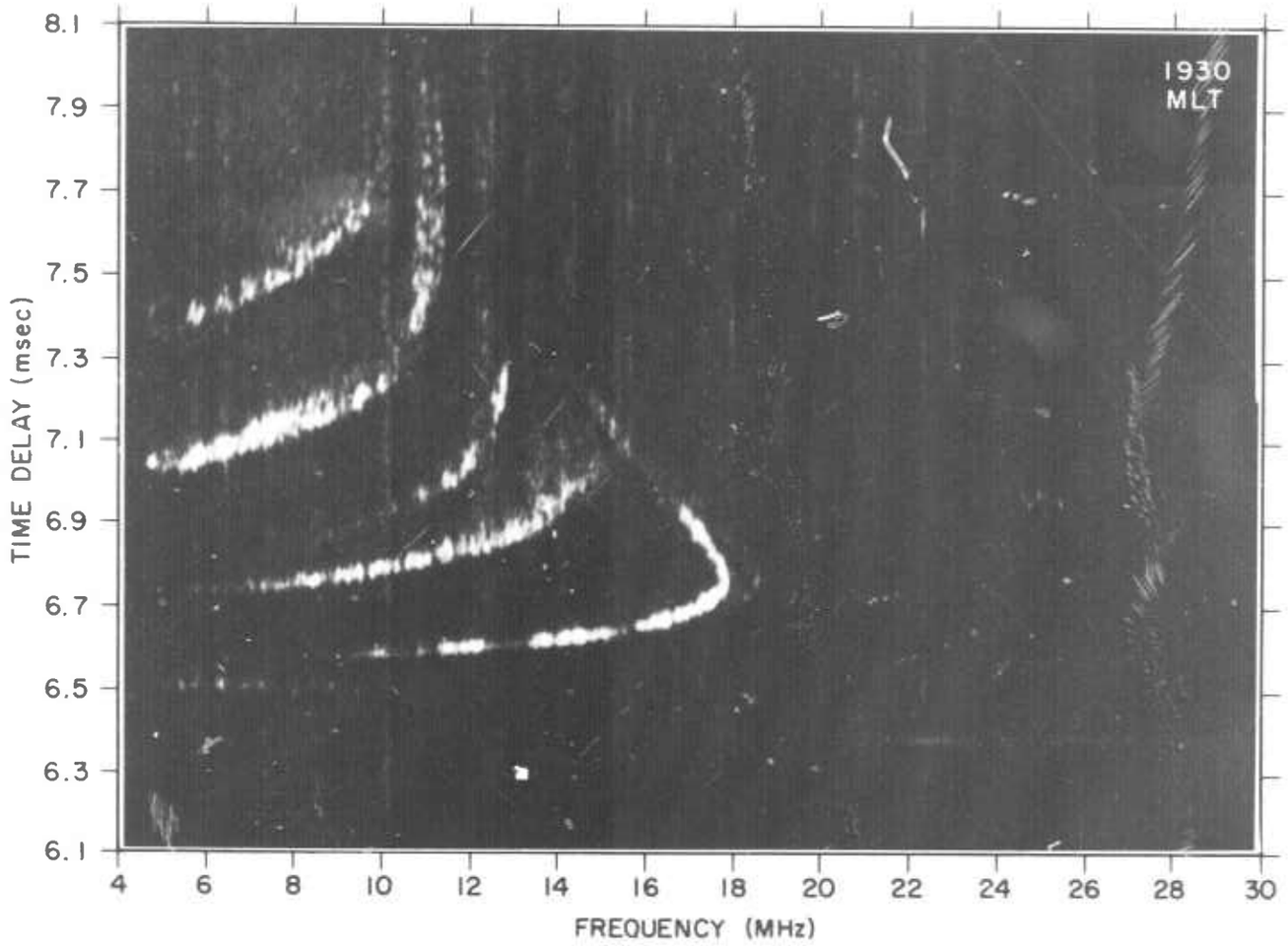

Fig. 11. EXPERIMENTAL CALIBRATED OBLIQUE IONOGRAM 11.

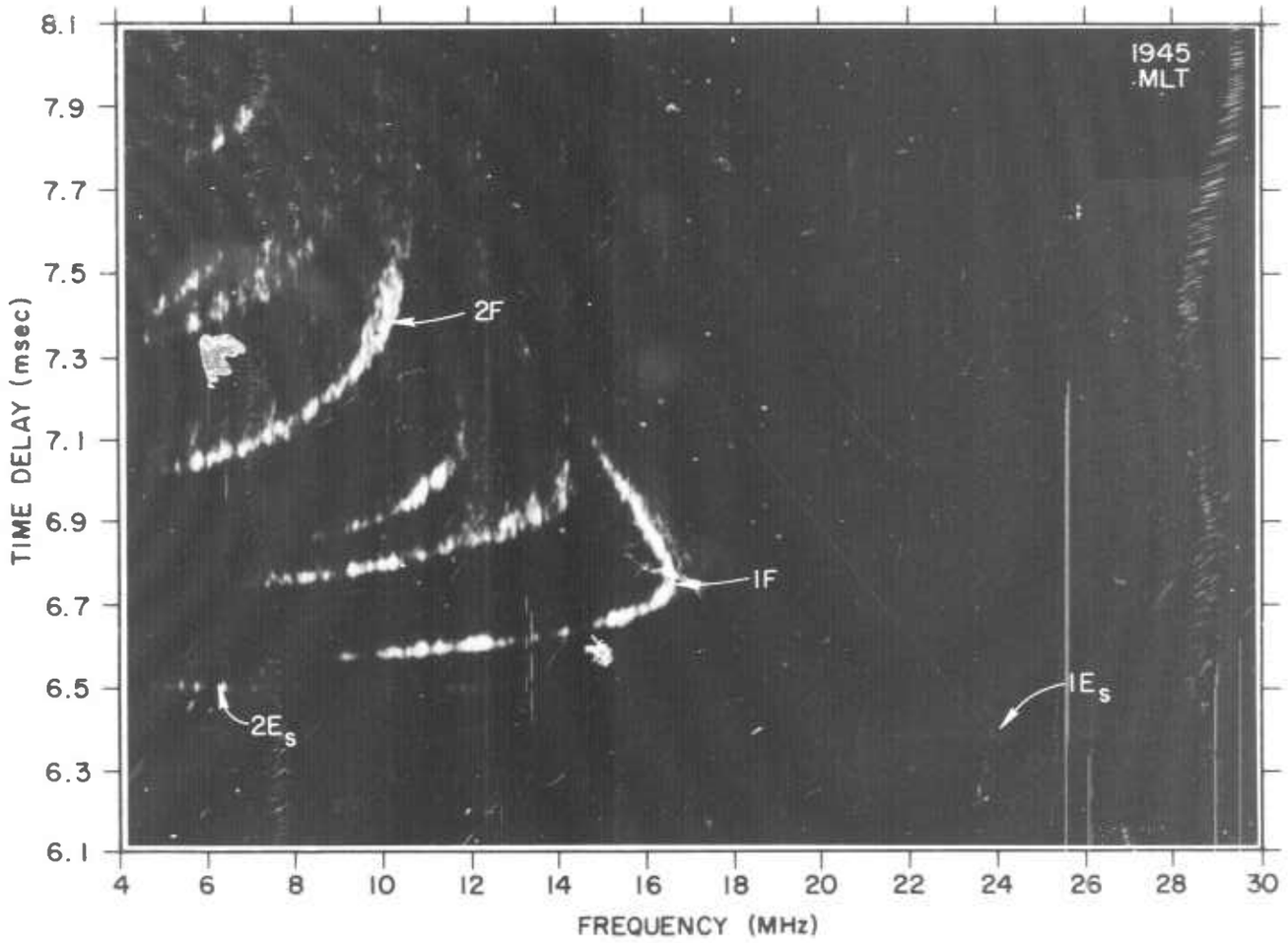

Fig. 12. EXPERIMENTAL CALIBRATED OBLIQUE IONOGRAM 12.

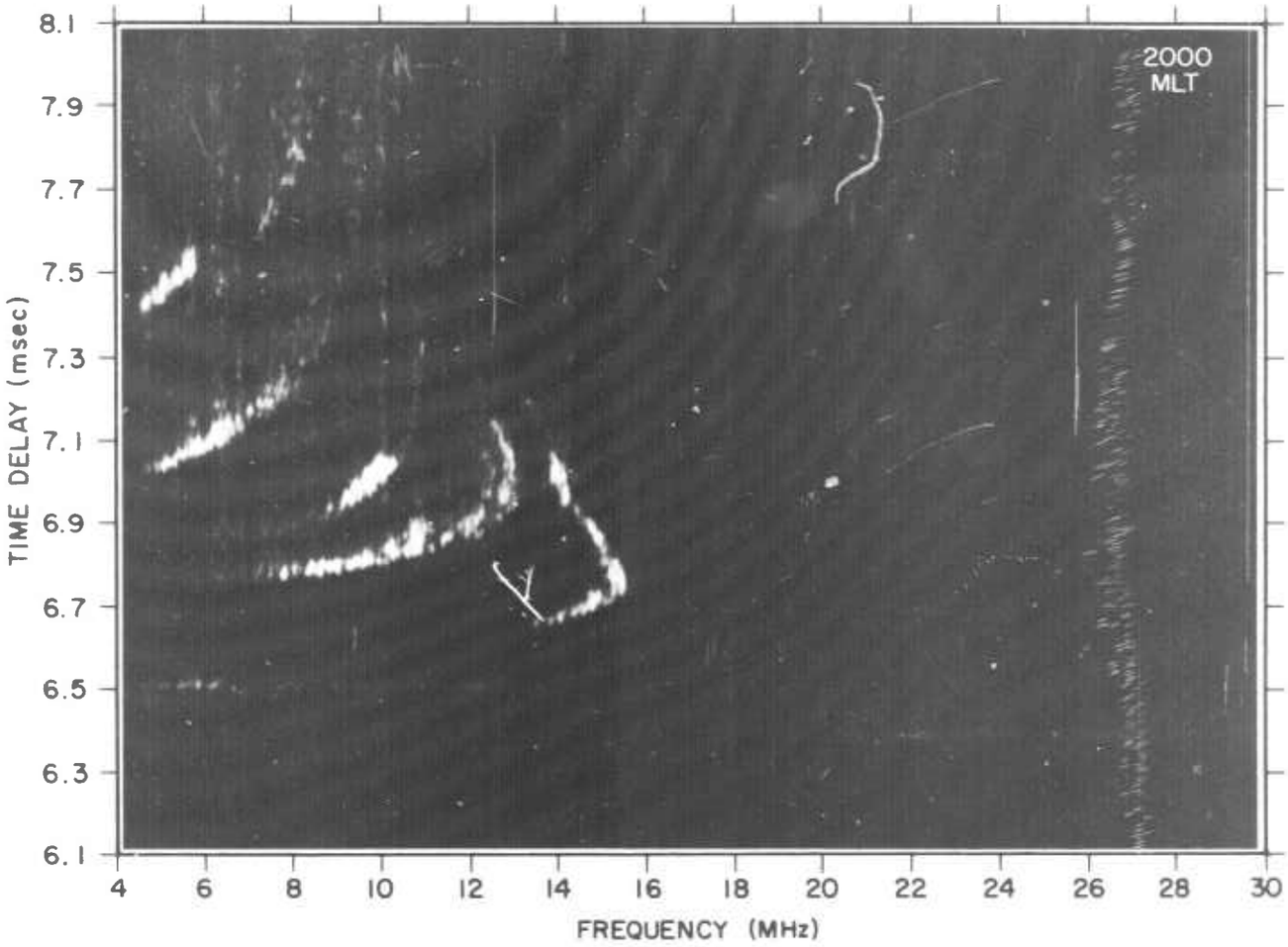

Fig. 13. EXPERIMENTAL CALIBRATED OBLIQUE IONOGRAM 13.

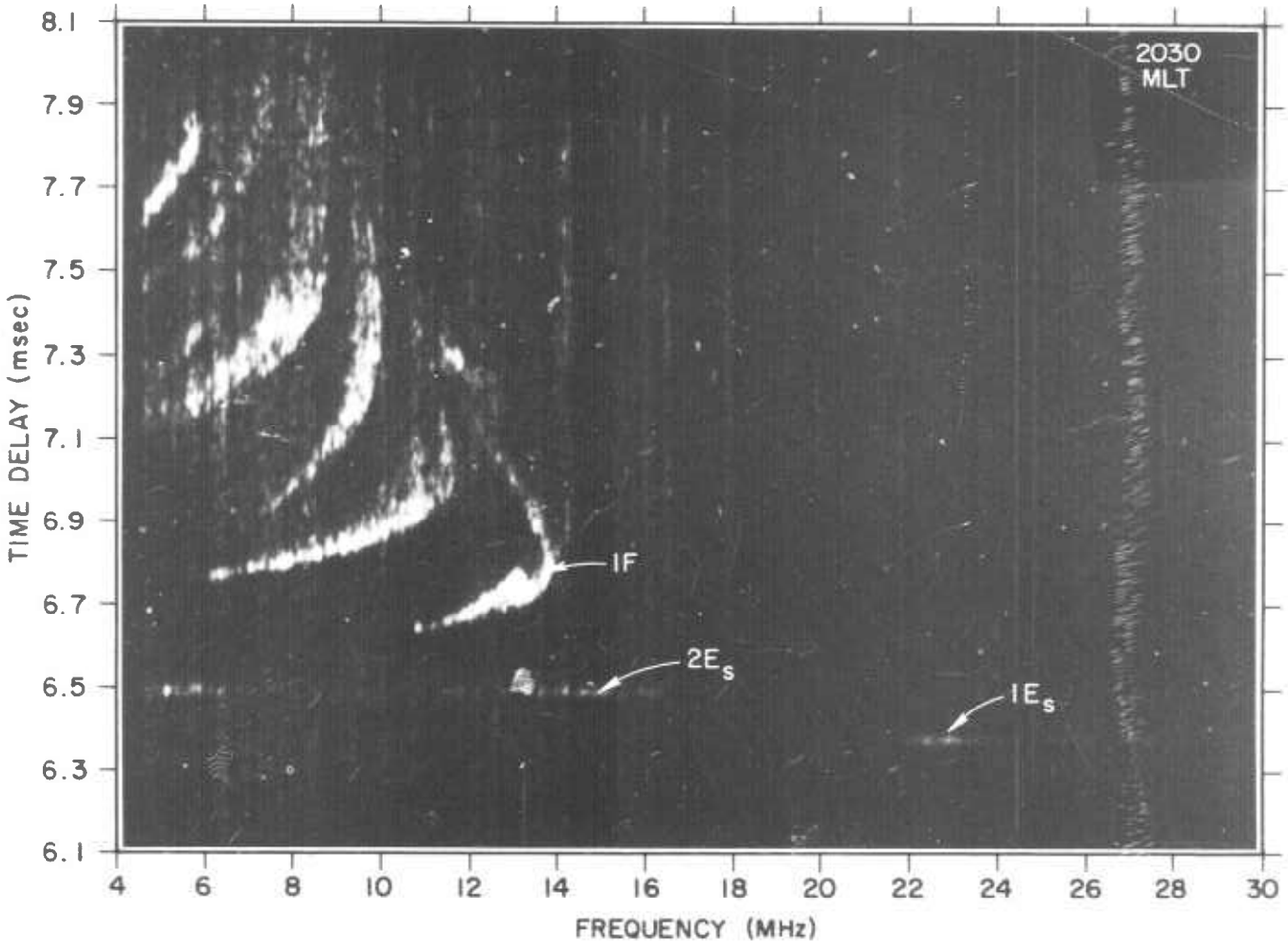

Fig. 14. EXPERIMENTAL CALIBRATED OBLIQUE IONOGRAM 14.

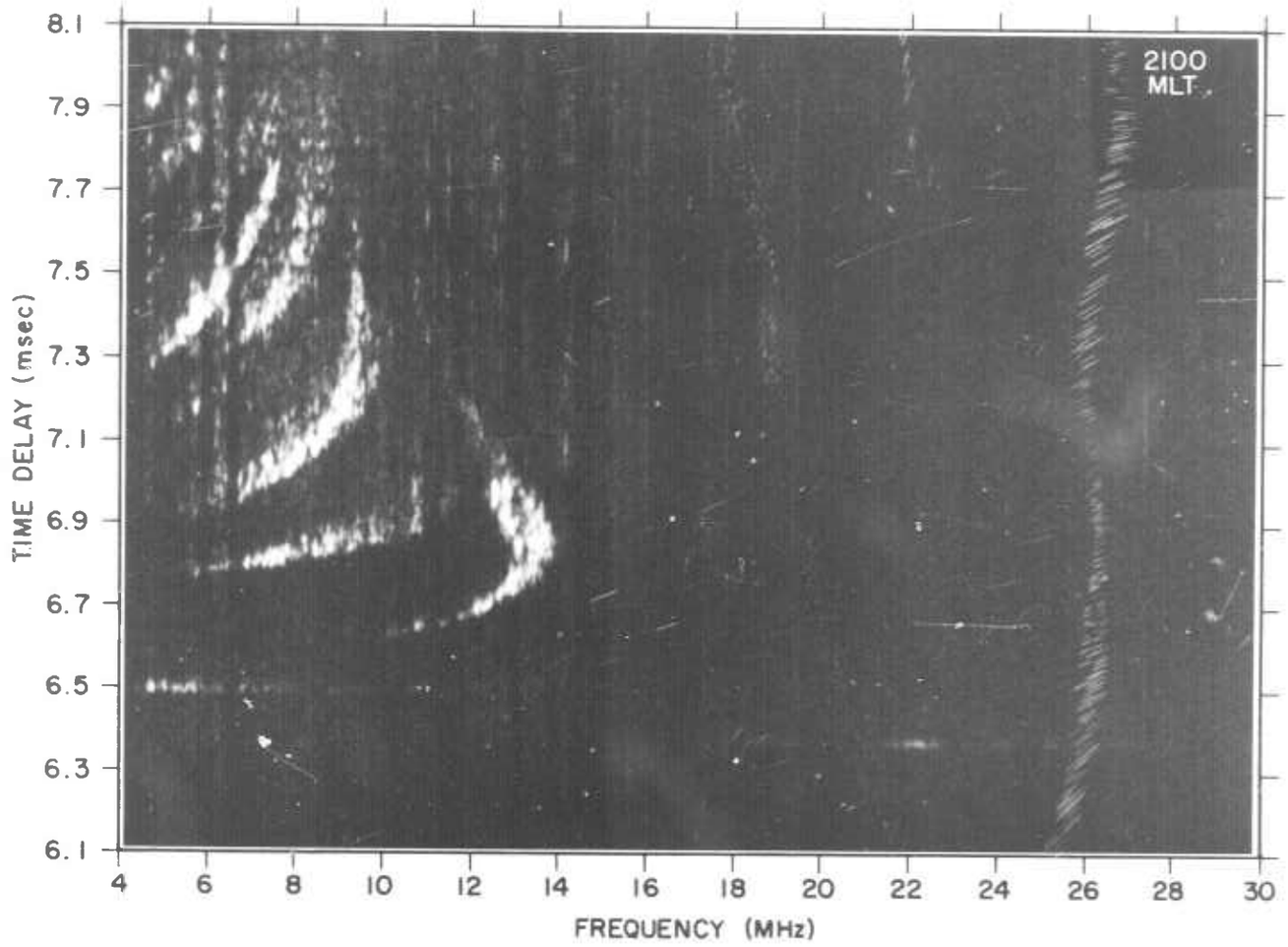

Fig. 15. EXPERIMENTAL CALIBRATED OBLIQUE IONOGRAM 15.

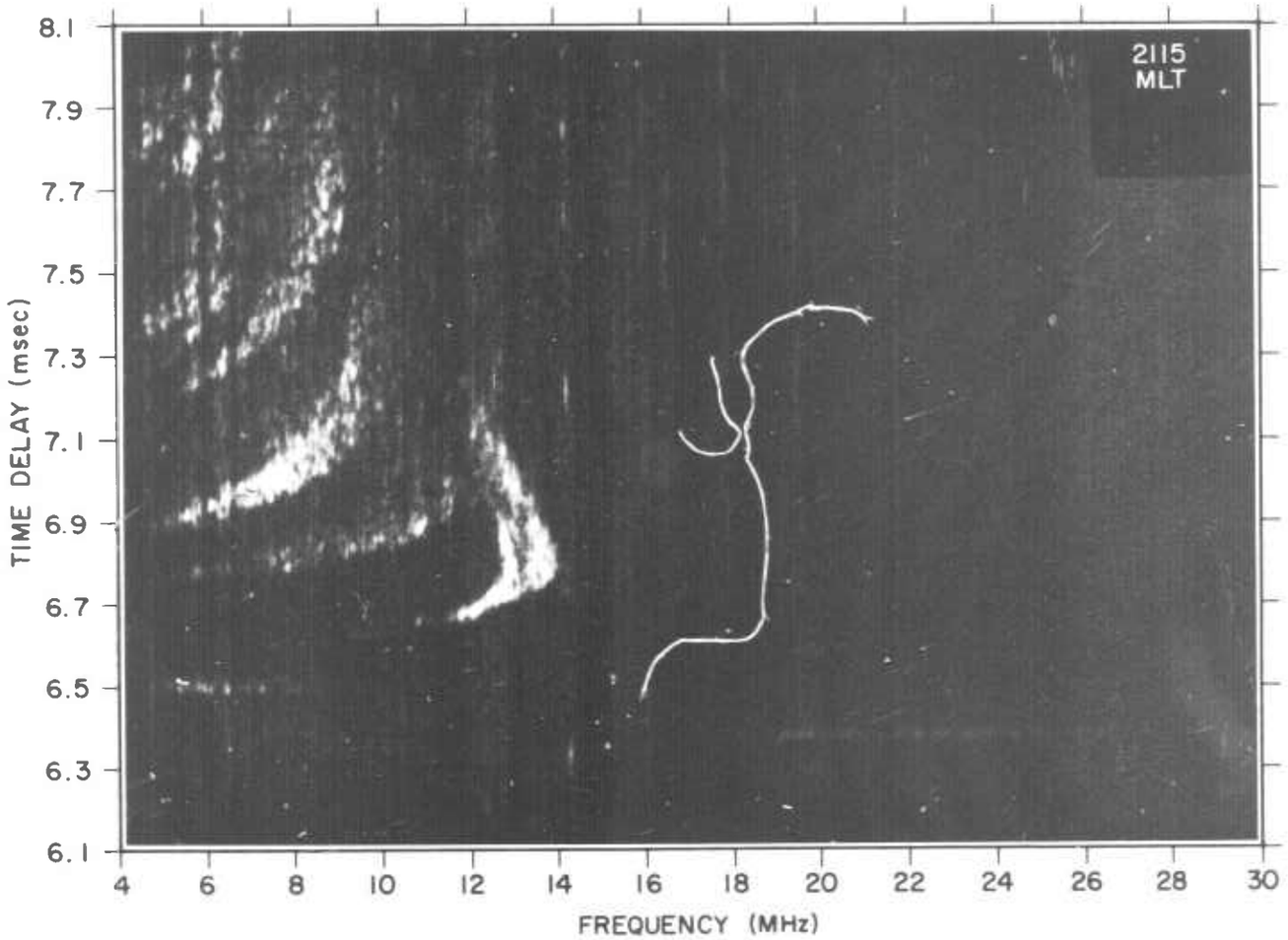

Fig. 16. EXPERIMENTAL CALIBRATED OBLIQUE IONOGRAM 16.

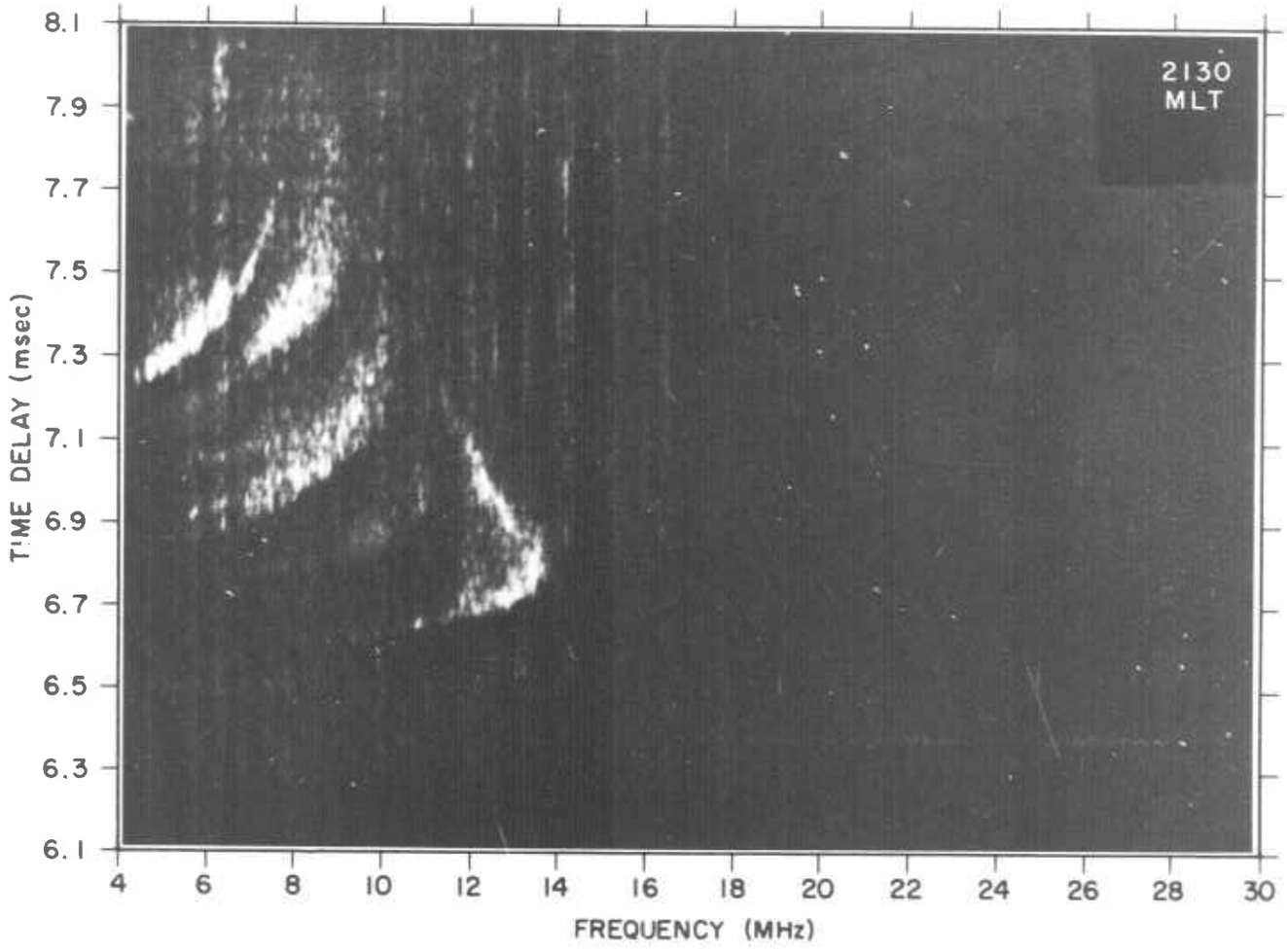

Fig. 17. EXPERIMENTAL CALIBRATED OBLIQUE IONOGRAM 17.

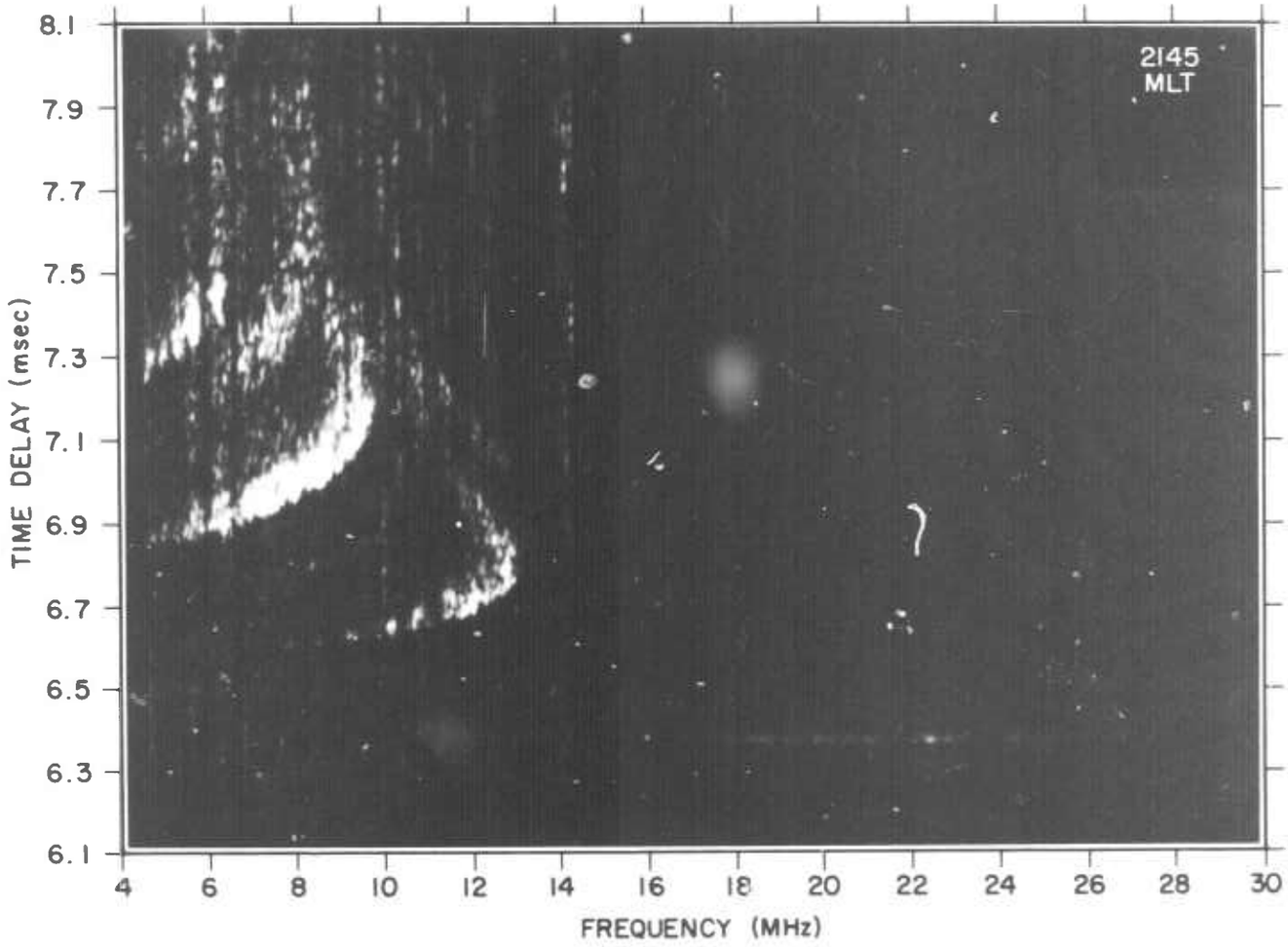

Fig. 18. EXPERIMENTAL CALIBRATED OBLIQUE IONOGRAM 18.

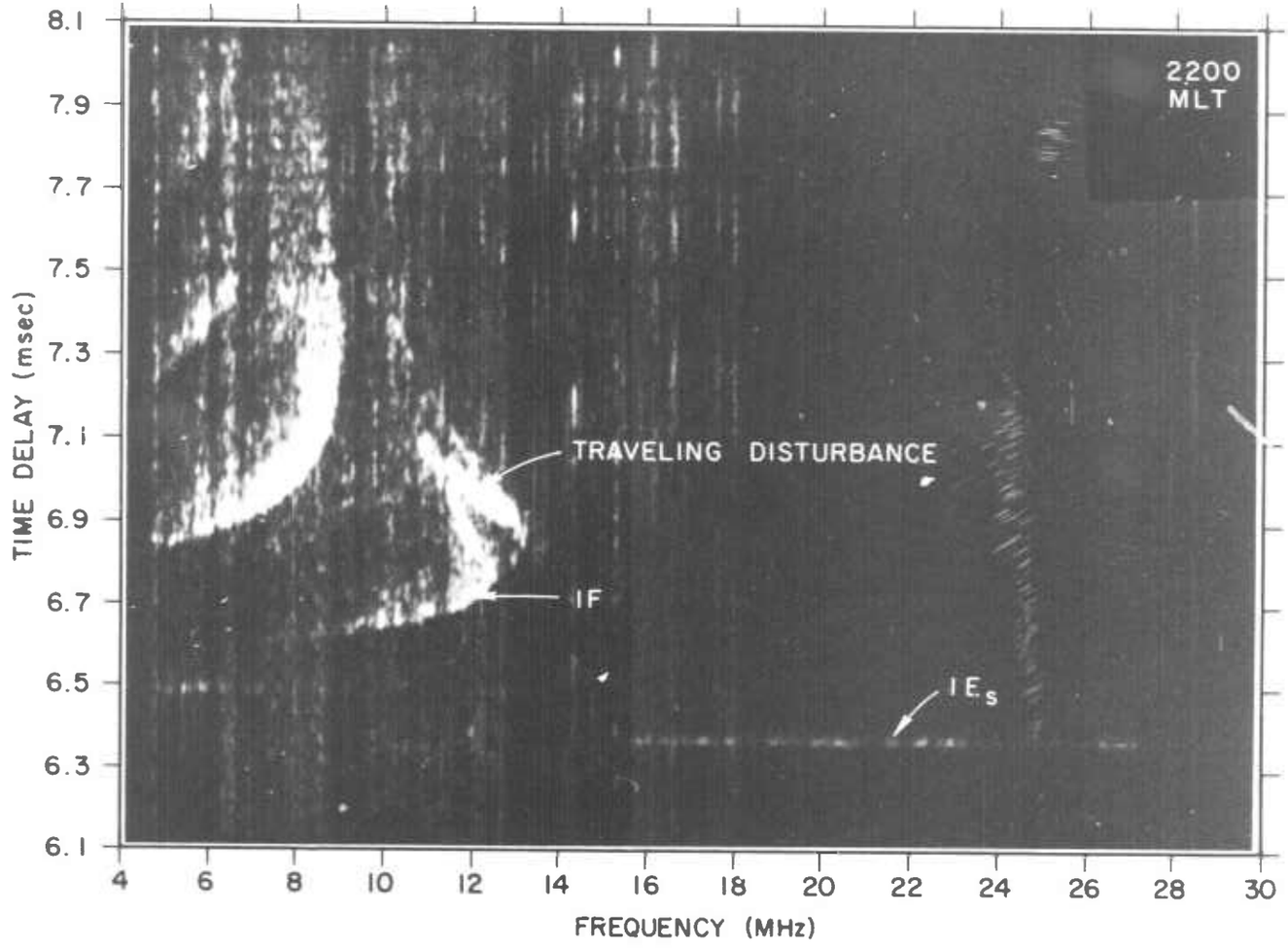

Fig. 19. EXPERIMENTAL CALIBRATED OBLIQUE IONOGRAM 19.

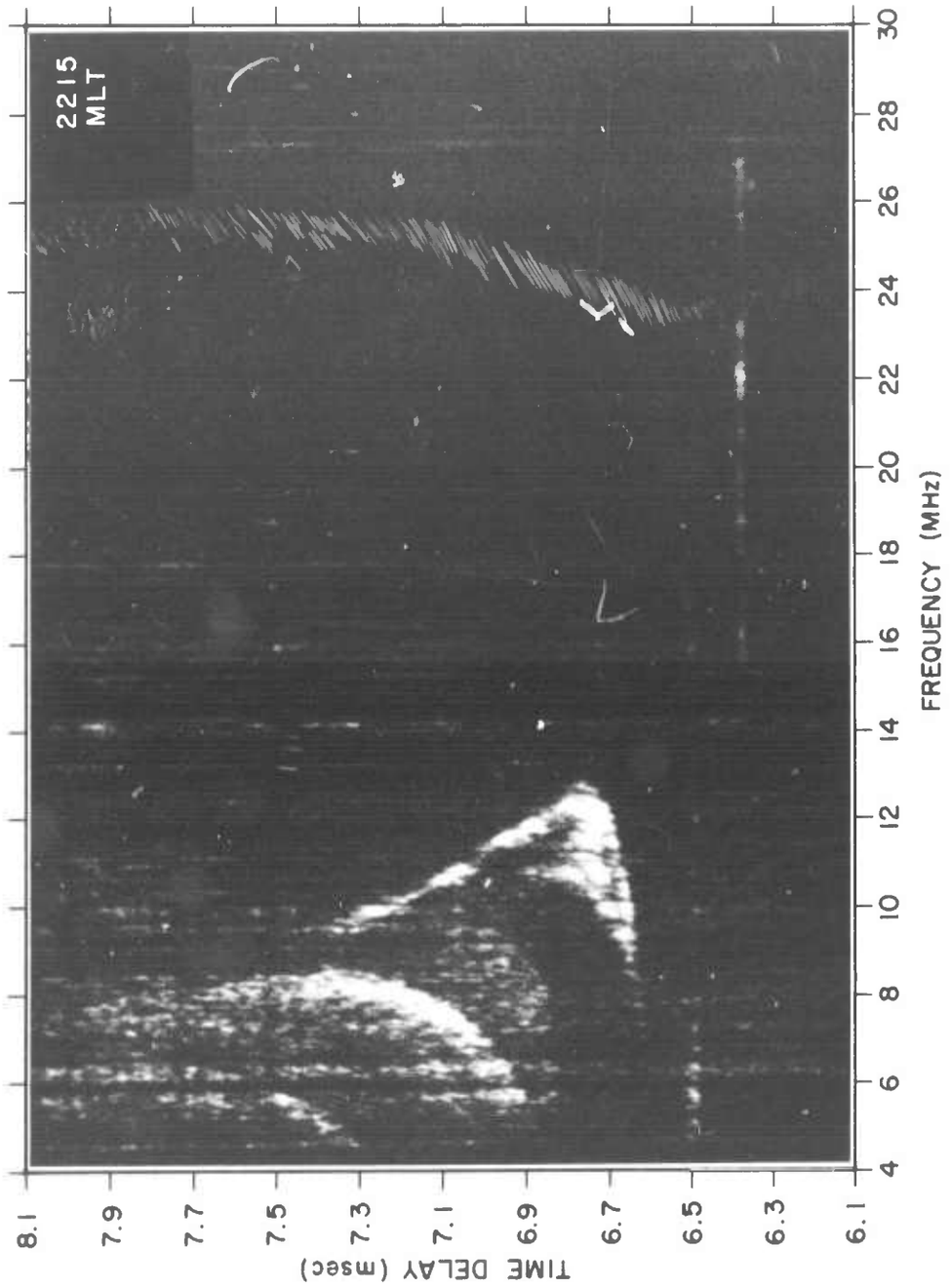

Fig. 20. EXPERIMENTAL CALIBRATED OBLIQUE IONOGRAM 20.

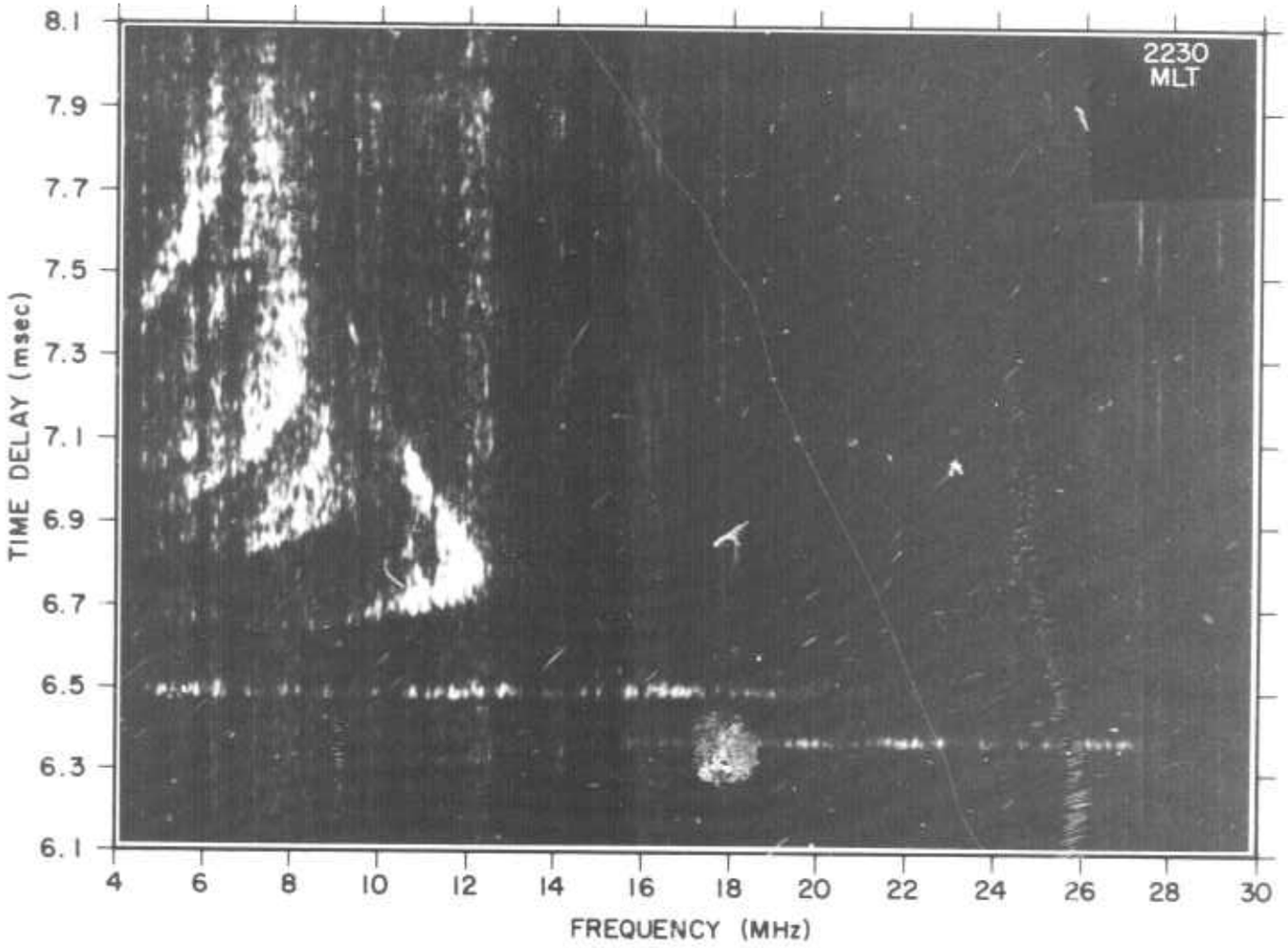

Fig. 21. EXPERIMENTAL CALIBRATED OBLIQUE IONOGRAM 21.

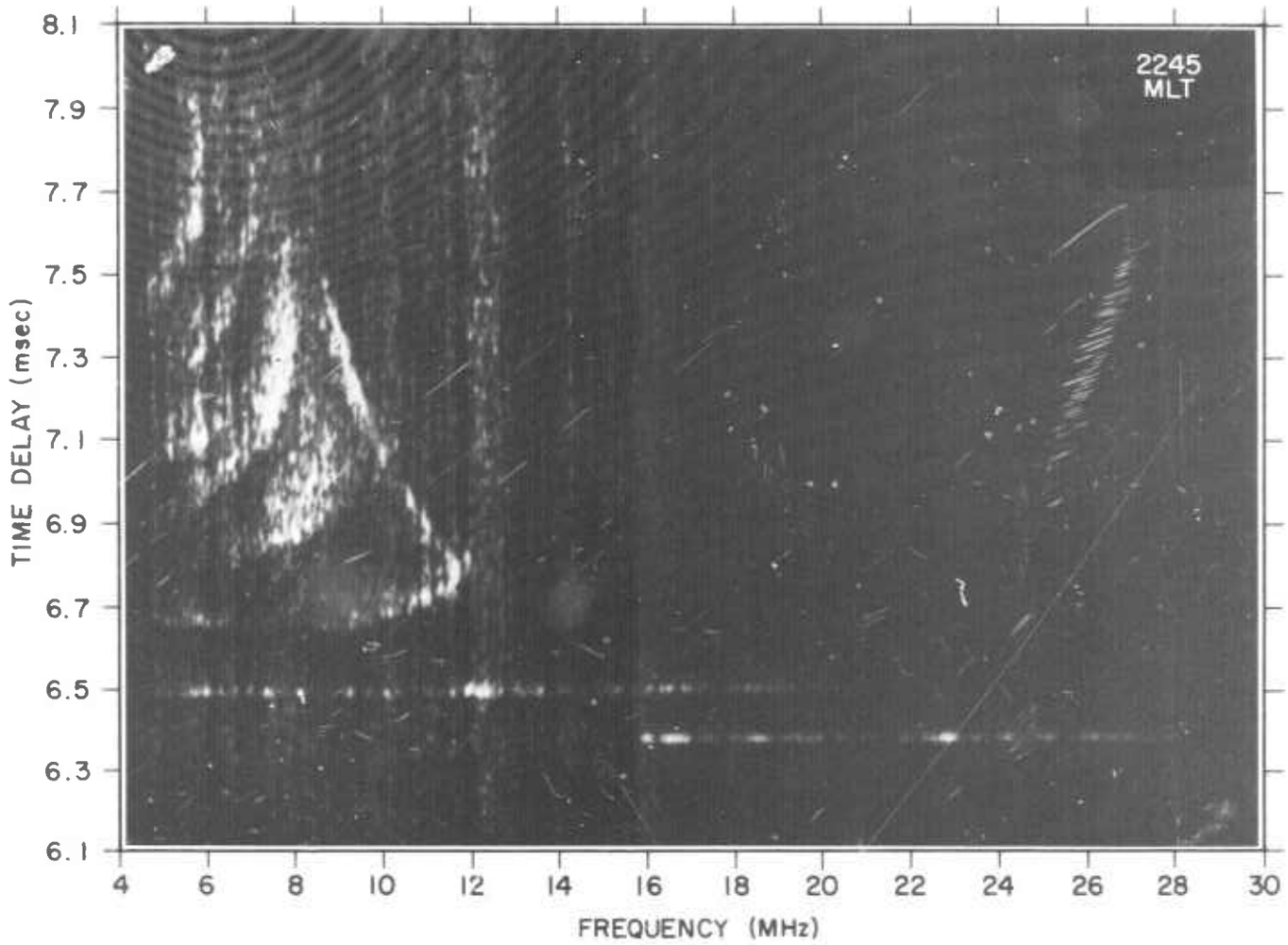

Fig. 22. EXPERIMENTAL CALIBRATED OBLIQUE IONOGRAM 22.

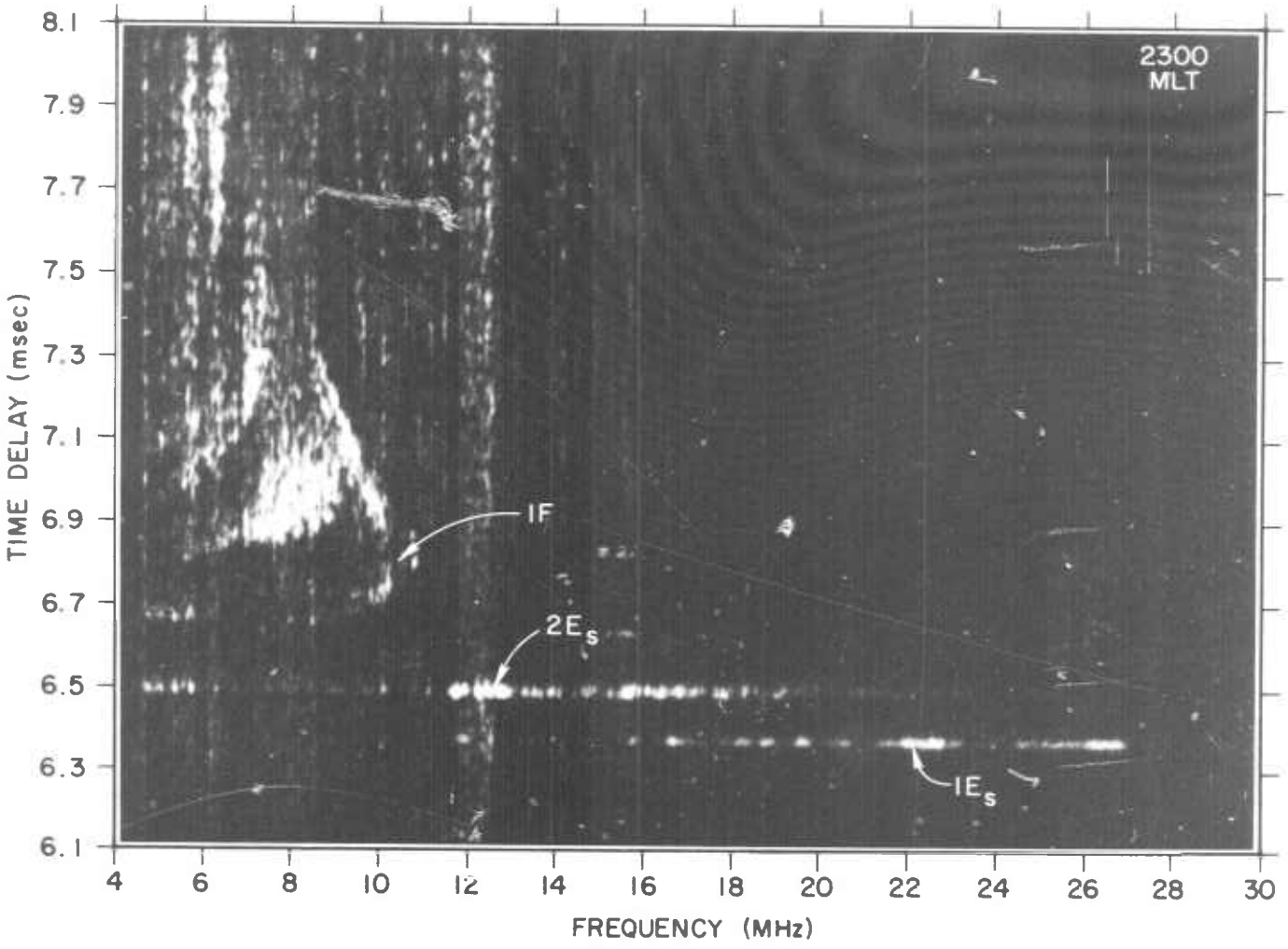

Fig. 23. EXPERIMENTAL CALIBRATED OBLIQUE IONOGRAM 23.

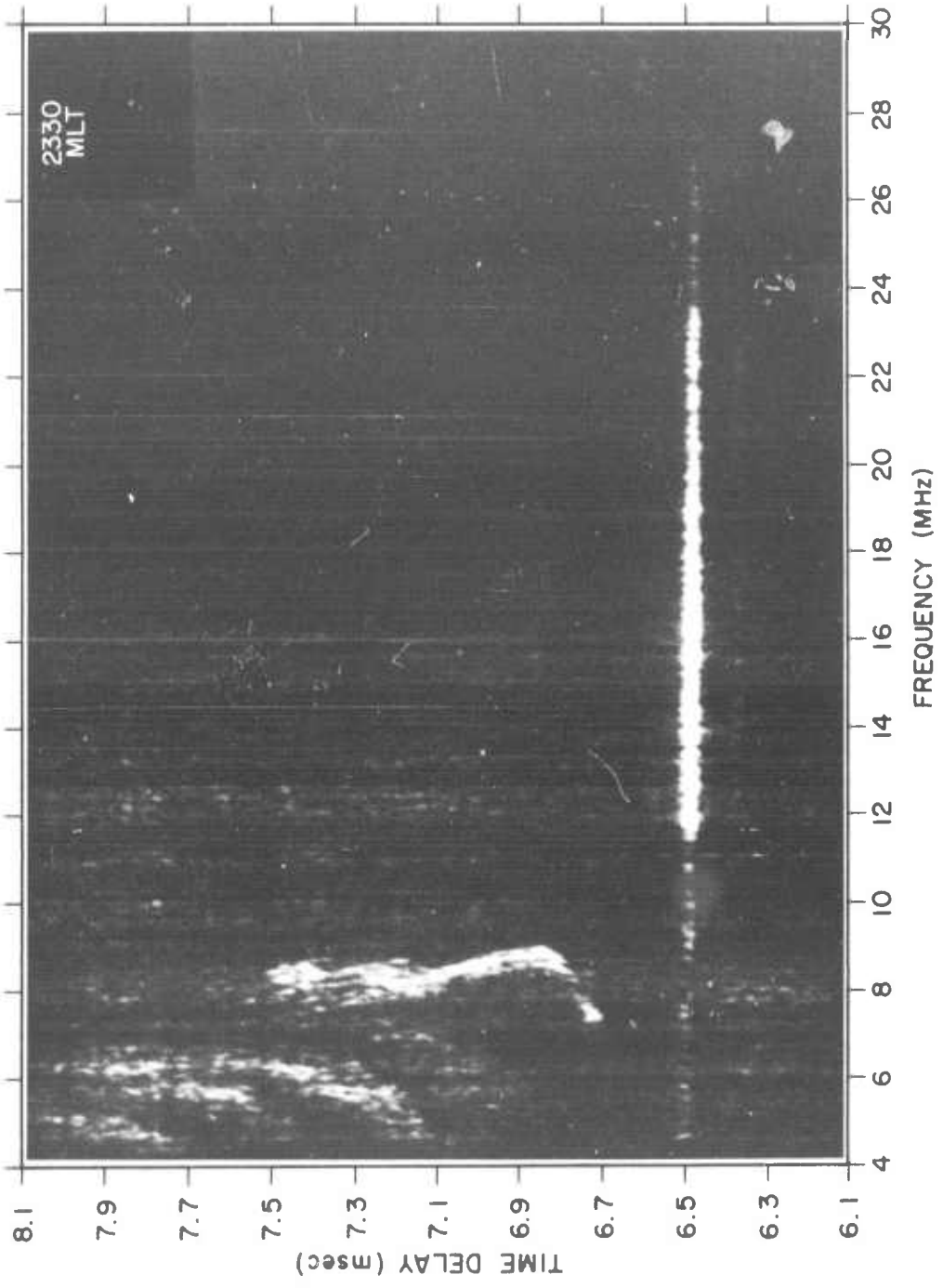

Fig. 24. EXPERIMENTAL CALIBRATED OBLIQUE IONOGRAM 24.

Several possible combinations of reflections are possible. Two of the simplest are the E-F or "N" mode and the FEF or "M" mode, as shown in Figs. 25 and 26. (Henceforth, within the multi-mode terminology, the sporadic-E-layer will be denoted by E, rather than by E_s.) The terminology adopted for the description of the modes is consistent with that adopted at the meeting in Lindau, May 1963 [Ref. 16, p. 189], and uses a dash to indicate the occurrence of a ground reflection. Thus, for example, the notation E-F (see Fig. 25) denotes first a reflection from the E_s-layer, then a reflection from the ground, followed by a reflection from the F-layer--in either direction. This path resembles a 2-hop F-mode path, but because of the lower height of the E_s-layer, the time delays for the E-F mode must be less than those for the 2-hop F-mode; furthermore, since the angles of incidence into the F-layer, ϕ_o, are greater than those for the 2F case, the maximum frequency that supports the E-F mode (MUF) should be higher than that for the 2F mode. These expectations were supported by the experimental records obtained.

Similarly, as shown in Fig. 26, the FEF mode denotes a reflection from the F-layer, followed by a reflection from the top of the E_s-layer, again followed by a reflection from the F-layer, which directs the wave down to the receiver.

Other possible multi-modes are (refer to Figs. 27-32): 2E-F, 2F-E, FEFEF, 3E-F, 2E-2F, FEF-E (which is identical to 2F if no tilts are present), and many others that neither are very likely (e.g., EFEFE), nor were visible within the time delays recorded on the experimental records (e.g., 3F-E). Occurrence of the FEF-F mode is also likely; however, it was not included in the present analysis.

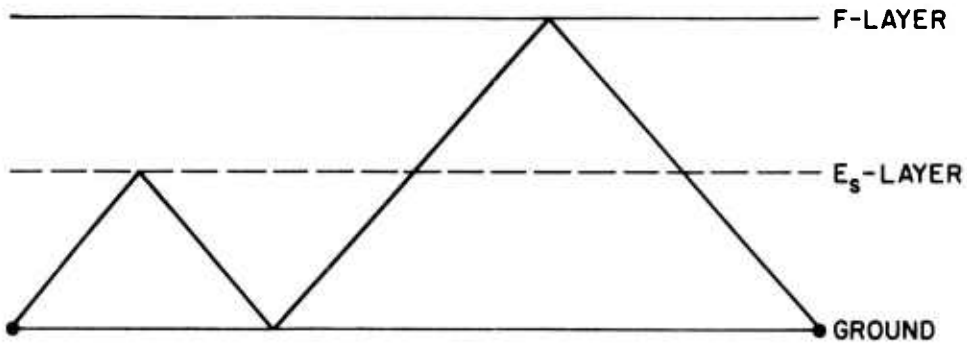

Fig. 25. MULTI-MODE DIAGRAM: E-F.

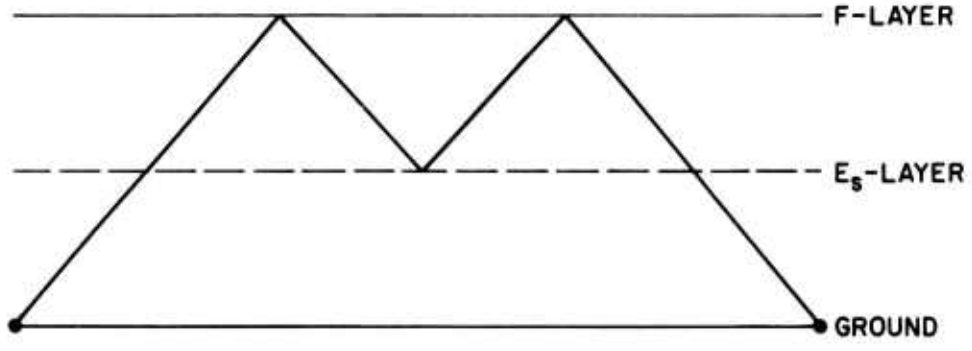

Fig. 26. MULTI-MODE DIAGRAM: FEF.

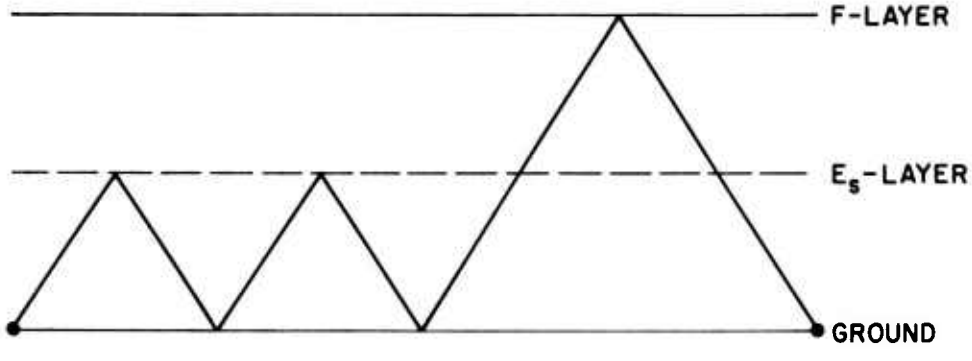

Fig. 27. MULTI-MODE DIAGRAM: 2E-F.

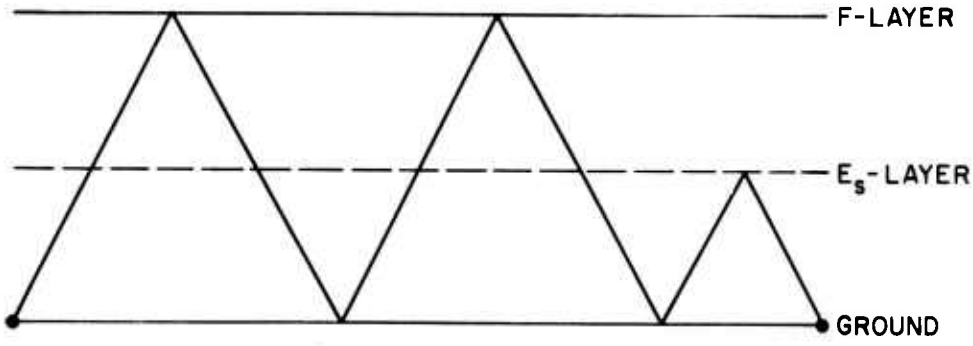

Fig. 28. MULTI-MODE DIAGRAM: 2F-E.

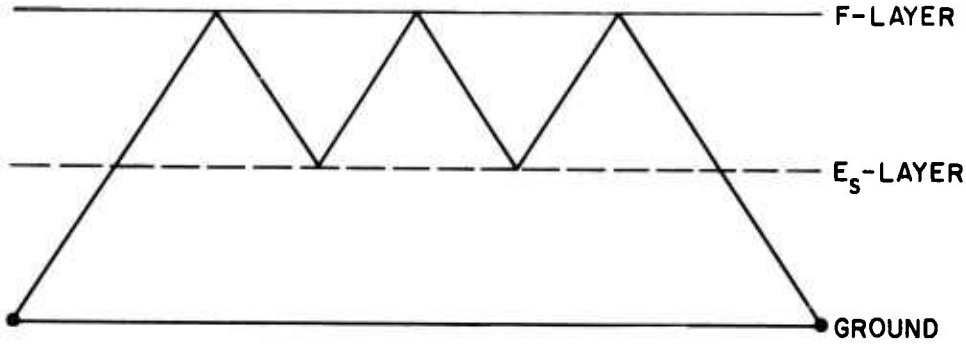

Fig. 29. MULTI-MODE DIAGRAM: FEFEF.

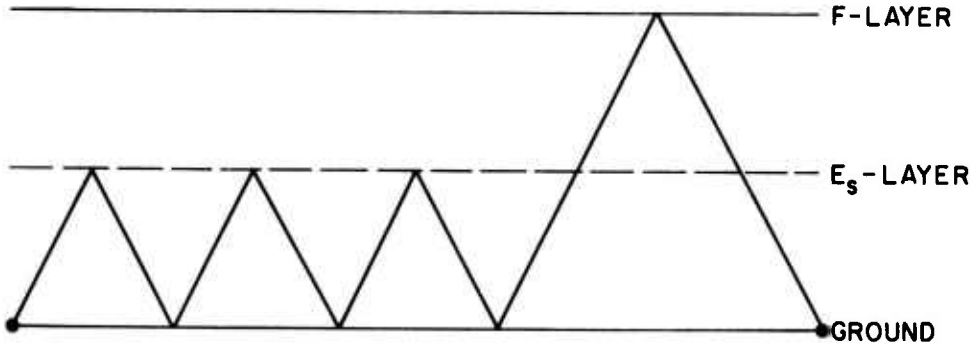

Fig. 30. MULTI-MODE DIAGRAM: 3E-F.

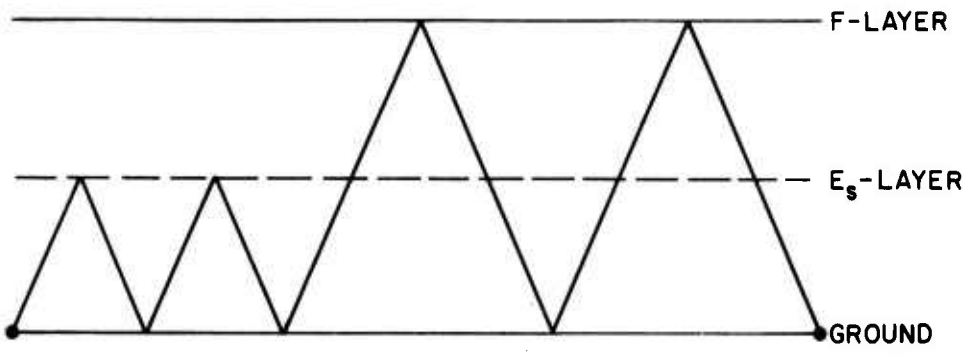

Fig. 31. MULTI-MODE DIAGRAM: 2E-2F.

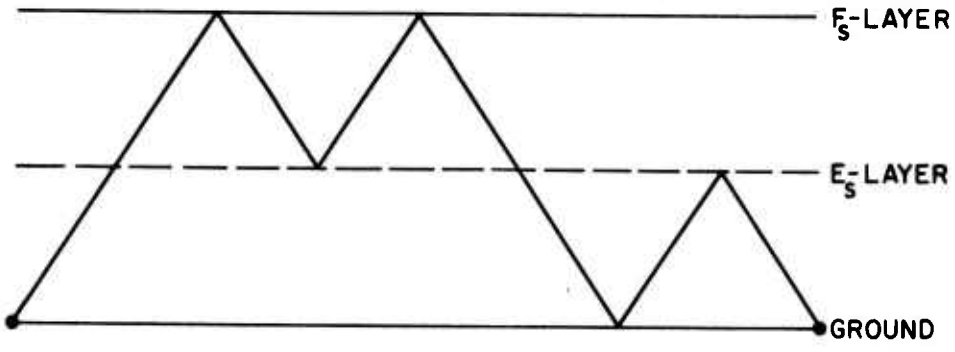

Fig. 32. MULTI-MODE DIAGRAM: FEF-E.

A. The Sporadic-E-Layer

Evidence of a sporadic-E-layer is shown by the horizontal traces on the records from 1130 hr on; some of the records in Figs. 1-24 are labeled accordingly. The evidence is even stronger on the records of 1830 on. A trace with this behavior is caused by an abrupt, very dense layer of electrons; this type of ionospheric layer permits very little ray penetration into the layer as the frequency is increased, and it usually enables the achievement of a rather high MUF.

Rays are permitted to pass to the F-layer over a wide range of take-off angles, as seen for 1-, 2-, and 3-hop F traces. Clearly, either the E_s-layer is confined to the center of the path and is limited in extent, or it extends perhaps over the entire path, but consists of irregularly sized and spaced, highly dense blobs of electrons. The latter would permit some of the wavefront energy to pass through the layer, while causing some of it to be reflected by the highly dense blobs. The author is inclined to accept this description of the layer, especially at the later times, since the presence of many different multi-modes suggests a fairly large E_s patch, capable of supporting reflections all along the path. Furthermore, it was also clear that $2E_s$ was present, suggesting a horizontal layer extent of at least 700 km. This size is consistent with other findings (e.g., see Ref. 21).

The thickness of the E_s-layer may be on the order of one to several kilometers. J. Carl Seddon [Ref. 22, p. 78] conducted a study that utilized measurements of electron density profile made by comparing the relative doppler shift of harmonically related signals radiated by a vertically ascending rocket. T. Croft [Ref. 23] has also compiled a set of records containing rocket measurements of ionospheric density, which involve E_s-layers. Both of these measurements confirm that the average "thickness" of the layer is about 2 km, and heights in the vicinity of 100 km occur. Typical profiles taken from Ref. 22 are reproduced in Fig. 33. The layer thickness is measured between points where the density is several orders of magnitude below the maximum density. Since a wave will penetrate the E_s-layer to a small degree--either from above or from below--the effective thickness of the layer

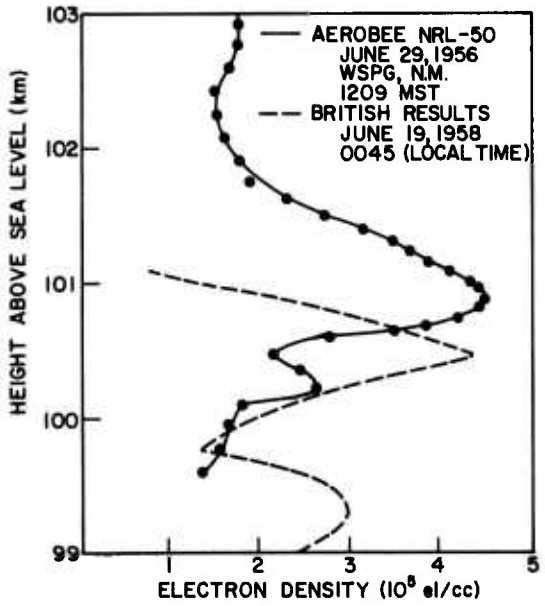

(a) Comparison of sporadic E at noon over New Mexico, U.S.A. with that over Woomera, Australia at midnight.

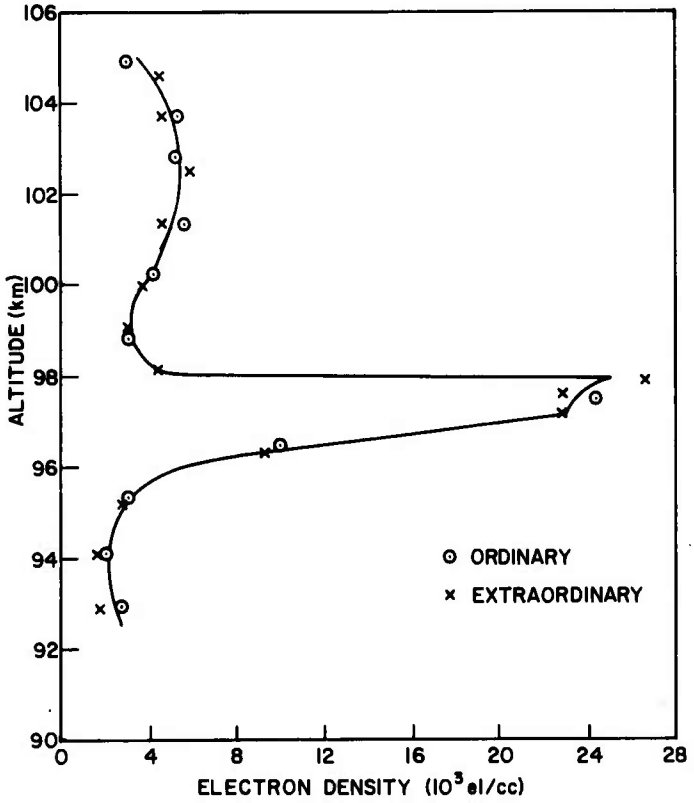

(b) Detailed profile of sporadic E over Ft. Churchill.

Fig. 33. ELECTRON DENSITY PROFILES MEASURED WITH ROCKETS. (From Smith and Matsushita, Ionospheric Sporadic E, The Macmillan Co., New York, 1962. Page 78.)

is probably on the order of 1 km. However, since the path length was appreciably greater than this thickness, it was assumed for greater simplicity that the layer was of zero thickness.

We then arrive at the following preliminary model assumptions:

(1) large extent, possibly over the entire path;

(2) very thin, highly dense blobby layer;

(3) nonblanketing (holes between blobs).

The height of the E_s-layer was determined through knowledge of the time delay of propagation over the path, and by assuming curved-earth geometry. The time delay, denoted hereafter by T_D, and height are related by

$$T_D = \frac{1}{150}\sqrt{2R(R+h)\left[1 - \cos\left(\frac{D_o}{2R}\right)\right] + h^2} \text{ msec} \quad \text{(for 1-hop)},$$

$$T_D = \frac{1}{75}\sqrt{2R(R+h)\left[1 - \cos\left(\frac{D_o}{4R}\right)\right] + h^2} \text{ msec} \quad \text{(for 2-hop)},$$

where

R = mean radius of earth, 6370 km,

D_o = path length, 1881.27 km,

h = height of E_s-layer.

These functions were plotted for this particular path, as shown in Fig. 34. The T_D's corresponding to the $1E_s$ and $2E_s$ modes were extracted from the records and are tabulated in Table 1. The corresponding E_s heights vs midpath time of day are plotted in Fig. 35; there are two curves, one for 1-hop, the other for 2-hop. For the later times, the 2-hop data indicated lower heights than those found in the 1-hop data. Ordinarily, one would expect the 2-hop mode to penetrate slightly deeper into the layer, and thus be reflected from a higher "virtual height" than the 1-hop mode--as seemed to be the case earlier in the day. In most cases, the 2-hop trace appeared at lower frequencies, and the 1-hop at higher frequencies; at these higher frequencies, there may have been deeper 1-hop mode-layer penetration. However, a more reasonable explanation for the inconsistency might be the existence of two or more different

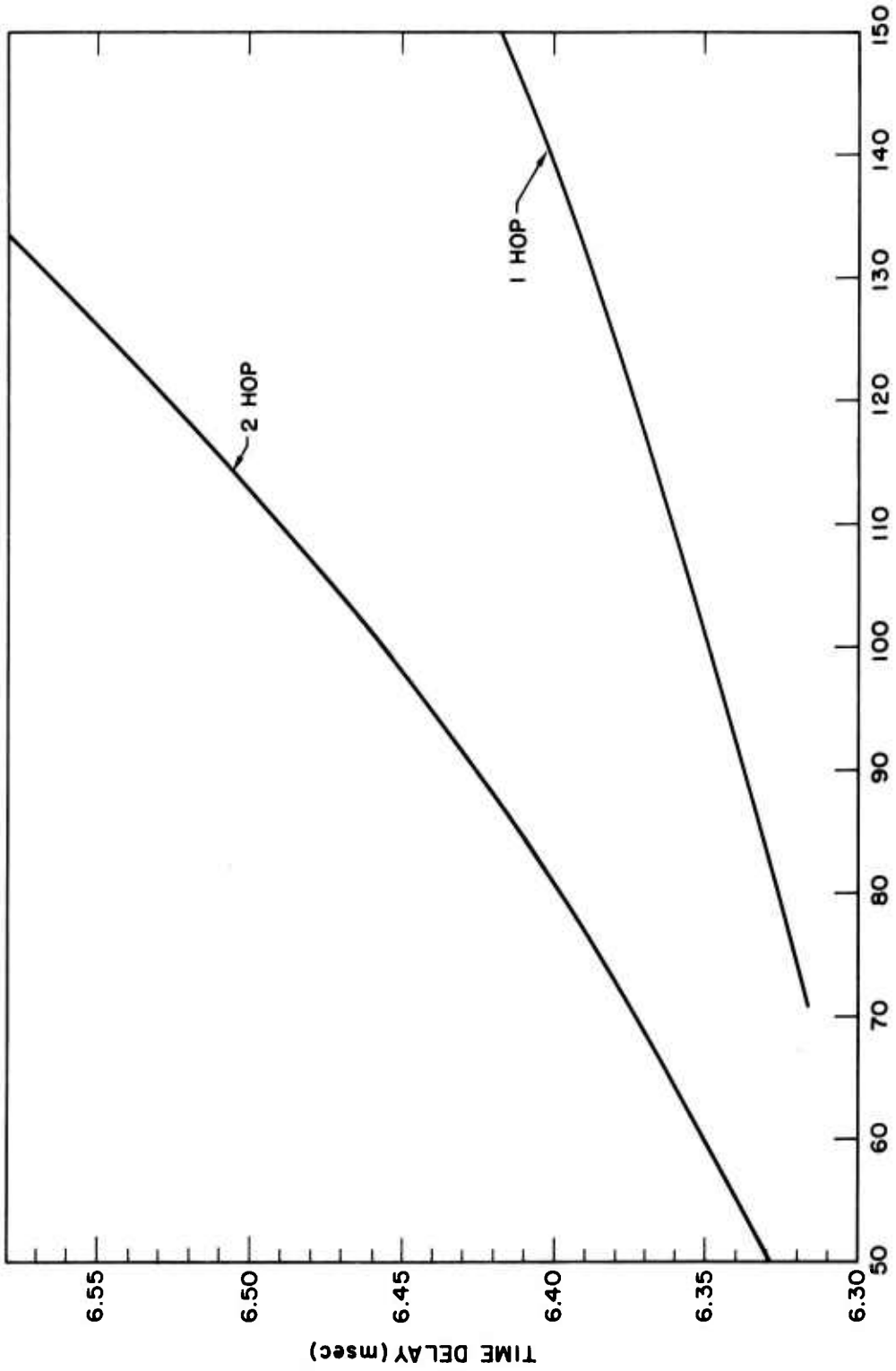

Fig. 34. TIME DELAY VS HEIGHT; 1- AND 2-HOP SPORADIC-E.

Table 1

TIME DELAYS AND VIRTUAL HEIGHTS FOR 1- AND 2-HOP SPORADIC-E

Ionogram Number	Midpath Local Time	Hops	Frequency Measurement (MHz)	Time Delay (msec)	Virtual Height (km)
1	0930	1 2	No sporadic-E-layer visible		
2	1130	1 2	16 11	6.380 6.480	124 107
3	1430	1 2	16 11	6.380 6.510	124 115
4	1600	1 2	16 10	6.380 6.520	124 118
5	1700	1 2	16 10	6.380 6.515	124 117
6	1730	1 2	10 8	6.380 6.530	124 121
7	1800	1 2	10 8	6.370 6.530	117 121
8	1830	1 2	18 8	6.380 6.520	124 118
9	1845	1 2	14 8	6.375 6.500	121 113
10	1900	1 2	20 10	6.375 6.515	121 114
11	1930	1 2	25 8	6.375 6.495	121 112
12	1945	1 2	25 10	6.375 6.500	121 113
13	2000	1 2	25 10	6.375 6.500	121 113
14	2030	1 2	25 10	6.375 6.495	121 112
15	2100	1 2	25 10	6.375 6.500	121 113
16	2115	1 2	25 10	6.378 6.500	123 113
17	2130	1 2	25 10	6.385 6.500	121 113
18	2145	1 2	25 10	6.375 6.490	121 110
19	2200	1 2	25 10	6.375 6.490	121 110
20	2215	1 2	25 15	6.375 6.500	121 113
21	2230	1 2	25 15	6.375 6.490	121 110
22	2245	1 2	20 10	6.375 6.495	121 112
23	2300	1 2	25 10	6.360 6.490	108 110
24	2330	1 2	20 20	6.370 6.490	117 110

levels of E_s ionization. Such an occurrence has been reported by observers in the past, and again just recently at Stanford by L. E. Sweeney, who is currently taking oblique-sounding records between Los Baños, California, and Bearden, Arkansas, using a very large aperture receiving array. Seddon [Ref. 22, p. 83] cites examples in which "preferred" levels of ionization separated by 6 km have been found. The existence of these levels correlated with the occurrence of wind shear levels separated by the same 6 km. It is therefore possible that a lower level was formed over midpath later in the day, accompanied by the disappearance of levels over other parts of the path.

From Fig. 35, it is impossible to tell whether an E_s-layer of higher (or lower) density occurred at the transmitter, middle, or receiver end of the path. Therefore, given a specific ray path for a particular mode from which an E_s reflection occurs at a specific range, the exact height of the E_s-layer cannot be deduced. An average E_s height was therefore determined by averaging the 1- and 2-hop E_s data of Fig. 35 at each time

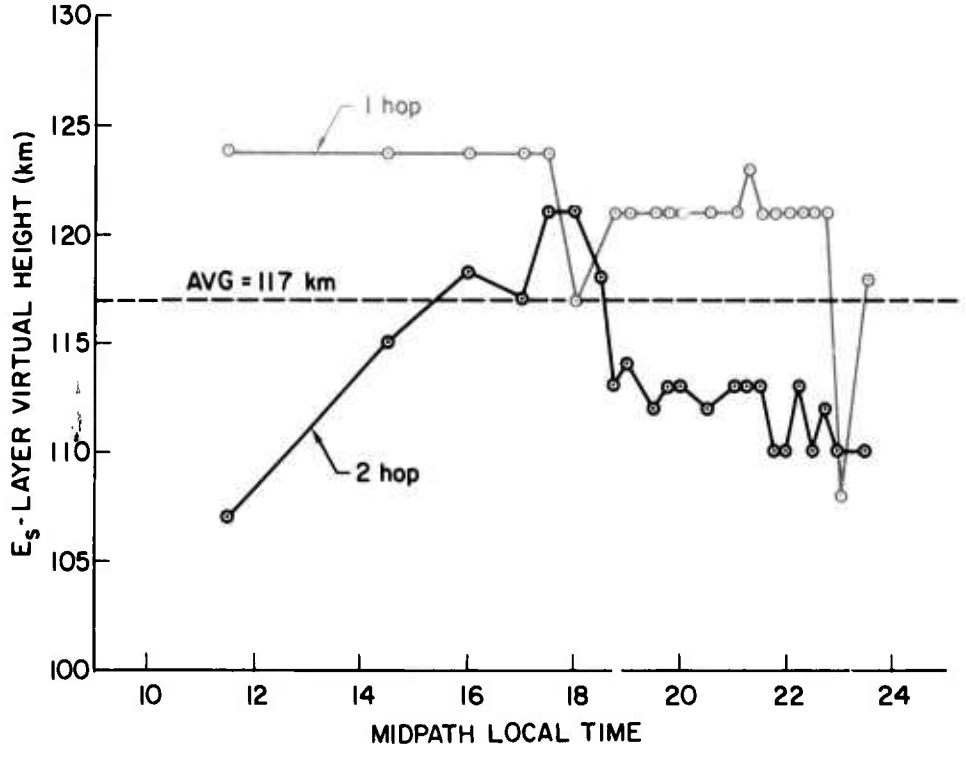

Fig. 35. SPORADIC-E HEIGHT VS MIDPATH LOCAL TIME (MLT).

of day; this is shown in Fig. 36. Furthermore, to make the models more consistent, all these values were averaged over the day's data, and an average height of 117 km was obtained; this height, by coincidence, is equal to one of Seddon's "preferred" heights. The height of 117 km proved quite successful for model matching, except at 1845 MLT, in which case a height of 105 km gave a much better fit. This exception could have been caused by the occurrence of a small, lower E_s patch, located over the appropriate reflection points along the path.

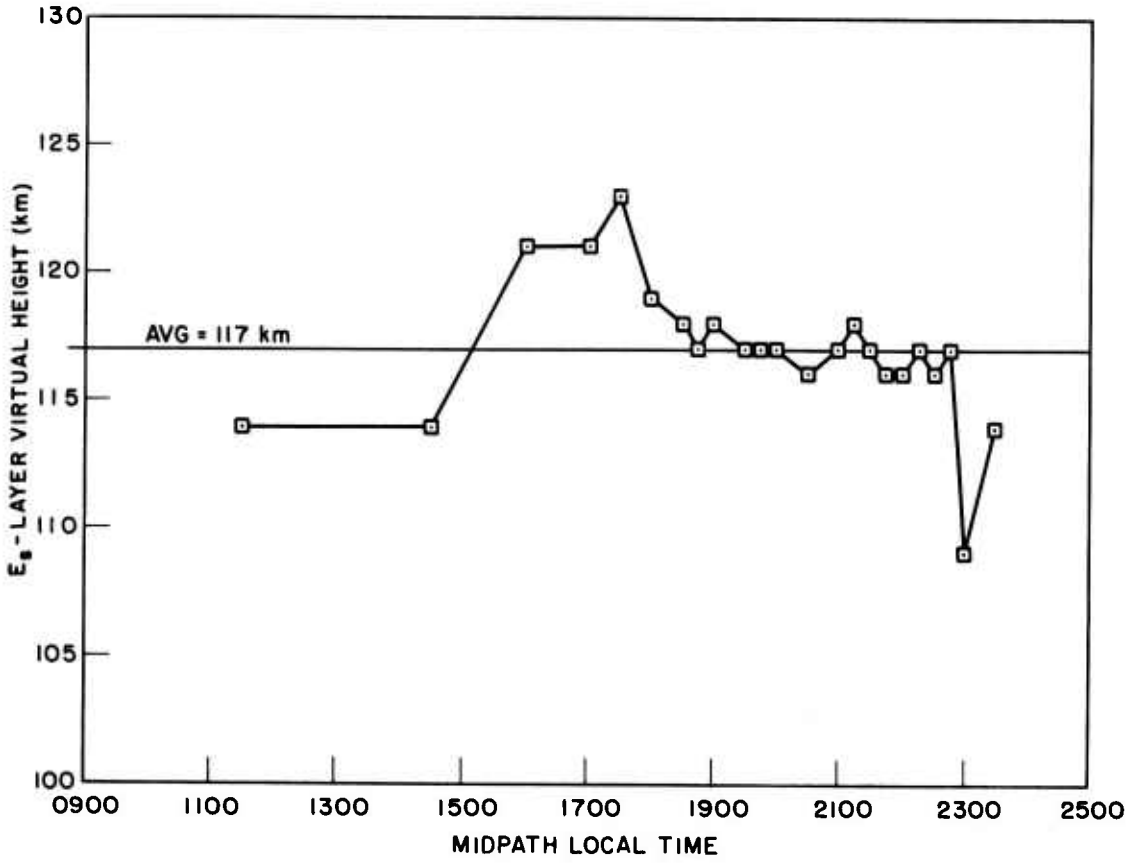

Fig. 36. AVERAGE HEIGHTS OF FIGURE 35 VS MIDPATH LOCAL TIME.

B. The F-Layer Models

1. The Initial Computer Models

One of the simplest possible, yet realistic, models for the F-layer is the β-Chapman layer, given by

$$N = N_o \exp(1 - z - e^{-z}) , \quad \text{where} \quad z = \frac{h - h_m}{H_s} ,$$

and

N = electron density,

N_o = maximum electron density,

h = height,

h_m = height of maximum ionization,

H_s = scale height in β-Chapman equation for density.

This model was quite successful, and with suitable modifications in N_o, h_m, and H_s, was used throughout the analysis. Table 2 lists the parameters used in the generation of these initial computer models.

Table 2

F-LAYER IONOSPHERES TRIED IN THE INITIAL MATCHING PROCEDURE

Model	Maximum Density N_o (electrons/cm^3)	Maximum Height h_m (km)	Scale Height H_s (km)
A	10^6	270	30
B	10^6	270	40
C	10^6	300	40
D	10^6	300	65
E	10^6	300	90
F	10^6	350	40
G	10^6	350	65

2. Modification of the Models To Match the MUFs

The synthesized ionograms are presented as plots of T_D vs frequency. The parameter that governs the behavior of a wave propagating through the ionosphere is the index of refraction, given by

$$\mu^2 = 1 - 80.6 \frac{N(h)}{f^2}$$

$$= 1 - 80.6 \frac{N_o g(h)}{f^2} ,$$

where

$N(h) \triangleq N_o g(h)$,

$g(h)$ = profile shape factor,

f = frequency in MHz.

Thus, if the density factor, N_o, is changed to $N_o' = kN_o$, where k is some constant, then μ^2 will be left unchanged, providing the frequency is scaled by the factor $\sqrt{k}$. Correspondingly, if we are given a synthesized ionogram on which the frequency scale is changed by the factor $\sqrt{k}$, the equivalent model density is changed again by the factor k. Therefore, to match the records, the model's frequency was scaled to give an MUF identical to the experimental MUF; both cases are for the 1F mode. It is perhaps easiest to visualize this by plotting the ionogram on a log-frequency scale; the scale may then be shifted along the horizontal axis to yield an ionogram for different values of N_o. Since the experimental data were recorded on linear scales, the shifting procedure was not feasible; no attempt was made to plot the experimental data on semilog coordinates.

The models for the sporadic-E- and F-layers mentioned above were employed in the generation of computer ionograms. The first task was to find a model that yielded an ionogram whose 1F mode matched the corresponding 1F mode of an experimental record.

Curved-earth geometry was employed, and horizontal tilts in electron density were ignored. The sporadic-E-layer was assumed to extend over the entire path at a constant height, and was made to be partially reflecting and partially transmitting (with time retardation ignored).

The ray-tracing procedure (denoted Ray-319) was developed by T. Croft and P. Fialer at the Stanford Radioscience Laboratory. Given the N(h) profile, the program specifies a frequency and take-off angle, and then follows the ray through the ionosphere. The refractive index is calculated at 1-km intervals; then Snell's law is solved at each successive level. The ray is followed until it strikes the ground, at which point its horizontal distance from the transmitter is recorded; the group and phase time delays and the true height of reflection are also recorded. A new take-off angle is then specified, and the process is repeated. The output was recorded on the line printer and was also put on punched cards for later use in an interpolation program.

A. Calculations

Given a particular mode, the height of the E_s-layer, a model F-layer, and a particular frequency, there are only two possible take-off angles that will support the propagation of a ray over the fixed distance between the transmitter and receiver, namely, the lower and upper (Pederson) rays in the F-layer (magnetoionic splitting is ignored).

Let us concentrate on the lower ray. To illustrate the method of calculation, we will consider the geometry presented by the E-F or "N" mode, shown in Fig. 37. As seen, the F-layer has been replaced by its equivalent virtual height of reflection, h'_F, which corresponds to the take-off angle solution, β, for the lower ray; h'_F will be a function of the frequency and ionospheric properties of the F-layer. We then see that, for a given E-layer height, h'_E, there will be a specific distance, D_E, which exists for the solution β. Moreover, there will be a specific

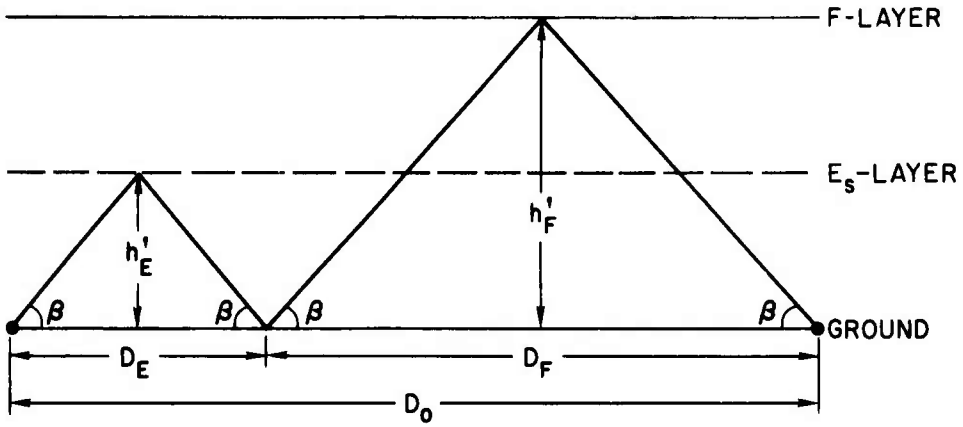

$$D_F = D_o - D_E$$

$$T_D = T_F + T_E$$

Fig. 37. GEOMETRY OF E-F MODE FOR CALCULATION OF TIME DELAYS.

distance, D_F, over which the F ray propagates. For the E-F mode, $D_E + D_F = D_o$. D_o was determined through knowledge of the latitude and longitude of the transmitter and receiver, and found to be 1881.27 km. D_E is a function of β, and is given by

$$D_E = 2R \left[\cos^{-1} \left(\frac{\cos \beta}{1 + h'_E/R} \right) - \beta \right],$$

where

R = 6370 km as before,

h'_E = specified 117 km in all cases but one, where 105 km was used.

Thus, the remaining distance D_F is given by $D_F = D_o - D_E$. Correspondingly, the ray-tracing program presents an output of skip distance vs β. We shall call this distance D'_F; the solution β exists where $D_F = D'_F$. Thus, D_F was tabulated for values of β ascending in short steps; then, both this table and the computer output were visually scanned for the approximate solution β, which was flanked by two values of β, above and below, in each table. The cards representing these values were inserted into a program that interpolated for the correct solution β;

this process is shown graphically in Fig. 38, where the two distance curves are plotted vs take-off angle and solutions are found for different frequencies. The solution β was then used to find the solution time delay for the F hop; finally the total time delay over the path at each particular frequency was determined. For the E-F case, $T_D = T_F + T_E$. At those frequencies for which an upper ray was supported, the process was repeated at a higher set of β's (Fig. 38). The frequencies were chosen 1 MHz apart; the set of solutions obtained for all the frequencies was plotted, and the points were connected to form the ionogram trace. The solution was always a smooth curve, since the F-layer profile was a monotonic function.

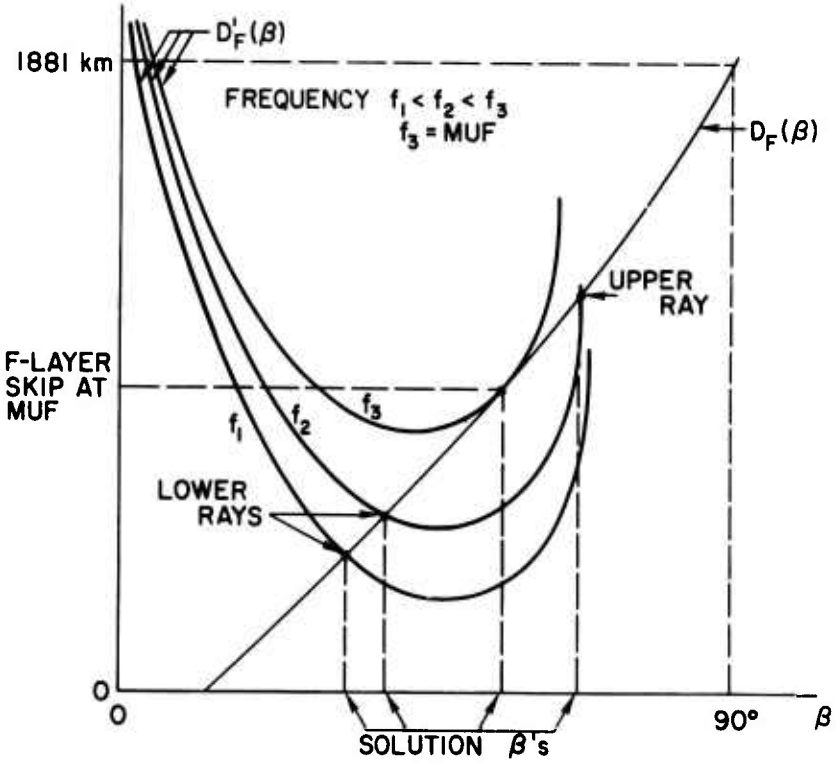

Fig. 38. F-LAYER GROUND DISTANCE VS TAKE-OFF ANGLES, ILLUSTRATING COMPUTER INTERPOLATION.

Before we generalize the procedure, consider for a second example the FEF, or "M" mode, shown in Fig. 39. For this mode,

$$D_F = \frac{D_o + D_E}{2} .$$

The function D_E is, of course, the same as before. However, a new set of curves $D_F(\beta)$ is obtained. The graphical (computer-interpolation) procedure is carried out as before. Finally, the time delay is obtained as $T_D = 2T_F - T_E$. Note that the E hop is fictitious; yet it is included to complete the geometry.

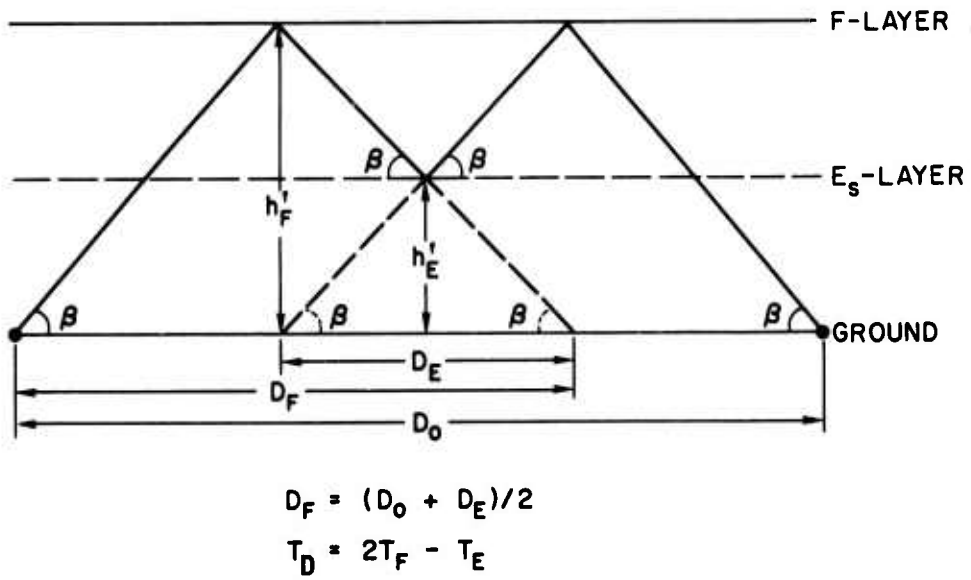

Fig. 39. GEOMETRY OF FEF MODE FOR CALCULATION OF TIME DELAYS.

The same procedure may be repeated for all other possible modes. For each mode, we will have a new set of functions for $D_F(\beta)$, calculated from knowledge of the geometry. These new functions will intersect the computer ray tracings $D'_F(\beta)$, as before, and a new ionogram trace is finally obtained by connecting the time-delay points obtained at each new frequency. Table 3 lists the various possible modes, together with their functions for D_F and T_D. Note that some modes could be expressed

Table 3

D_F AND T_D FORMULAS FOR EACH MODE

Mode	D_F Formula	T_D Formula
E-F	$D_F = D_o - D_E$	$T_D = T_F + T_E$
FEF	$= (D_o + D_E)/2$	$= 2T_F - T_E$
2E-F	$= D_o - 2D_E$	$= T_F + 2T_E$
E-2F	$= (D_o - D_E)/2$	$= 2T_F + T_E$
FEFEF	$= (D_o + 2D_E)/3$	$= 3T_F - 2T_E$
3E-F	$= D_o - 3D_E$	$= T_F + 3T_E$
2E-2F	$= (D_o - 2D_E)/2$	$= 2T_F + 2T_E$
FEF-E	Identical to 2-Hop F	

differently; for instance, 2E-2F could be 2F-2E, E-F-E-F, F-E-F-E, E-2F-E, or F-2E-F. If tilts in electron density were present, these modes would be separated; otherwise, they would all appear superimposed.

B. Matching the Models to 1F and 2F Traces

The model-matching procedure is essentially a "cut-and-try" process; however, certain guidelines may be followed in order to make a good guess at the first "cut." The following is an account of how the models used were derived through trying different values of h_m, H_s, and the modified N_o.

Model E (Table 2) was tried first, since it had been used on numerous occasions in other studies by T. Croft at Stanford (the Stanford number is IID 165). The T_D at the MUF of model E closely matched the MUF of Ionogram 14 (Fig. 14); however, the MUFs were different. Therefore, the frequency scale of the model was modified according to the technique mentioned above:

Model MUF = 20.8 MHz.

Experimental MUF = 13.8 MHz.

Therefore, $\sqrt{k} \triangleq K_f = 13.8/20.8 = 0.663$. The frequency scale of model E was multiplied by this factor. The result is shown in Fig. 40. As seen, at lower frequencies the model's time delays are too low. The scale height was reduced to $H_s = 40$ km, and the maximum height was increased to $h_m = 350$; model F resulted. The time delay at the MUF was 7.0 msec, which was much too high, even for records at later times of the day. The scale height was increased to 65, and model G resulted; unfortunately, the MUF T_D was still too high.

It was noted, however, that when the scale height is decreased, the ionization becomes more concentrated at heights near h_m, which raises the T_D's at the lower frequencies. Therefore, h_m was returned to 300 km, and H_s was left at 65 km; model D resulted. When this model's MUF was matched to Ionogram 14, a successful match was obtained. K_f was found to be 0.640, and the new model is given the number D1, where it differs from model D by its maximum density, $N_o' = K_f^2 N_o = 4.09(10)^5$.

It was also noted that Ionogram 15 gave time delays somewhat higher at lower frequencies; however, the T_D at its 1F MUF was approximately the same as that of Ionogram 14. Hence, h_m was left at 300 km, and H_s was lowered to 40 km; model C resulted, whose MUF was scaled to Ionogram 15 with $K_f = 0.622$. This yielded model C1, with its $N_o' = K_f^2 N_o = 3.87(10)^5$.

Third, note that the MUF T_D's are somewhat lower at earlier times of the day, as in Ionograms 9 through 13. Therefore, since it was apparent that the drop in MUF T_D could be realized by lowering h_m, the height of maximum ionization was dropped to 270 km. Two values of H_s, 30 and 40 km, were tried, and models A and B resulted. Model A yielded too high time delays at lower frequencies. Model B, however, through proper adjustment of the frequency scale, gave good matches to the 1F traces of Ionograms 9, 12, and 13. The results were

Ionogram 9, $K_f = 0.816$, $N_o' = 6.65(10)^5$---model B1

Ionogram 12, $K_f = 0.705$, $N_o' = 4.96(10)^5$---model B2

Ionogram 13, $K_f = 0.654$, $N_o' = 4.27(10)^5$---model B3.

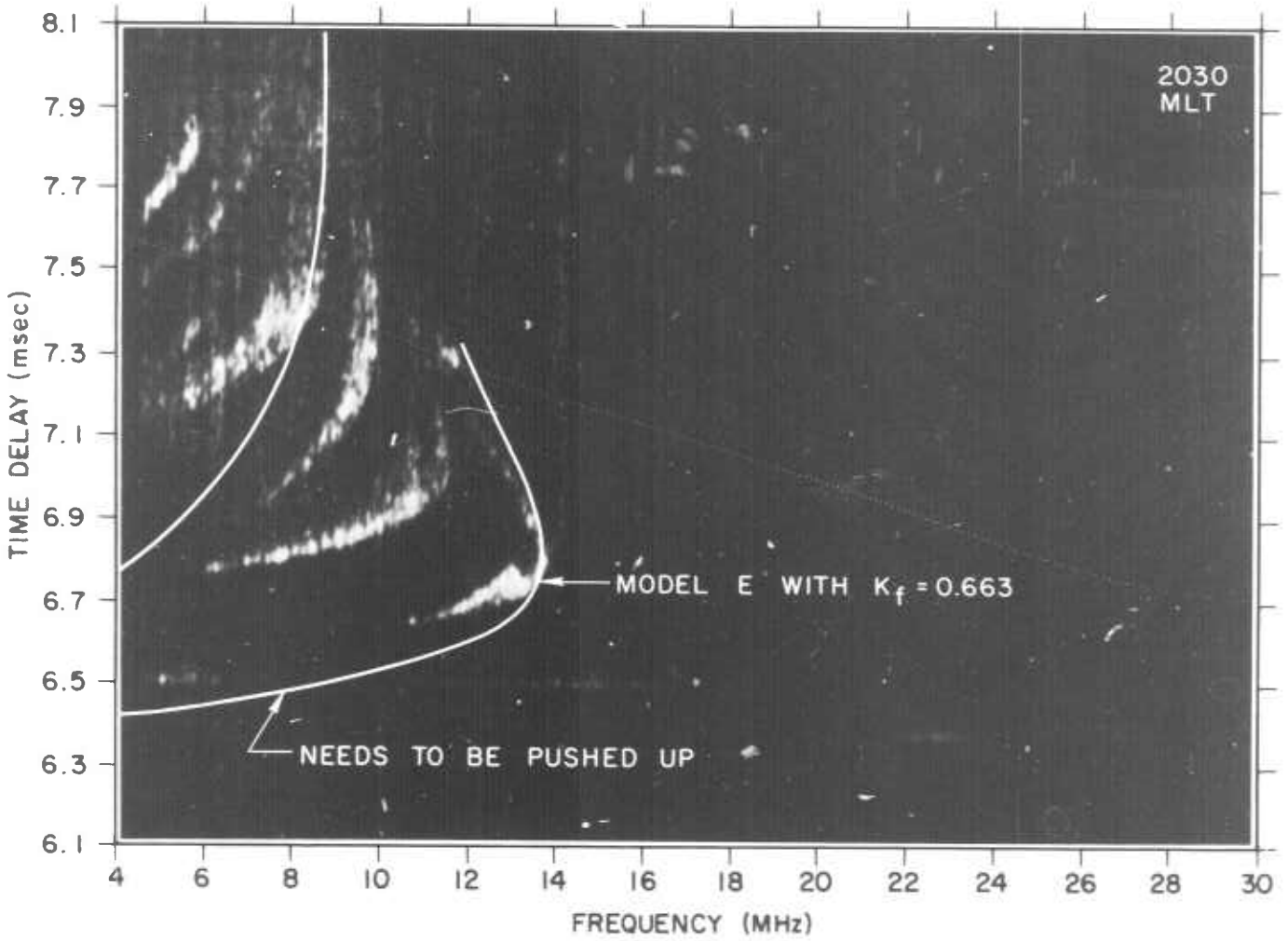

Fig. 40. EXAMPLE OF IONOGRAM MODEL MATCHING. Poor match--Ionogram 14 is matched to model E with K_f = 0.663.

The five models, B1, B2, B3, D1, and C1, are plotted in Figs. 41 and 42. Note the change in the F-layer ionosphere as the day progresses.

C. Including the E_s-Layer: Generation of Multi-Modes

For Ionograms 12 through 15, an E_s-layer height of 117 km was employed in the programs used to generate the multi-modes. For Ionogram 9, an E_s height of 105 km gave a much closer match. The effect of varying this height may be seen in Chapter VII, Error Analysis. The results are shown in Figs. 43-47. They are discussed individually below.

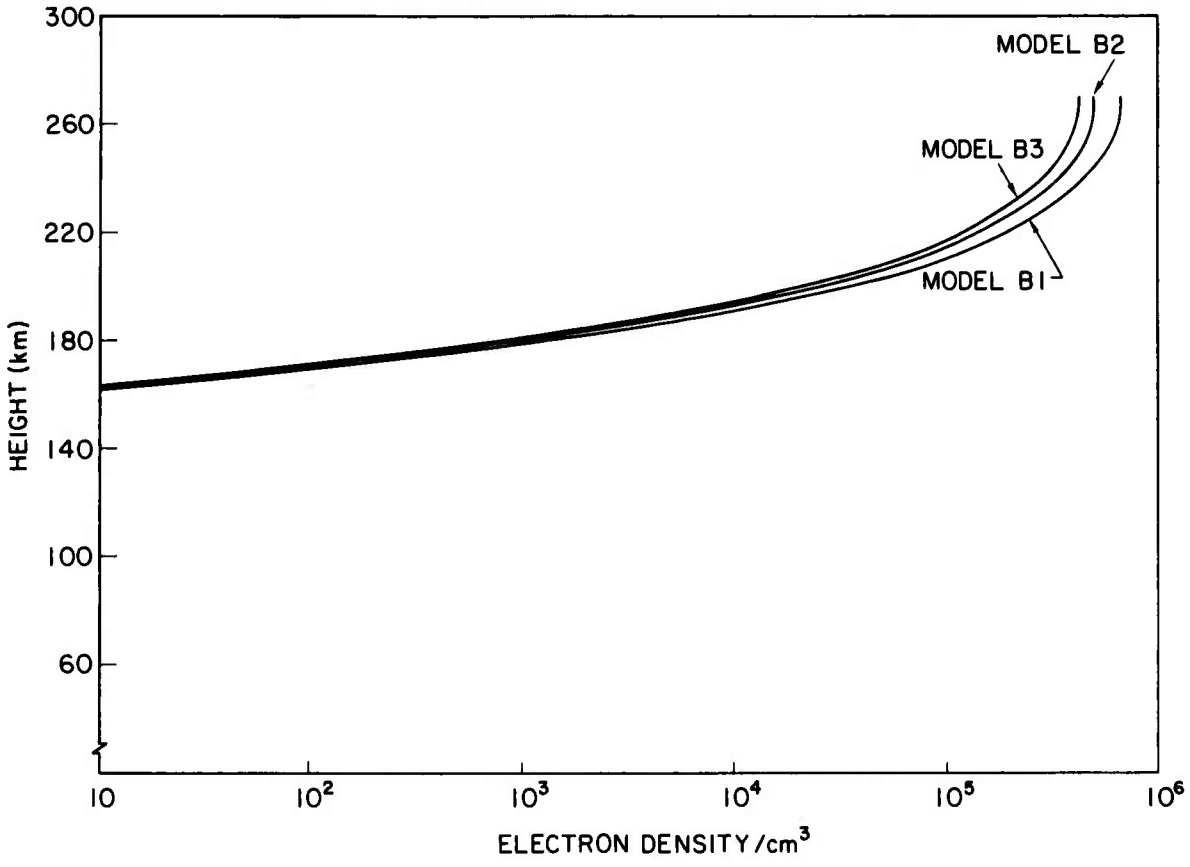

Fig. 41. PROFILES OF IONOSPHERIC MODELS USED: MODELS B1, B2, AND B3.

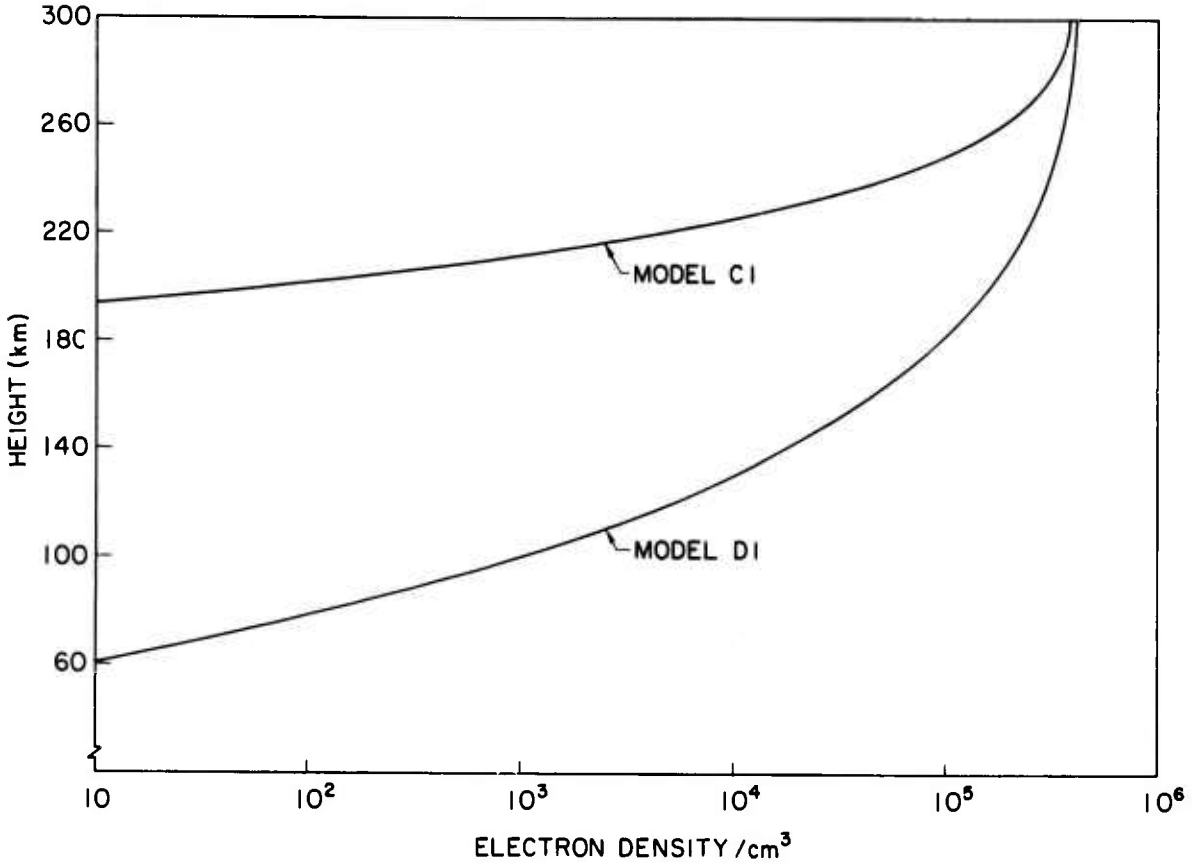

Fig. 42. PROFILES OF IONOSPHERIC MODELS USED: MODELS D1 AND C1.

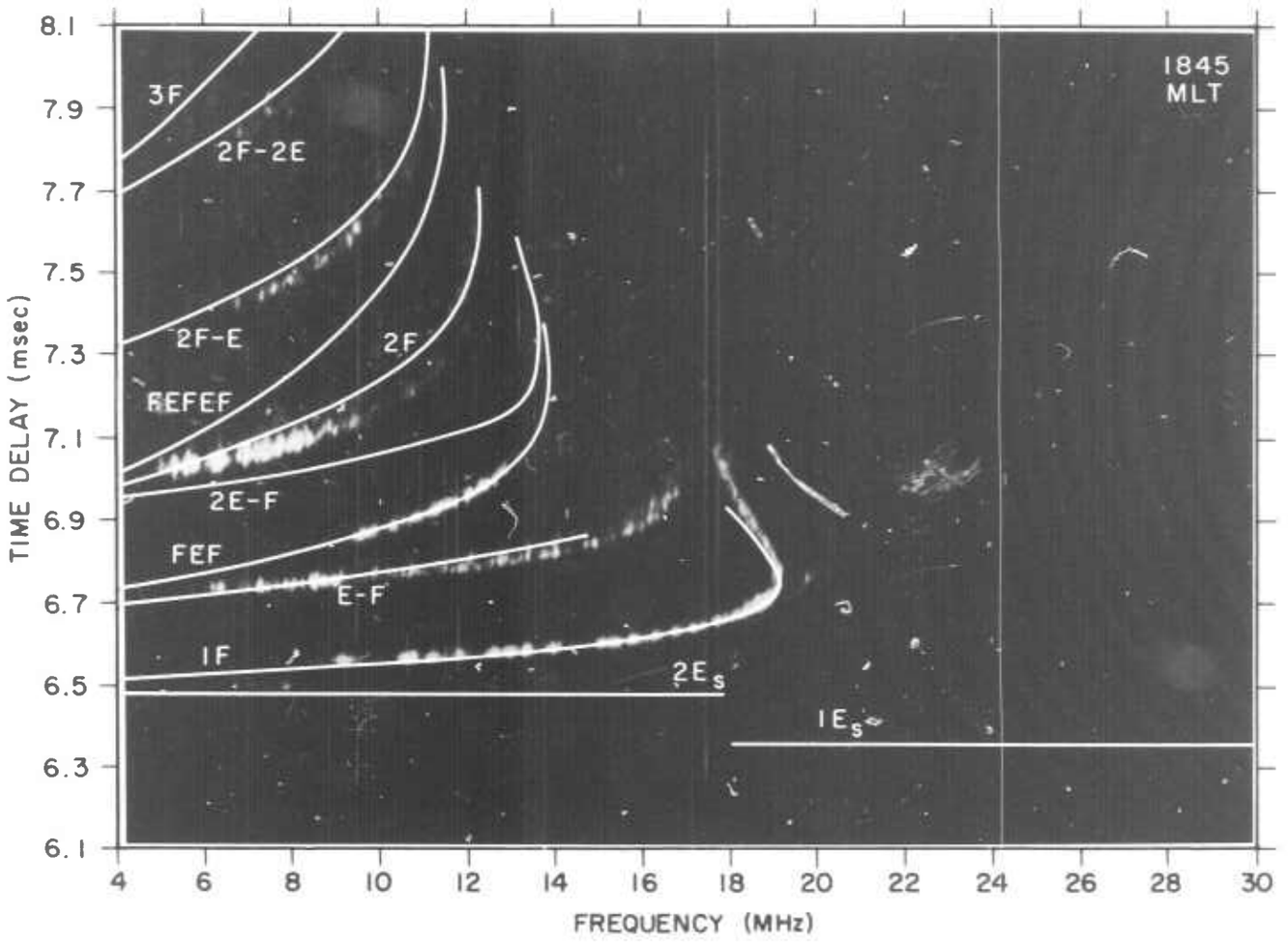

Fig. 43. RESULTS OF IONOGRAM MATCHES: IONOGRAM 9, MODEL B1.

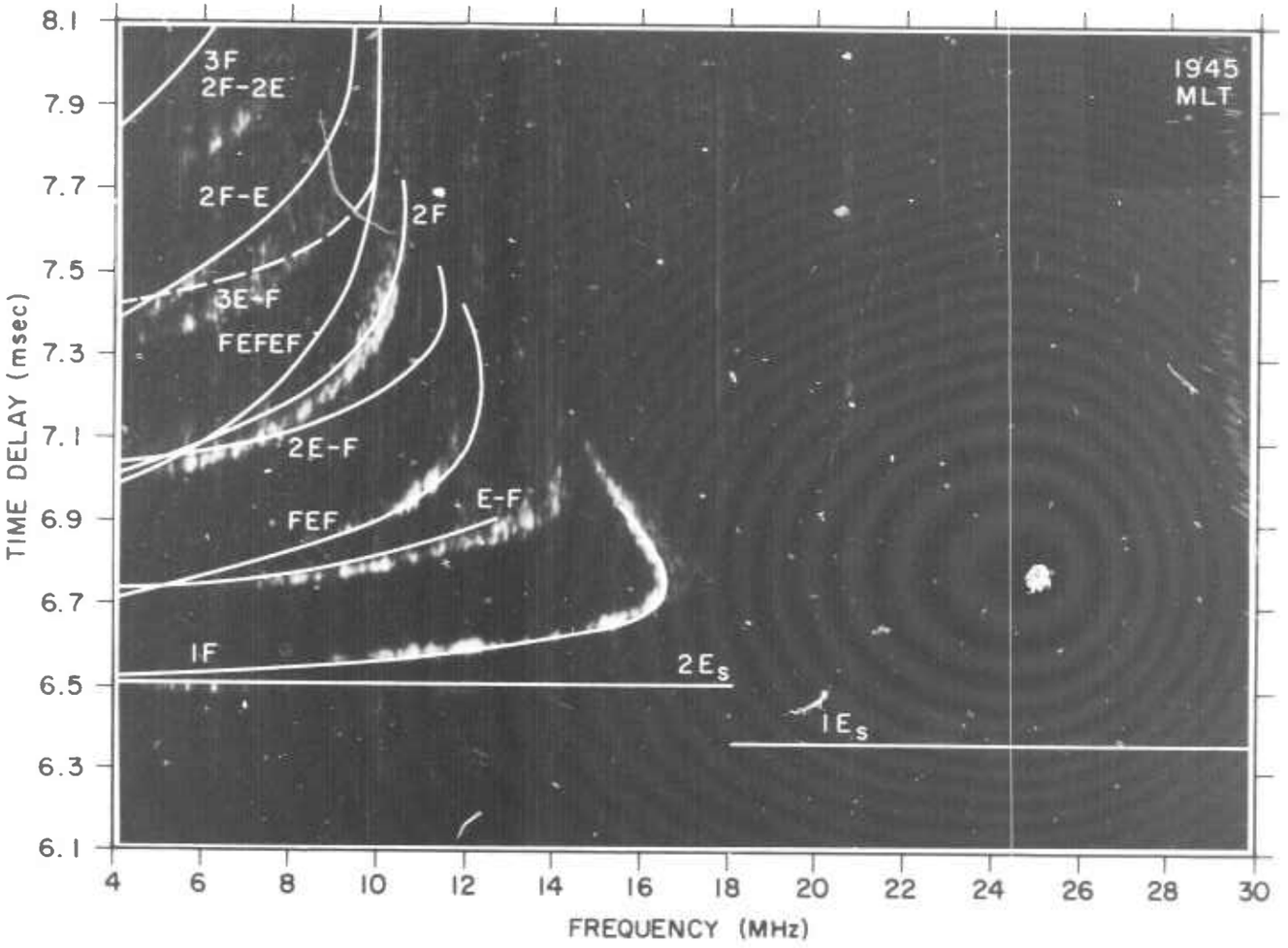

Fig. 44. RESULTS OF IONOGRAM MATCHES: IONOGRAM 12, MODEL B2.

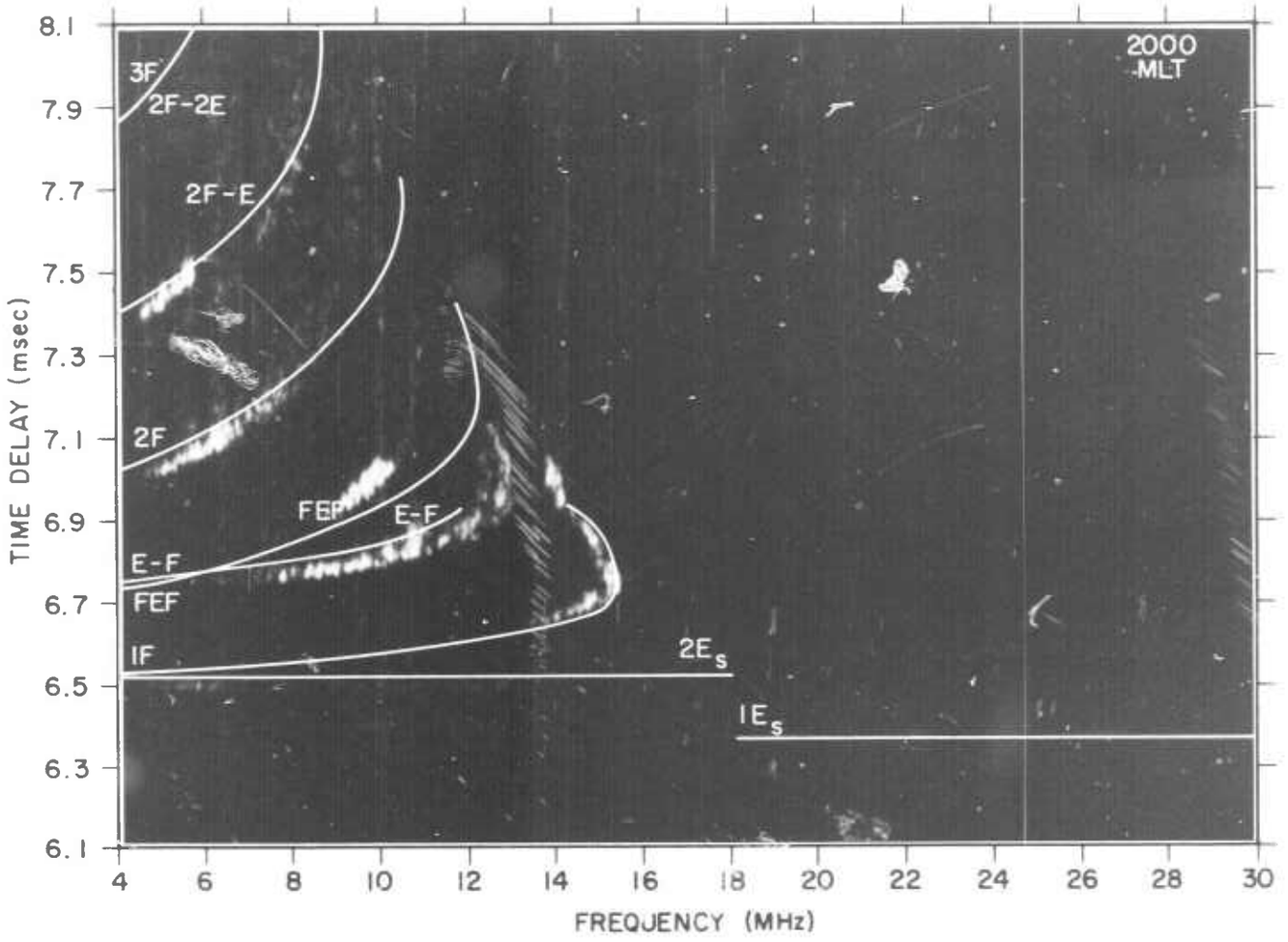

Fig. 45 . RESULTS OF IONOGRAM MATCHES: IONOGRAM 13, MODEL B3.

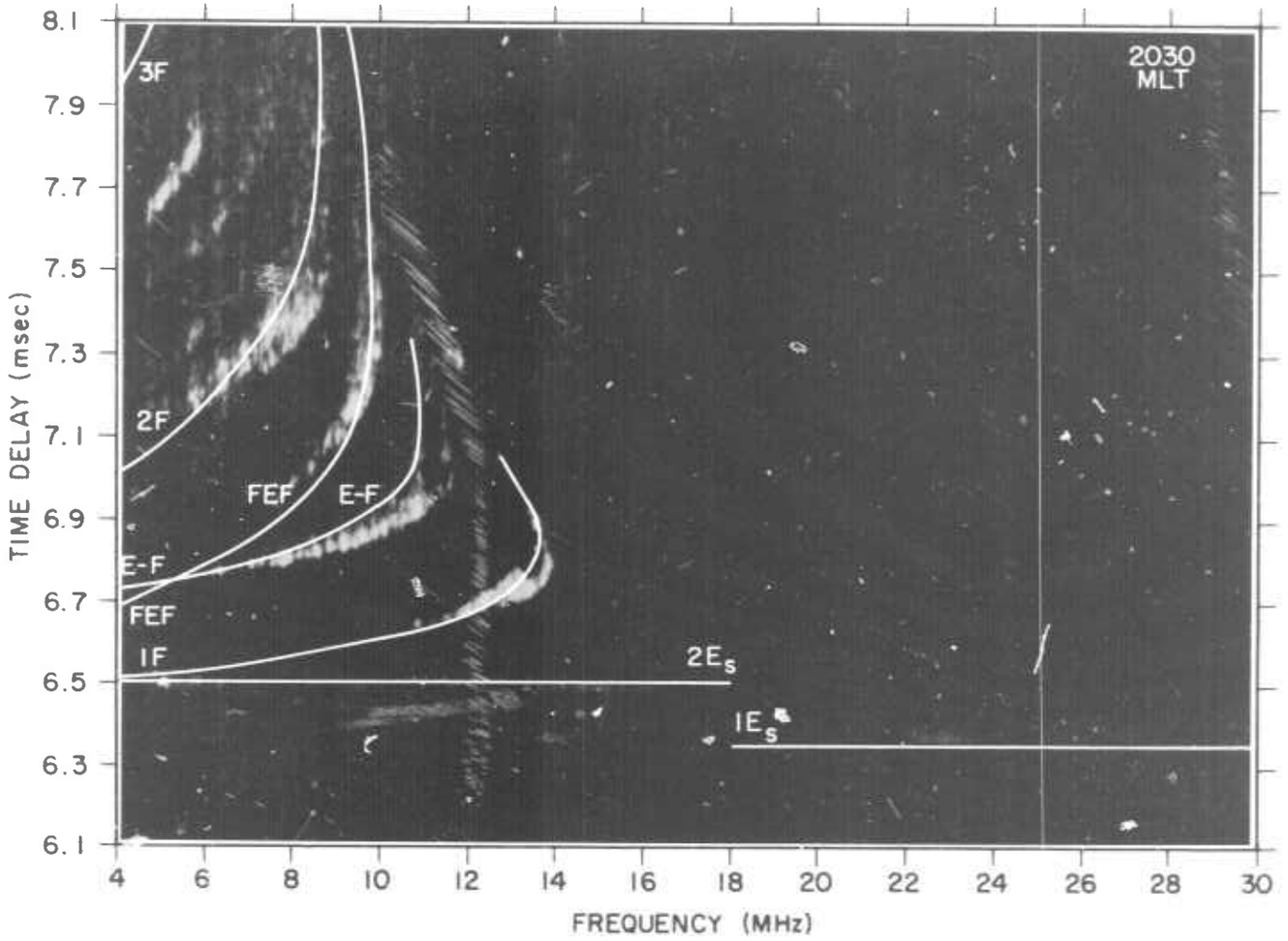

Fig. 46. RESULTS OF IONOGRAM MATCHES: IONOGRAM 14, MODEL D1.

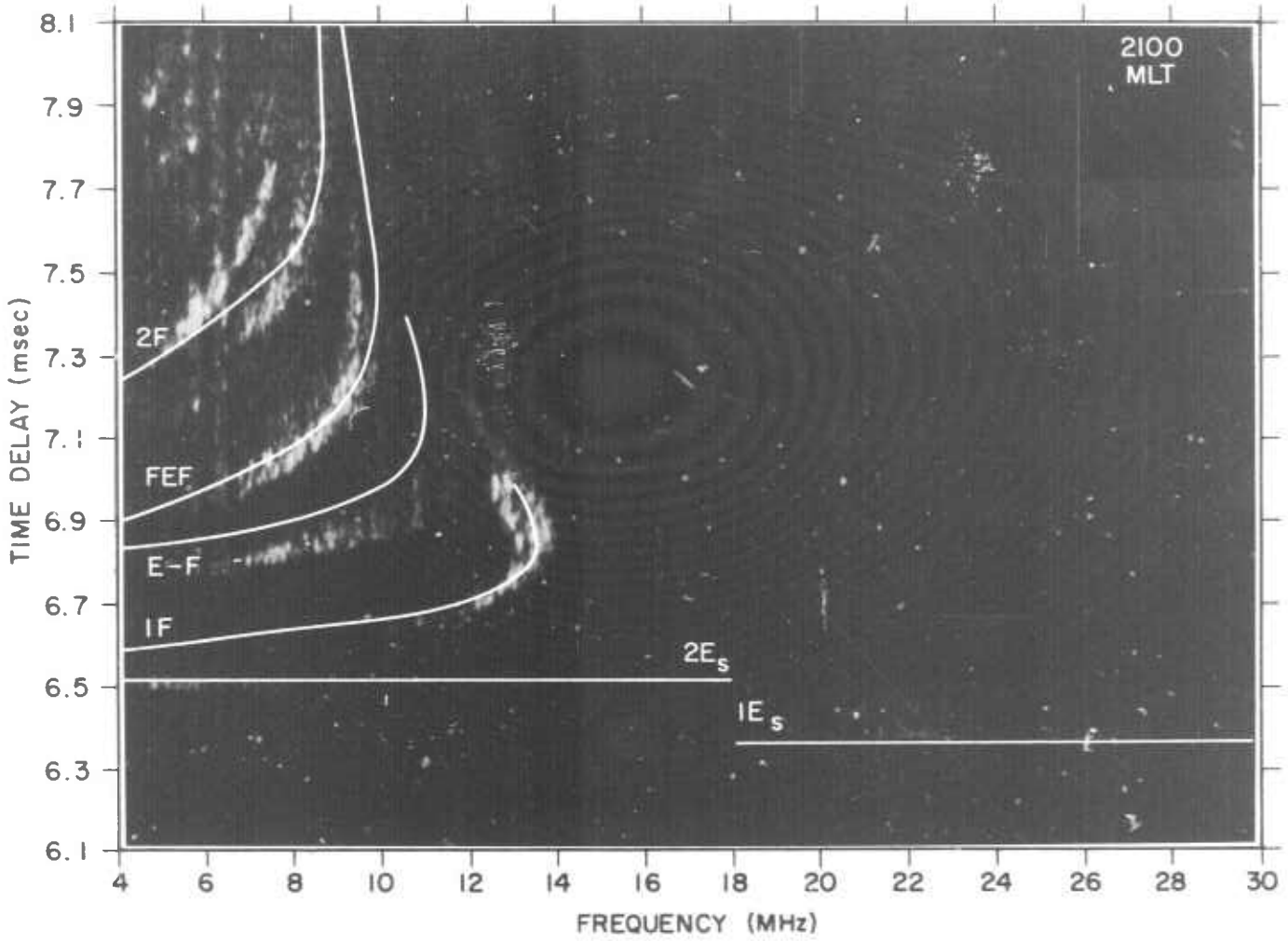

Fig. 47. RESULTS OF IONOGRAM MATCHES: IONOGRAM 15, MODEL C1.

D. Observations

1. Ionogram 9: 1845 MLT (Fig. 43)

This was the best match obtained. As seen, modes 1F, E-F, FEF, 2F-E, and 2F-2E are clearly explained. However, it is not clear what occurred near the 2F mode. For frequencies below about 11 MHz, it appears that a 2F or FEF-E mode is present. At 11 MHz, a peculiar splitting of the mode suggests that both 2F and FEF-E are present; 2F is the most probable, since we are not sure about the extent of the E_s-layer. Therefore, the trace at the lower frequencies is probably 2F, while the trace above 11 MHz is probably FEF-E. Furthermore, note that, if the FEF portion of the latter mode occurred at the east end of the path, its higher time delays would be explained because the electron density for the two F hops would be slightly lower than for the 2F mode. (The subject of tilts is discussed later.)

As noted, an E_s height of 105 km was employed in this model. Reference to Fig. 35 does not suggest this height. However, when 117 km was used, there was a fairly large discrepancy between the model and the record trace. As mentioned in Chapter IV-A, a small E_s patch at a lower height may have occurred somewhere along the path; or an error in time-delay calibration on the experimental records caused an error in the estimation of E_s virtual heights.

2. Ionogram 12: 1945 MLT (Fig. 44)

This was also a fairly good match. The modes 1F, E-F, FEF, and, seemingly, 2F-E are explained. The occurrence and splitting of the modes 2F and FEF-E are also apparent.

The group of modes around 2F-2E could very well be modes such as F-E-F-E and 2E-2F (as mentioned in Chapter III) which have the same model, but which see slightly different ionospheres in ray travel. Because it is even possible that 3E-F was present in this group, this mode is dotted-in for reference; however, it is not probable, since $3E_s$ was not evident on the records.

3. Ionogram 13: 2000 MLT (Fig. 45)

This was not a very exceptional match; nevertheless, we may still identify the 1F, 2F, E-F, and FEF modes. It seems also clear that the 2F-E mode was present. We note that $1E_s$ and $2E_s$ are becoming more pronounced in this and the following records.

4. Ionogram 14: 2030 MLT (Fig. 46)

Modes 1F, E-F, and FEF are clearly identifiable. Modes 2F and/or FEF-E also appear with 2F again the most probable.

5. Ionogram 15: 2100 MLT (Fig. 47)

Although this was a poor match, we may still label the 1F, E-F, and FEF modes. Because of the model/experiment discrepancy for 1F, we may identify 2F as the major trace just above the FEF mode, since the model gives time delays too high at the lower frequencies.

Note some general characteristics that occur on each model ionogram with respect to

(1) the general location of the modes with respect to 1F, 2F, and 3F traces (see Chapter VI);

(2) the extent of the upper ray into higher time delays, which is determined by the distribution of ionization near the maximum density;

(3) the fact that if the upper ray of the 1F trace were extended to higher time delays, to the top of the record, and if no tilts were present, all mode traces would appear to the left, and above, the 1F trace--except the $1E_s$ and $2E_s$ modes, which do not depend on the F-layer.

To measure the effectiveness of the aforementioned model-comparison technique, a simpler model was used to predict the FEF and E-F mode structure. Both the E_s- and F-layers were assumed to be copper sheets--the mirror analogy; additionally, the E_s-layer was allowed to transmit part of the energy incident upon it, so that it was nonblanketing.

The E_s-layer was assumed to be 117 km high; the height of the F-layer was varied. Curved-earth geometry was assumed, and the appropriate formulas were programmed into a digital computer to calculate the time delay and F-layer virtual height which would support propagation of a particular mode at a given take-off angle. A similar analysis was conducted by Bowhill [Ref. 24] in 1961. The formulas used are as follows:

The take-off angle β is specified; then

$$D_E = 2R\left[\cos^{-1}\left(\frac{\cos\beta}{1 + h'_E/R}\right) - \beta\right] \quad \text{as before,}$$

where

$$R = 6370 \text{ km},$$
$$h'_E = 117 \text{ km}.$$

Also

$$D_F = (P_1 \times D_o + P_2 \times D_E)/P_3 ,$$

where for each mode, P_1, P_2, and P_3 are defined by the corresponding equation for D_F appearing in Table 3.

Then

$$h'_F = R\left[\frac{\cos\beta}{\cos\left(\frac{D_F}{2R} + \beta\right)} - 1\right] \quad \text{km}$$

$$T_E = \frac{1}{150}\sqrt{2R(R + h'_E)\left[1 - \cos\left(\frac{D_E}{2R}\right)\right] + h'^2_E} \quad \text{msec},$$

$$T_F = \frac{1}{150}\sqrt{2R(R + h'_F)\left[1 - \cos\left(\frac{D_F}{2R}\right)\right] + h'^2_F} \quad \text{msec},$$

$$T_D = Q_1 \times T_F + Q_2 \times T_E \quad \text{msec},$$

where Q_1 and Q_2 are specified for each mode according to the T_D equations in Table 3. The time delays vs F-layer virtual height were plotted as shown in Fig. 48.

To predict the time delays at which a particular mode would occur, it was necessary first to choose a frequency, and then to estimate the average virtual height for the F-layer, from the 1F and 2F modes, according to Fig. 48. We note that the 2F virtual height will be greater than

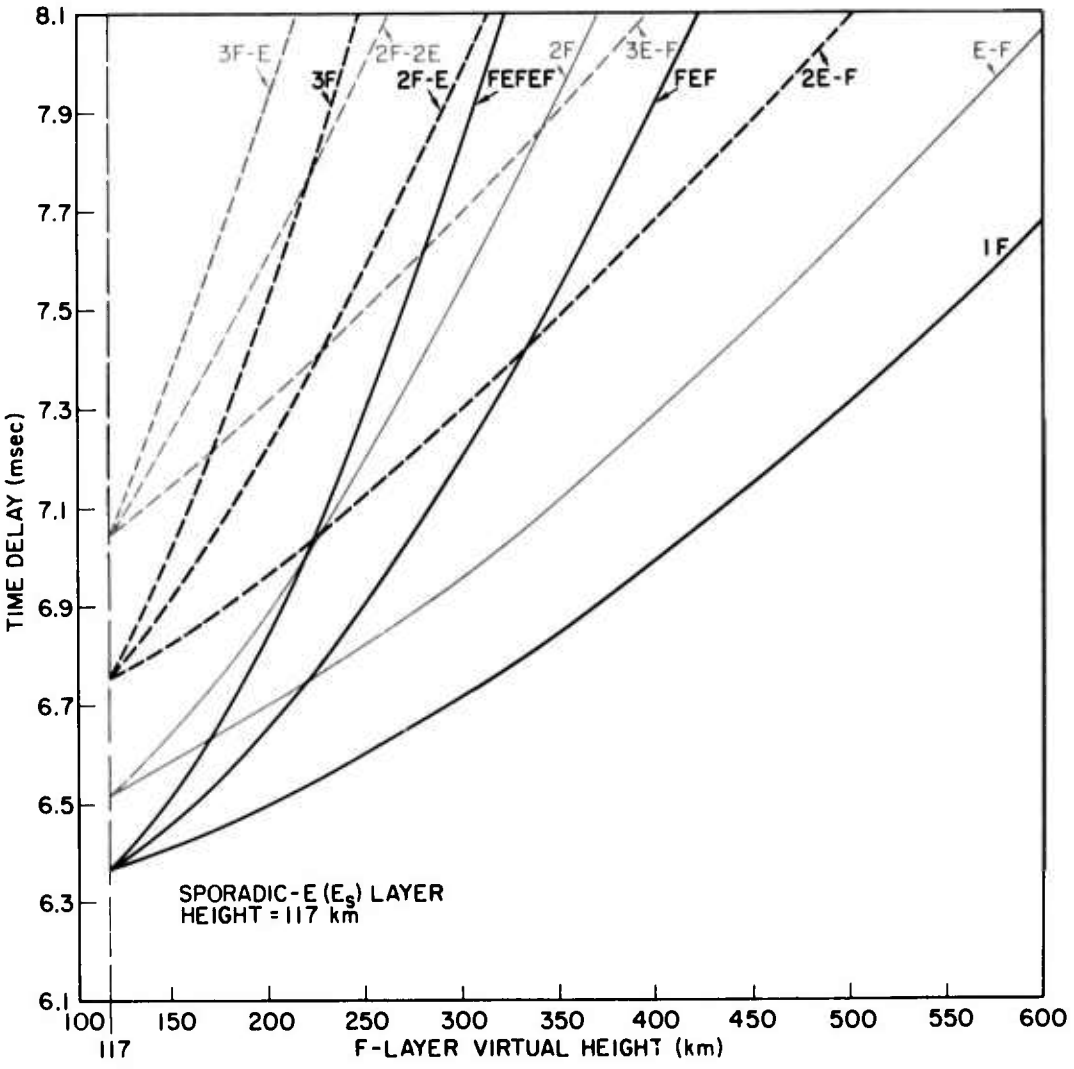

Fig. 48. TIME DELAY VS F-LAYER VIRTUAL HEIGHT FOR SEVERAL MODES--MIRROR-ANALOGY MODEL.

the 1F virtual height, since in the latter case the wave does not approach the layer from as steep an angle. Table 4 lists these results.

Table 4

1F AND 2F VIRTUAL HEIGHTS (h'_F) FOR EACH IONOGRAM AT SPECIFIC FREQUENCIES

Ionogram	Frequency (MHz)	T_D-1F (msec)	T_D-2F (msec)	h'_F-1F (km)	h'_F-2F (km)	h'_F(avg) (km)
9	9	6.57	7.13	237	238	238
12	9	6.58	7.23	240	253	247
13	8	6.56	7.25	232	257	245
14	7	6.54	7.30	221	264	243
15	7	6.60	7.44	250	284	267

The F-layer virtual heights were then used to predict time delays for the FEF and E-F modes. Also, at the frequencies specified for each ionogram, the time delays for the two modes (FEF and E-F) appearing between the 1F and 2F modes were recorded. The results appear in Table 5.

Table 5

COMPARISON OF MIRROR-ANALOGY MODEL AND EXPERIMENTAL IONOGRAM TIME DELAYS AT SPECIFIC FREQUENCIES OF TABLE 4, USING h'_f(average)

Ionogram	Frequency (MHz)	T_D E-F (msec)		T_D FEF (msec)	
		Calculated	Observed	Calculated	Observed
9	9	6.79	6.77	6.84	6.85
12	9	6.82	6.78	6.89	6.87
13	8	6.84	6.78	6.88	6.87
14	7	6.80	6.80	6.87	6.91
15	7	6.87	6.80	7.00	7.00

It is clear from the aforementioned model predictions that, at the frequencies considered, the lower of the time delays observed correspond to the E-F mode. This fact is also predicted by the simpler model, as seen in Table 5. It is probably most reasonable to consider the average calculated time delays, since the virtual height of the F-layer that supports propagation of the E-F and FEF modes must lie somewhere between the 1F and 2F virtual heights. This may be easily seen by noting that the equivalent F-hop distance, D_F, is always greater than $\frac{1}{2}D_O$, but less than D_O, for both modes, for all virtual heights above 117 km. (A longer D_F results in a lower virtual height.)

All but Ionogram 14 have given FEF predictions within 0.02 msec, and Ionogram 14 gives it within 0.04 msec. The predictions for the E-F mode are almost as accurate: within less than 0.04 msec for Ionograms 9, 12, and 14, less than 0.06 msec for Ionogram 13, and less than 0.07 msec for Ionogram 15.

This comparison gives further justification to the computer-modeling procedure, and could even be used as a rough estimation of mode structure, when only a good guess at the type of mode is needed.

The presentation of Fig. 48 looks quite similar to an oblique ionogram, with the frequency scale replaced by F-layer virtual height. The similarity lies in the fact that for higher frequencies, the virtual height of reflection does go up, because refraction by the ionosphere is less pronounced at these higher frequencies. The exact relationship between virtual height and frequency will depend on the electron profile over the path (or the model assumed).

Figure 48, probably one of the most significant in the report, shows in a general way how modes are likely to be placed in relationship to each other, especially when a single F-layer is present. The similarity may be seen through comparison with the model-matches done previously. Note in particular the FEF and E-F modes of Fig. 46. The modes cross at about 5.3 MHz, with the E-F mode remaining the lower after the cross-over. Exactly the same effect occurs in Fig. 48, where the cross-over occurs at h'_F = 220 km. The time delay at the cross-over is the same for both models--6.76 msec. Reference to the models in Figs. 44 and 45

shows the same cross-over. In Figs. 43 and 47, the cross-over occurs at a much lower frequency, if at all; the E-F mode is still the lower of the two. Precisely the same effect is noted for the 2E-F, 2F, and FEFEF combination in Figs. 43 and 44, when compared again with Fig. 48.

The simple model predictions of Fig. 48--or curve sets like it for different ranges and E_s heights--should provide a valuable tool for deducing the types and positions of modes. On a long path, and especially if severe tilts occur, the simple model could prove to be entirely inadequate; however, a relatively good "guess" is still possible.

Various possible errors can occur within the mode-matching or predicting analysis. Basically, we are comparing the traces on the experimental data with calculated or synthesized traces from a model. The following problems could exist:

(1) Noisy data: ground forward scatter, spread-F (if present), Faraday-rotation-with-frequency blobs (Ref. 25), blanketing that causes cut-off at lower frequencies, excessive interference from broadcast stations, and other interference.

(2) Time-delay error and smearing of traces due to propagation of waves through a blobby E_s-layer--poor resolution.

(3) Improper calibration of data time-delay scales.

(4) Misalignment of time-delay scales and broadening of ticks due to photograph scale expansion--poor resolution.

(5) Inadequate model for F and E_s layers. Most of the error in the latter is attributable to errors in measurement of virtual height.

The errors due to (1) and (2) are very difficult to discuss quantitatively. Those due to (3) are assumed not to exist, although such errors could explain why a lower-than-expected E_s height gave a better match in Ionogram 9, and would probably also yield closer matches in the other ionograms. The inaccuracies caused by (4) were minimized by care in data reproduction and model-experiment scale-matching. The errors due to (5) are probably the greatest, and may be discussed quantitatively.

The F-layer model could be modified to any desired extent. A parabolic layer might be tried; it has given good matches. Extra electrons could be substituted into any model on a trial-and-error basis to match to the 1F and 2F traces more closely. This is a very slow process, although the technique could be improved by having the computer do all the interpolation procedures, etc., so that, given inputs of distance, E_s-layer height, earth radius, F-layer model, and type of mode desired, an ionogram output is produced. One could also tell the computer what the desired MUF is, and it would modify the frequency scale accordingly. A most extravagant idea would be to devise a self-adapting program to

match to any desired accuracy.

To estimate the error in time delay due to an error in E_s-layer height, ionosphere model A (Table 2) was used in the calculations of 1F, 2F, E-F, FEF, 2E-F, and FEFEF modes. Heights of 105, 117, and 124 km were used to produce 3 ionogram sets, as shown in Figs. 49-51. Comparison of the figures is self-explanatory. An example of the uncertainty in time delay may be calculated at 11 MHz for the FEF mode, where the time delay for E_s-layer heights of 105, 117, and 124 km are 6.90, 6.87, and 6.84 msec, respectively. If a height of 117 km is assumed (as it was), then an error of 0.03 msec will occur if the height is actually 105 or 124 km. This T_D error is of the same order obtained with the simplified model, and is also of similar order to that observed in the Chapman model-matching. Note that over the day of measurement, the E_s-layer height varied between 107 and 124 km.

There are also some approximation errors in the calculations due to the linear interpolation done in the computer; however, these are of no great significance compared with the resolution obtained in the data of Figs. 1-24, which are limited by factors of equipment and data reproduction.

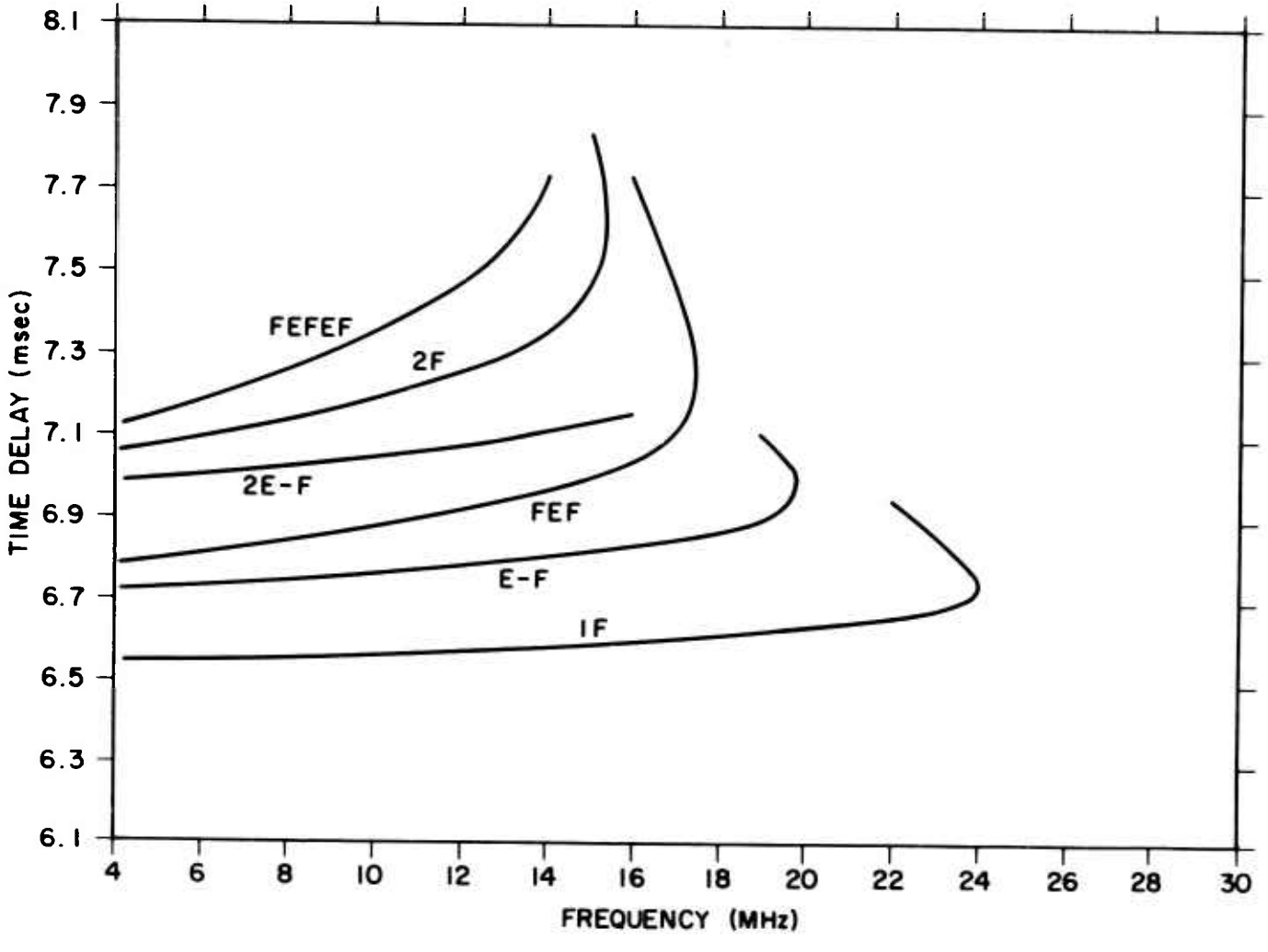

Fig. 49. ERROR ESTIMATE: MODEL IONOGRAMS FOR SPORADIC-E HEIGHTS OF 105 KM.

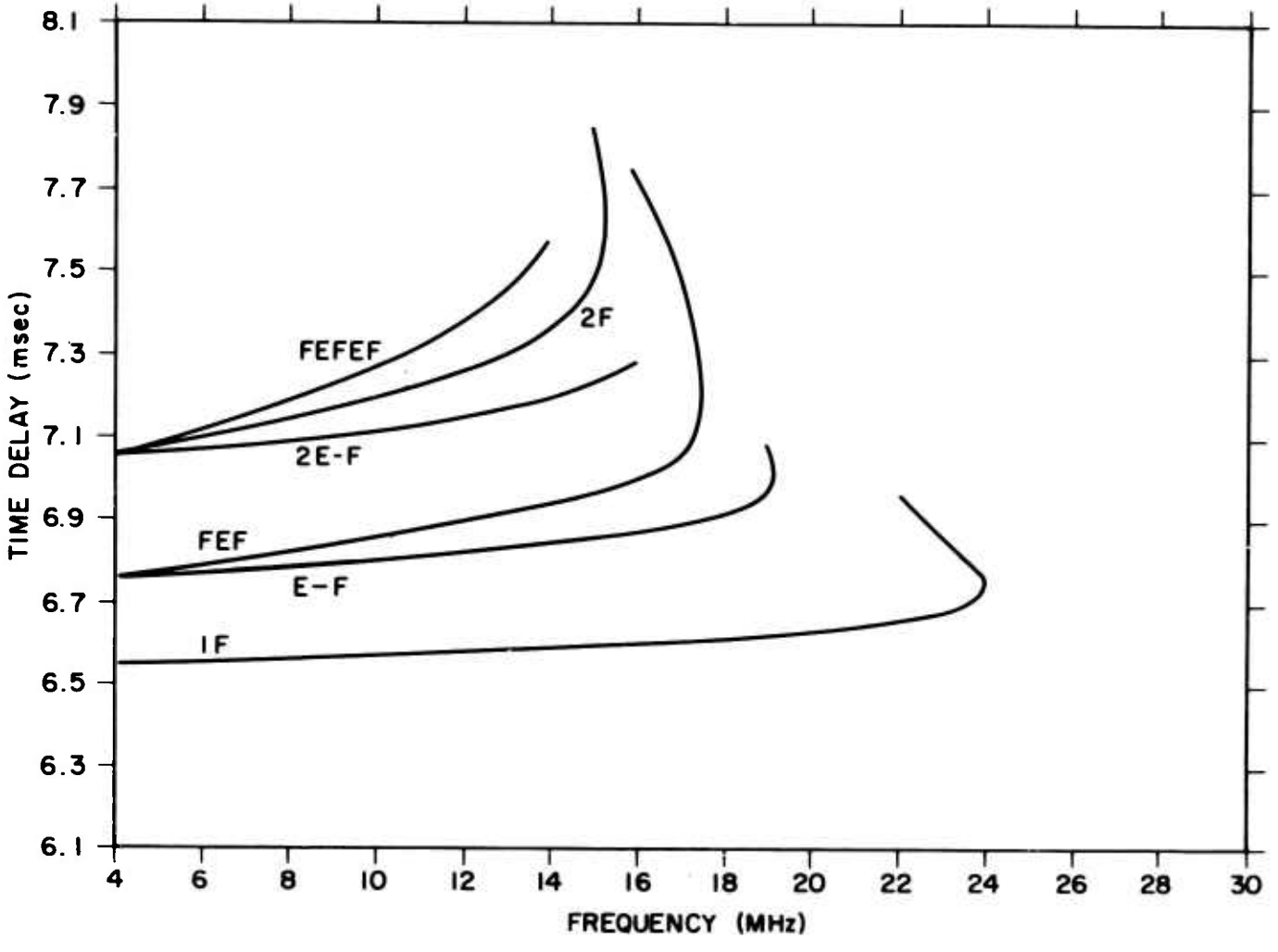

Fig. 50. ERROR ESTIMATE: MODEL IONOGRAMS FOR SPORADIC-E HEIGHTS OF 117 KM.

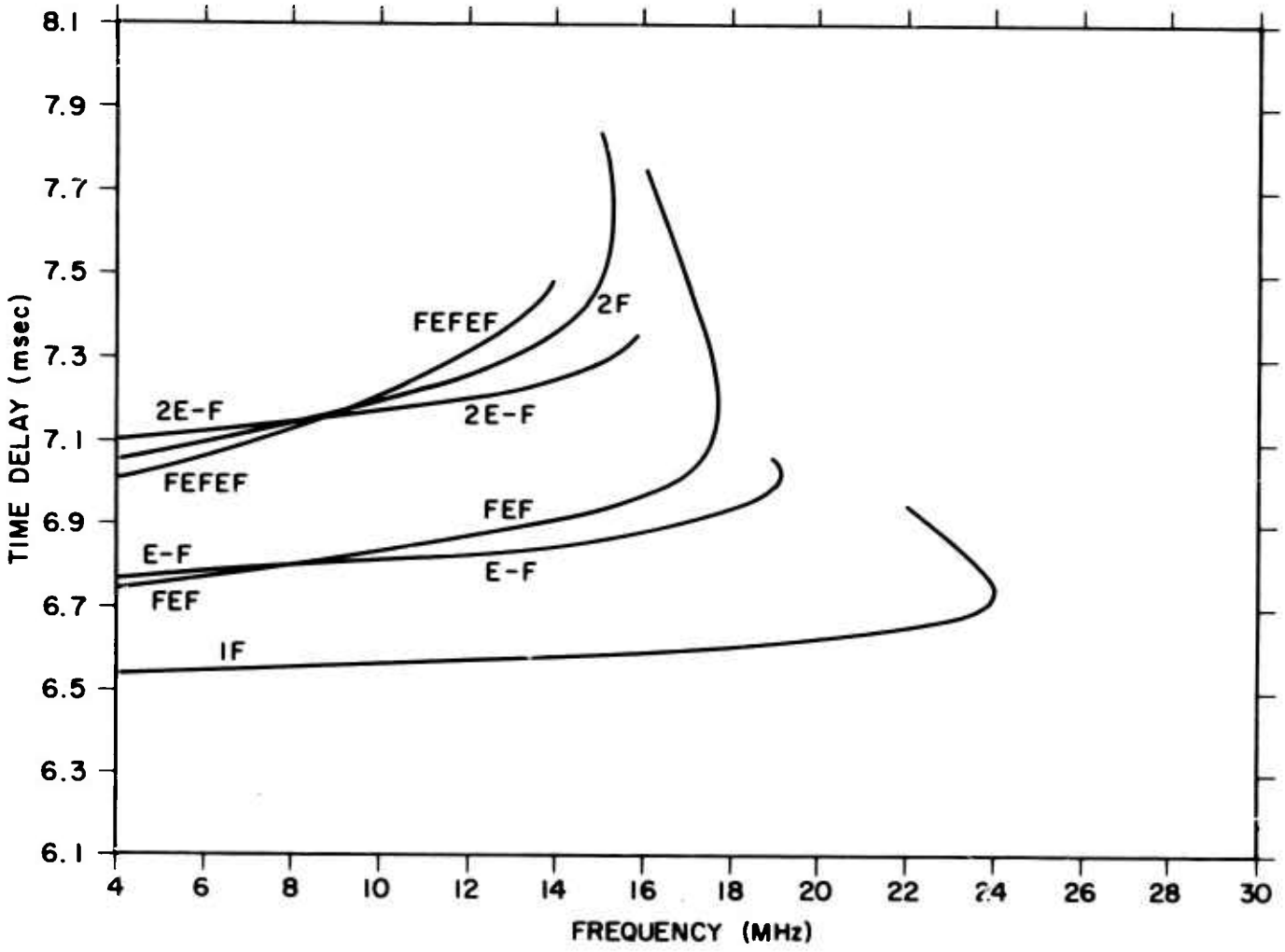

Fig. 51. ERROR ESTIMATE: MODEL IONOGRAMS FOR SPORADIC-E HEIGHTS OF 124 KM.

VIII TILTS IN ELECTRON DENSITY: MODELING SUGGESTIONS

It is highly probable that the electron density profile was not at all times constant over the E-W path between Stanford and Lubbock, since the sun's zenith angle was different over the path.

Because each mode propagates through different sections of the ionosphere, a simple laterally constant model would not be adequate to explain a complete mode structure. (The simple model is, however, useful to gain a first-order understanding of the mode structure, as was done in the analysis above.)

An example of a complication that could arise is with the "N" mode. Notice that this mode can be expressed either as E-F or F-E, with the F reflection occurring at either the transmitter or receiver end of the path. If both modes propagate and a tilt exists, the τ_D for each will be different; hence, the mode will split into the E-F and F-E modes. The degree of this split will, of course, be a function of the nature and magnitude of the tilt.

Furthermore, a model that is adequate to account for the effects on one mode--say a 2F mode--will not be adequate to explain the structure of some other mode. For instance, suppose that the ionosphere that supports the 2F mode was modeled by assuming two different electron profiles over the path--one for each hop. If this model was used to explain an FEFEF mode, there would be an error in the F reflections, especially at the center of the path. However, a model consisting of three or four separate F-layers over the path might be adequate to explain the simpler modes, which involve only two or at most three F-layer reflections. Before approaching such a modeling technique, however, the nature and degree of tilt over the path must be considered.

As time progresses, the solar zenith angle changes over the path. Correspondingly, the ionosphere also changes. Therefore, a tilt over the path will, in some way, be related to the time difference over the path, as well as to the midpath time. To calculate the time difference, the coordinates of the transmission end-points must be known. These were found to be

Stanford: Latitude 37.408 degrees N
Longitude 122.183 degrees W

Lubbock: Latitude 33.600 degrees N
Longitude 101.840 degrees W.

An approximate value for the time difference between stations may be calculated from the longitude values. Given that 1 hr equals 15 degrees of longitude, there is 1.36 hr difference between stations.

The solar zenith-angle variation vs time of day for February was obtained from the Central Radio Propagation Laboratory (CRPL) Handbook 90. An average latitude of 35 degrees was assumed. The variation is plotted in Fig. 52. If the sun is not below the horizon, and if something is known about the nature of density variation with solar zenith

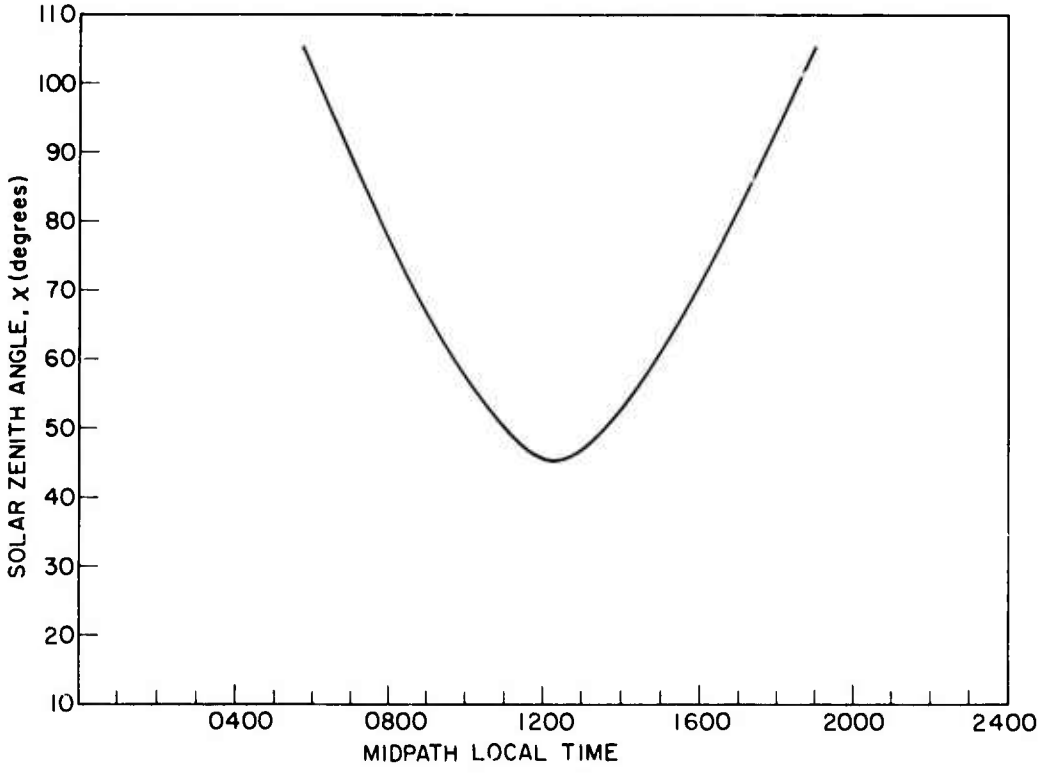

Fig. 52. SOLAR ZENITH ANGLE VS TIME OF DAY FOR FEBRUARY: LATITUDE 35 DEGREES.

angle χ, then a tilt model could be deduced. For example, the Chapman model,

$$N = N_o \exp(1 - z \sec \chi \, e^{-z}) ,$$

could be used. This model could be initially matched to the 1F trace, according to the midpath time--hence, solar zenith angle--conditions. However, in our case, the data used in the mode comparison were taken later in the day, when density conditions are primarily determined by electron-ion recombination processes. The sun was well over the horizon, and ion generation was nearly absent.

The best idea concerning the profile changes over the path can be obtained from the records themselves. By studying the properties of the 1F trace as time progresses, we obtain properties of the ionosphere located roughly over midpath, vs time of day. With some degree of accuracy, one may then assume that the ionosphere will be equivalent at a certain time anywhere along the path. Thus, a model derived for the midpath ionosphere at a specific time may be used later in the day to model the ionosphere at the point more westward along the path which has the same local time as the midpath model.

Now, the number of models needed will depend upon the degree of tilt over the path. To gain some idea of how the tilt varies with time of day, two very useful techniques may be employed with a sequence of records such as those used by the author. For means of illustration, these were tried with the sequence of 24 records in Figs. 1-24:

(1) the 1F maximum observed frequency (MOF) was plotted vs midpath local time of day, as seen in Fig. 53;

(2) the 1F virtual height of reflection was obtained from the time-delay information and plotted vs time of day for several different frequencies. A few of these plots appear in Figs. 54-56.

These two techniques, if done with sufficiently small time separation, and at enough frequencies, supply all needed information with which a

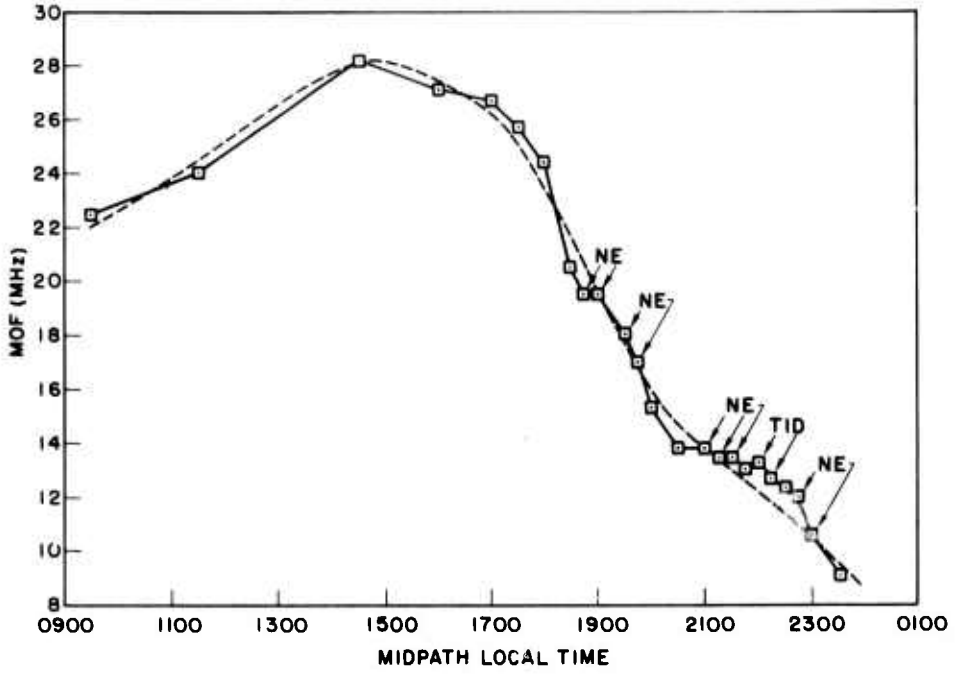

NE ≙ "Nose Extension at MOF"

TID ≙ "Traveling Ionospheric Disturbance at MOF"

Fig. 53. MOF VS TIME OF DAY FOR 1F TRACE OF FIGURES 1 THROUGH 24.

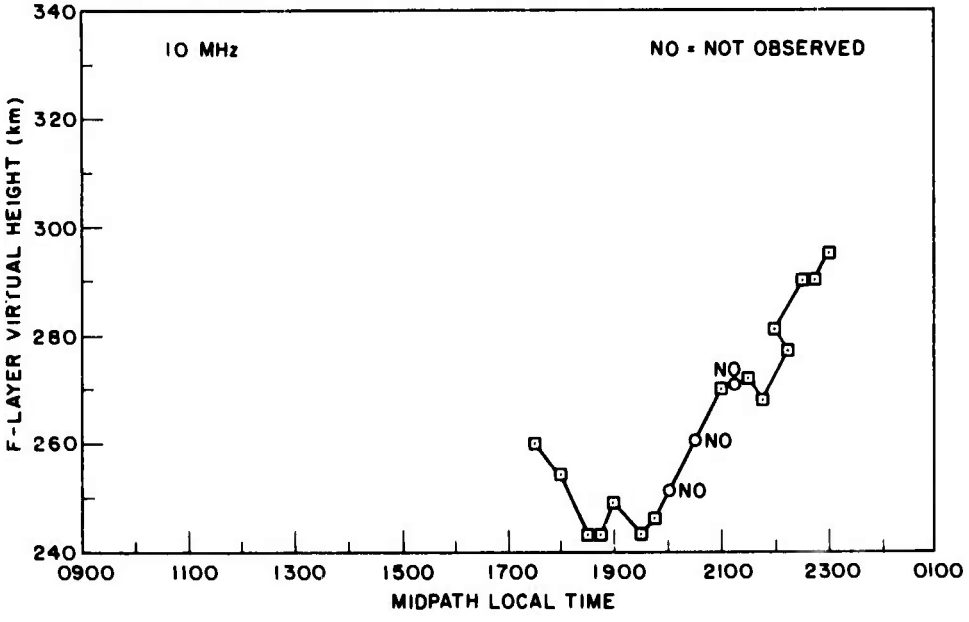

Fig. 54. F-LAYER VIRTUAL HEIGHT VS TIME OF DAY; TILT STUDY--10 MHz.

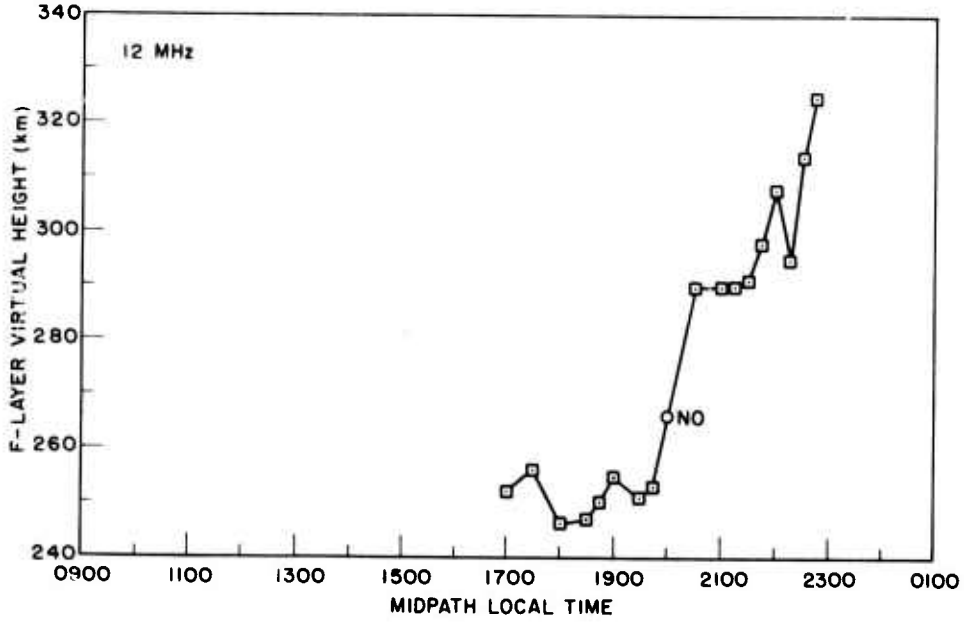

Fig. 55. F-LAYER VIRTUAL HEIGHT VS TIME OF DAY; TILT STUDY--12 MHz.

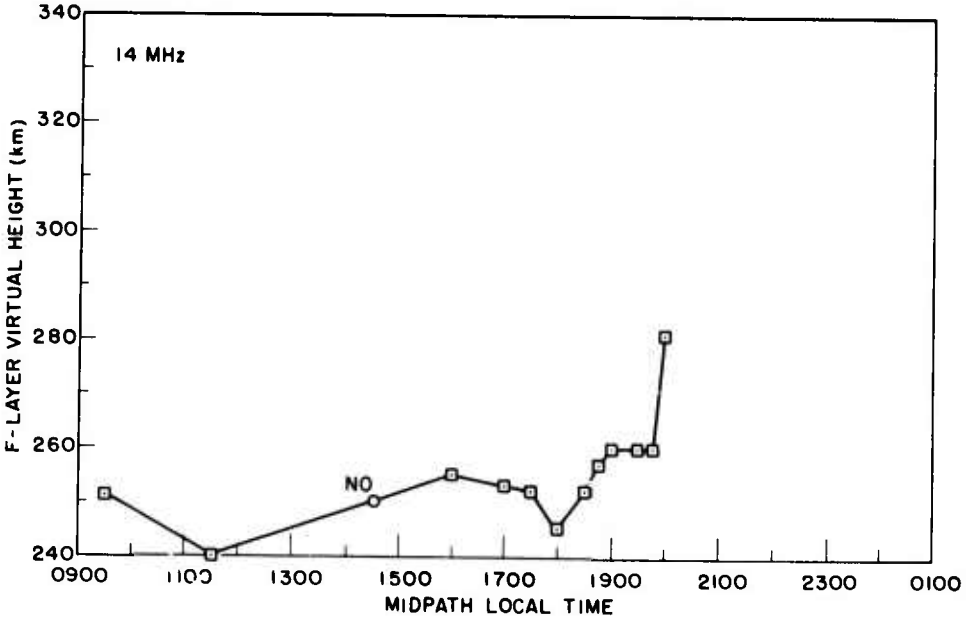

Fig. 56. F-LAYER VIRTUAL HEIGHT VS TIME OF DAY; TILT STUDY--14 MHz.

sequence of Chapman models may be derived. However, it is surely easier to obtain the models by direct experiment-model ionogram comparison, as was done earlier in this report.

At certain times of day--such as at noon--the tilts are very small, and therefore do not warrant the more complicated modeling analysis. However, later in the day, tilts should be considered, as seen in Figs. 53 and 54-56 by the steeper curve slopes.

We would need, therefore, a modified ray-tracing/interpolation procedure to accommodate the extra models. In a conference with Dr. Croft, the following ideas were suggested:

(1) A few individual models could be inserted into the computer. When the range is reached at which the ionosphere shifts to the adjacent model, the calculations proceed with the new model. Figure 57 illustrates this technique.

(2) If the scale height, H_s, and maximum height, h_m, of the Chapman model were the same over the path--such as through a sequence of records resembling Ionograms 13, 14, and 15,--the change in the maximum electron density, N_o, could be modeled by

$$N_o(\theta) = N_o\left(1 + k_1\theta + k_2\theta^2\right)$$

where

$$\theta = \frac{\text{actual range - starting range}}{1881.27 \text{ km}}$$

and k_1, k_2 are determined from the known N_o's at the starting ranges.

This provides a continuous model, and necessitates changing the ionosphere at each calculation level.* Similar work was done by Dayharsh [Ref. 9, p. 43].

---

* Suggested by T. A. Croft at Stanford University.

(3) Higher powers of θ could be used, which depends on the number of models matched along the path. This in turn determines the number of starting ranges and constants k.

If further investigation of multi-modes is to be done, the above techniques should surely be tried, as they most certainly enable a closer match to nature.

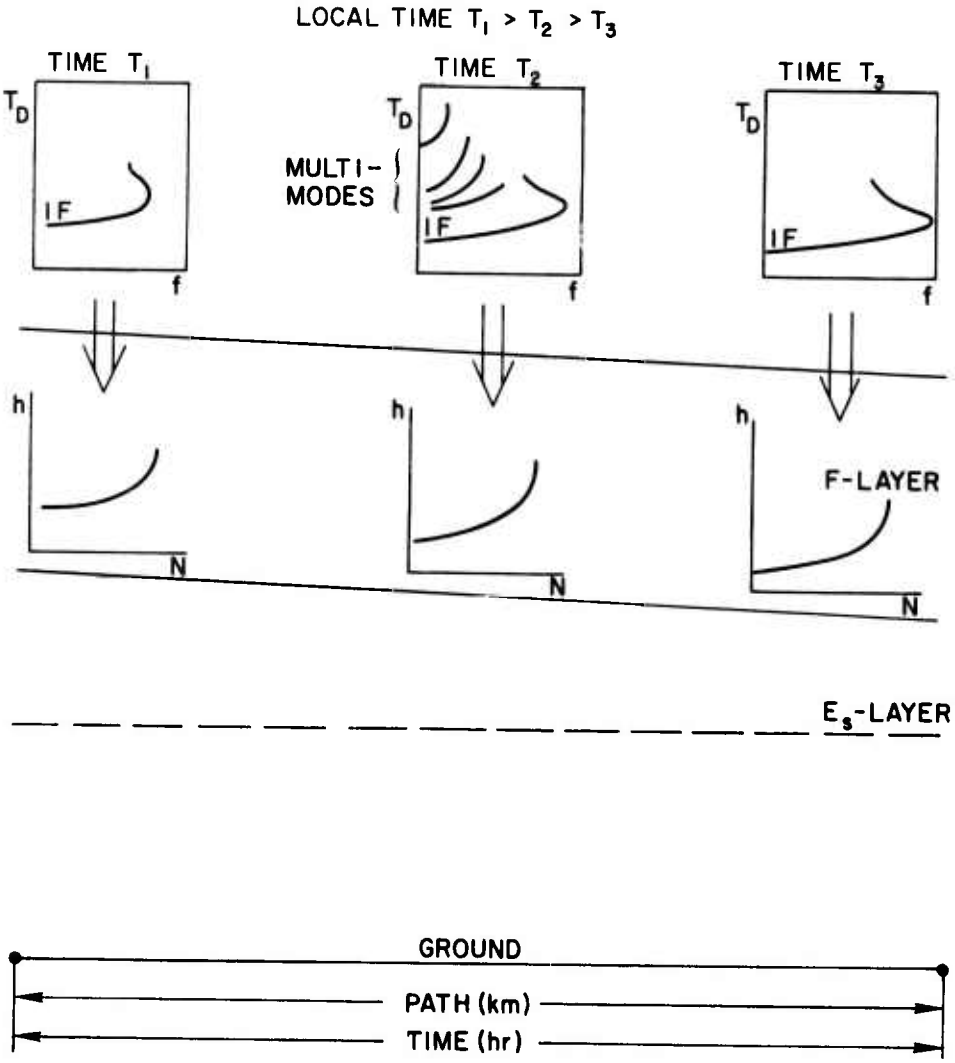

Fig. 57. SCHEMATIC DIAGRAM OF TILT-MODELING PROCEDURE USING DISCRETE MODELS. Use 1F trace to obtain computer models at a few points in time at midpath. Distribute models according to time along the path and thence synthesize multi-modes from distributed model.

Finally, as mentioned previously, tilts could severely hamper predictions based on the simple mirror analogy model, especially over long paths. This problem could be partially circumvented by examining records spaced in time over the path, and thence distributing the F-layer virtual height over the path on a proportional basis. The h'_F (virtual height) scale of Fig. 48 would then represent the F-layer virtual height at one end of the path, and other heights would be related to this height by some constant. For instance, suppose we have three separate layers, denoted by a, b, and c. We might then have: $h'_b = 1.1h'_a$, and $h'_c = 1.2h'_a$. The formulas for the simple layer could be modified to include the new layers by

(1) modifying the interpolation ranges;

(2) including more terms in the calculations of path length to take into account the different path lengths for each hop. We note that the angle of reflection at the ground and the top layers, β, is always the same.

IX CONCLUSIONS

A. Summary

The aim of the work was fulfilled. An electron density model for the F-layer was found in 5 cases, which yielded computer-synthesized ionogram traces which, in turn, matched 5 experimentally obtained ionograms reasonably well. An average E_s-layer height was determined through measurement of time delays associated with $1E_s$ and $2E_s$ modes. The F-layer models and E_s-layer heights were used in computer ray-tracing/interpolation programs to produce model ionogram traces representative of 2F, E-F, FEF, FEFEF, 2E-F, 2F-E, 3E-F, 3F-E, and 2F-2E propagation modes. In almost all cases, a very good prediction of modes--based on close experiment-model correspondence--was possible, as seen in Figs. 43-47. Because tilts were not included in the F-layer models, it was not possible to resolve fine-scale splittings such as appear in the 2F/FEF-E combination.

Successful comparisons to a simpler mirror-analogy model were made, which verified the model ionogram synthesis prediction made previously. Figure 48, based on this simpler model, shows in a general way how we expect the mode structure to appear.

Errors were analyzed, and the degree of inaccuracy caused by an improper choice of E_s height was derived quantitatively by employing a typical F-layer model in a synthesis procedure, which used E_s heights of 105, 117, and 124 km. An error on the order of $\pm$ 0.03 msec might be expected in an average model-experiment comparison, in which the FEF and E-F modes are under study.

Tilts were studied, and it was suggested that these could be modeled by employing a sequence of ionograms, to derive a sequence of F-layer models, spaced in local time, which could then be distributed over the path. This technique would enable more fine-scale predictions to be made.

B. Applications and Suggestions For Future Work

Most HF radio engineers need a greater understanding of ionospheric mode structure. A wave that traverses a given distance, over several different paths, will arrive at the receiver with several different time

delays, magnitudes, phases, and polarizations. If, in addition, there is magnetoionic splitting into O and X rays (which is usually the case), one may double the number of modes, and hence the complications. A comprehensive communication design must account for such effects. More notable problems would exist when some pulse encoding scheme is used, such as RTTY or facsimile, where there could be severe pulse overlap, which, to make problems worse, would change with time of day. Note that the range of modes extends over some 1.5 msec; this number will be a function of the path length. Satisfactory and reliable encoding would, under severe conditions, need to place pulses at least this far apart. If concurrent oblique studies are made, it might be possible to make a judicious choice of frequencies--such as to use only the E_s-layer, or to rely on the F-layer near its MUF where signals would be the strongest. D. K. Bailey [Ref. 26] has done some notable work in this area already. He has defined a certain "multipath reduction factor" (MRF), which was derived statistically over several different paths. The MRF measures the ratio of the operating frequency to the MOF of the 1F trace, for which a certain minimum overlap time may be realized.

More recent work has been done in the area of communication error rate, notably by E. M. Young of SRI [Ref. 14]. Young discusses several sources of communication error, and attempts some predictions. His method is based on the long-term HF propagation predictions of CRPL and USARPA, and on estimates of the "channel-scattering function" [Ref. 7], which forms a basis for determining time- and frequency-selective fading effects caused by ionospheric variations.

It would seem that (over suitable propagation paths--the shorter, the better) the techniques of the present work should be of value in facilitating communication problem calculations. Through the use of computer ray-tracing techniques, with reliable ionospheric models--which are conveniently described by exponential functions--several types of communicative systems could be programmed. When a Chapman ionosphere proves to be wholly inadequate for modeling, it should still be possible to arrive at some analytical model for the ionosphere that yields well matched oblique modes.

Parameters are time delay and frequency; furthermore, by changing a model's parameters with time, the effective ionospheric doppler shifts could also be modeled. Work similar to this was done by Young [Ref. 14, p. 30], although he generally found poor agreement with measured data.

Through some modification of the computer ray-tracing program, it is also possible to include amplitude variation by computing range attenuation, including antenna pattern values, and estimating ionospheric absorption; Ref. 16 provides at least an introduction to these computation techniques. To make these calculations more realistic, the earth's magnetic field also could be included within the description of the ionosphere. This would determine a "coherent bandwidth" through the propagating medium--as was discussed by M. R. Epstein in Ref. 27.

Ionospheric physicists can also gain some understanding of the behavior of the ionosphere by studying the model variations with time of day. In this connection, it would also be instructive to consult some of the literature regarding the analysis of ionograms for electron density profiles; the oblique ionograms could be transformed to equivalent vertical ionograms, if tilts were not too extensive. A very good source is Ref. 28, which is a special issue on this subject.

The types of modes that occur are also functions of ionospheric parameters, such as the type and extent of sporadic-E-layers. Furthermore, there are some interesting changes in structure along the path which occur quite rapidly--not in accord with normal diurnal changes. There seem to be indications that these are some type of traveling irregularity. If so, their extent, position, and velocity will affect all the modes in a different way. It seems that information could be gained about both the mode structure and the nature of the irregularity if such a study were undertaken.

As mentioned, the influence of tilts should be explored, and a subsequent attempt should be made at the fine-scale resolution of nearby modes.

An exhaustive analysis of multi-modes over several paths could be conducted ultimately to yield some statistical information regarding the occurrence of each type of mode, and its relationship to other types, as

was done by Dayharsh [Ref. 12]. The results, no doubt, would follow some diurnal and seasonal variation. One may conclude even now (see Figs. 1-24 and the subsequent matches of Figs. 43-47) that earlier in the day, the FEF and E-F modes are the most likely candidates of the multi-mode family. Later in the day, as D-layer absorption apparently drops, other modes appear, which require more hops, and E_s-layer traces become much more pronounced. In general, it appears that most probable modes are those which require the least number of reflections and which are likely to suffer the least amount of attenuation.

It is clear that reliable prediction of complex mode structure will not come until E, F, and particularly E_s structure and statistics are understood more thoroughly.

The techniques of mode estimation (modeling) are so far a fairly time-consuming process, and several more sophisticated computer techniques would be needed (as well as an on-site computer) to enable nearly real-time mode analysis and subsequent prediction of communication effects. Simplified graphical techniques are still most efficient for rapid mode analysis work; however, there is still need for a reliable graphical technique with which one could quickly explain complex mode structure appearing on oblique ionogram data. The author is currently working on such a technique.

1. A. F. Wilkins and F. Kift, "Characteristics of H.F. Signals," Elec. and Radio Engineer, Sep 1957, pp. 335-341.

2. R. Silberstein, "A Long-Distance Pulse-Propagation Experiment on 20.1 Megacycles," J. Geo. Res., 63, Sep 1958, pp. 445-466.

3. K. Kift, "The Propagation of High-Frequency Radio Waves to Long Distances," The Inst. Elec. Engineers, Mar 1960, pp. 127-140.

4. E. V. Appleton and W. J. G. Beynon, "The Application of Ionospheric Data to Radio Communication Problems: Part I," Proc. Phys. Society, 52, 1940, p. 518.

5. J. B. Lomax, "HF Communication Effects: Executive Summary," Final Report, SRI Project 3670, DASA 1724, Stanford Research Institute, Menlo Park, Calif., Aug 1965.

6. R. A. Shepherd, B. C. Tupper, and J. B. Lomax, "HF Communication Effects: Phase-Stable Data Reduction Techniques and System Test Results," Final Report, SRI Project 3670, DASA 1691, Stanford Research Institute, Menlo Park, Calif., Aug 1965.

7. R. A. Shepherd, "HF Communication Effects: Frequency Dispersion and Doppler Shift," Final Report, SRI Project 3670, DASA 1697, Stanford Research Institute, Menlo Park, Calif., Aug 1965.

8. R. A. Shepherd and J. B. Lomax, "Frequency Spread in Ionospheric Radio Propagation," IEEE T. on Comm. Tech., COM-15, No. 2, Apr 1967, pp. 268-275.

9. T. I. Dayharsh, W. E. Blair, et al, "HF Communication Effects: Propagation in the High-Latitude Ionosphere," Final Report, SRI Project 3670, DASA 1700, Stanford Research Institute, Menlo Park, Calif., Aug 1965.

10. T. A. Croft, "The Synthesis of Oblique Ionograms By Digital Computer," Rept. SEL-64-106 (TR No. 89), Stanford Electronics Laboratories, Stanford, Calif., Sep 1964.

11. A. K. Paul and J. W. Wright, "Some Results of a New Method of Obtaining Ionospheric N(h) Profiles and Their Bearing on the Structure of the Lower F Region," J. of Geo. Res., 68, No. 19, Oct 1, 1963, pp. 5413-5420.

12. T. I. Dayharsh, "HF Communication Effects: Ionospheric and Mode-of-Propagation Measurements," Final Report, SRI Project 3670, DASA 1701, Stanford Research Institute, Menlo Park, Calif., Aug 1965.

13. P. L. George, "The Application of Model Techniques to the Reduction of Oblique Ionospheric Data," Tech. Note CPD(T) 147, Department of Supply, Australian Defense Scientific Service, Weapons Research Establishment, Salisbury, South Australia, Dec 1967.

14. Edel M. Young, "HF Communication Effects: Prediction of Propagation Parameters Affecting Error Rate," Final Report, SRI Project 3670, DASA 1723, Stanford Research Institute, Menlo Park, Calif., Aug 1965.

15. T. A. Croft, "Interpreting the Structure of Oblique Ionograms," Rept. SEL-66-010 (TR No. 114), Stanford Electronics Laboratories, Stanford, Calif., Feb 1966.

16. K. Davies, Ionospheric Radio Propagation, NBS Mono. 80, Superintendent of Documents, U.S. Govt. Printing Off., Washington, D.C., 1965.

17. R. B. Fenwick and G. H. Barry, "Generation of Accurate Frequency-Sweep Waveforms by Direct Synthesis," Rept. SEL-64-130 (TR. No. 99), Stanford Electronics Laboratories, Stanford, Calif., Dec 1964.

18. R. B. Fenwick and G. H. Barry, "Step by Step to a Linear Frequency Sweep," Electronics, Jul 26, 1965, pp. 66-70.

19. R. B. Fenwick and G. H. Barry, "Sweep-Frequency Oblique Ionospheric Sounding at Medium Frequencies," IEEE T. on Broadcasting, BC-12, Jun 1966, pp. 25-27.

20. R. L. Murphy, R. B. Fenwick, and G. H. Barry, "Sweep-Frequency CW Ionospheric Sounding Over an 8000-km Path," Rept. SEL-66-071 (TR No. 120), Stanford Electronics Laboratories, Stanford, Calif., Aug 1966.

21. P. B. Gallagher, "Analysis of a New Type of Radio Scattering from the Ionospheric E-region," Rept. TR No. 107, Stanford Electronics Laboratories, Stanford, Calif., May 7, 1956.

22. E. K. Smith and S. Matsushita, Ionospheric Sporadic E, The Macmillan Co., New York, 1962.

23. T. A. Croft, "Rocket Measurements of the Electron Density in the Ionosphere," Rept. SEL-65-017 (TR No. 98), Stanford Electronics Laboratories, Stanford, Calif., Mar 1965.

24. S. A. Bowhill, "Diversity Effects in Long Distance High Frequency Radio Pulse Propagation," J. of Res. of NBS, 65D, May-Jun 1961, pp. 213-223.

25. M. R. Epstein and O. G. Villard, Jr., "Received Polarization of Ionospherically Propagated Waves as a Function of Time and Frequency," Rept. SEL-68-014 (TR No. 145), Stanford Electronics Laboratories, Stanford, Calif., Jan 1968.

26. D. K. Bailey, "The Effect of Multipath Distortion on the Choice of Operating Frequencies for High-Frequency Communication Circuits," IRE T. PGAP, Ap-7, Oct 1959, pp. 397-404.

27. M. R. Epstein, "Polarization of Ionospherically Propagated Waves," Rept. SEL-67-091 (TR No. 143), Stanford Electronics Laboratories, Stanford, Calif., Oct 1967.

28. Radio Science, Special Issue on Analysis of Ionograms for Electron Density Profiles, 2, Oct 1967.

DISTRIBUTION LIST

U-Series

NAVY

Chief of Naval Research
Department of the Navy
Washington, D.C. 20360
2 Attn: Code 418
1 Attn: Code 2027

Director
U.S. Naval Research Lab
Washington, D.C. 20390
1 Attn: Code 5320
(Mr. E. Zettle)
1 Attn: Code 5320
(Mr. J.M. Headrick)
1 Attn: Code 5432C
(Mr. F.A. Polinghorn)
1 Attn: Code 2027

Chief of Naval Operations
Department of the Navy
The Pentagon
Washington, D.C. 20350
1 Attn: OP-07TE
1 Attn: OP-723E

Commander
U.S. Naval Missile Center
Point Mugu, California 93041
1 Attn: Code N03022

Commander
Naval Weapons Center
China Lake, California 93555
1 Attn: Code 4025
(Mr. R.S. Hughes)

Commander
Naval Command Control Communications Laboratory Center
San Diego, California 92152
1 Attn: Mr. H.J. Wirth
1 Attn: Library

Commander
Naval Weapons Center
Corona Laboratories
Corona, California 91720
1 Attn: Mr. V.E. Hildebrand

Director
Office of Naval Research
Branch Office
495 Summer Street
Boston, Massachusetts 02210
1 Attn: Mr. Stan Curley

AIR FORCE

Headquarters, USAF
The Pentagon
Washington, D.C. 20330
1 Attn: AFNICAD
(MAJ Nyquist)
1 Attn: AFRDDF

Headquarters, USAF
Office of Assistant Chief of Staff, Intelligence
Washington, D.C. 20330
1 Attn: AFNICAA

Commander
Rome Air Development Center
Research & Technology Div.
Griffiss AFB, New York 13442
1 Attn: EMASO
(Mr. S. DiGennaro)
1 Attn: EMAES
(MAJOR D.R. Wipperman)
1 Attn: EMASR
(Mr. V.J. Coyne)
1 Attn: EMASA

Headquarters, AF Systems Command
Foreign Technology Division
Wright-Patterson AFB,
Ohio 45433
1 Attn: TDC (Mr. Zabetakis)
1 Attn: TDEED
(Mr. W.L. Picklesimer)
1 Attn: TDCES
1 Attn: TDCE
(Mr. M.S.J. Grabener)

Headquarters
AF Systems Command
Research & Technology Division
Bolling AFB, Washington D.C.
20332
1 Attn: RTTC
(Mr. Philip Sandler)

Headquarters
USAF Security Service (OSA)
San Antonio, Texas 78241
1 Attn: Mr. W.L. Anderson
ODC-R

Headquarters
Air Defense Command
Ent AFB, Colorado Springs,
Colorado 80912
1 Attn: NPSD-A
1 Attn: ADLPC-2A
(LCOL R.J. Kaminski)
1 Attn: ADOAC-ER
1 Attn: NELC-AP

Electronics Systems Div. (ESSL)
L. G. Hanscom Field
Bedford, Massachusetts 01731
1 Attn: 440L

Headquarters SAC (OAI)
Offutt AFB
Omaha, Nebraska 68113
1 Attn: Mrs. E. G. Andrews

Headquarters, AFCRL
L.G. Hanscom Field
Bedford, Massachusetts 01731
1 Attn: CRUI
1 Attn: CRUP (Dr. G.J. Gassman)

U.S. Air Force
Western Test Range
Vandenberg AFB,
California 93437
1 Attn: WTGT
(Mr. Stanley Radom)

Headquarters, USAF AFTAC
Washington, D.C. 20333
1 Attn: TD-3

Major T.D. Damon
Hqtrs. Air Weather Service
(AWVDC)
1 Scott Air Force Base, Illinois
62265

ARMY

Office of the Assistant Chief
of Staff for Intelligence
Department of the Army
The Pentagon, Room 2B 457
Washington, D.C. 20310
1 Attn: Mr. Joseph Grady

U.S. Army SLAG
The Pentagon, Room 1B 657
Washington, D.C. 20310
1 Attn: Mr. N.R. Garofalo

Chief, Army Security Agency
Arlington Hall Station
Arlington, Virginia 22212
1 Attn: Mr. R.R. Neill
1 Attn: IAOPS-O(SA)

Commanding Officer
U.S. Army Security Agency
Processing Center
Vint Hill Farms Station
Warrenton, Virginia 22186
1 Attn: LT Alan Bagully
1 Attn: Technical Library

Commander, Electronics
Warfare Lab
Mt. View Office, USAEC
P.O. Box 205
Mt. View, California 94040
1 Attn: Mr. Joseph Bert

U.S. Army Foreign Science &
Technology Center
Munitions Building
Washington, D.C. 20315
1 Attn: Communications &
Electronics Division

Commanding General
U.S. Army Missile Command
Redstone Arsenal, Alabama 35809
1 Attn: AMSMI-RES

DEPT. OF DEFENSE

Director
Advanced Research Projects Agency
The Pentagon
Washington, D.C. 20301
1 Attn: Mr. Alvin Van Every

Office of the Assistant Director
Intelligence & Reconnaissance
Office of the Director of Defense
Research & Engineering
The Pentagon, Room 3E 119
Washington, D.C. 20301
1 Attn: Mr. H.A. Staderman

Director
National Security Agency
Ft. George G. Meade
Maryland 20755
1 Attn: K-344 (Mr. C. Gandy)
1 Attn: C3-TDL

Deputy Director
Research & Technology
Office of the Director of
Defense Research & Engineering
The Pentagon, Room 3E 1030
Washington, D.C. 20301
1 Attn: Dr. C.W. Sherwin

Office of the Assistant
Director (Defense Systems)
Defense Research & Engineering
The Pentagon, Room 3D 138
Washington, D.C. 20301
1 Attn: Mr. Daniel Fink

Director, Defense
Intelligence Agency
The Pentagon, Room 3B 259
Washington, D.C. 20301
1 Attn: DIACO-4
1 Attn: DIAST-2B

Director, Weapons Systems
Evaluation Group
Office of the Director of
Defense, Research & Engineering
1 Washington, D.C. 20301

Defense Documentation Center
Cameron Station
20 Alexandria, Virginia 22314

National Aeronautics & Space
Administration
Ames Research Center
Moffett Field, California 94035
1 Attn: Dr. Kwok-Long Chan
1 Attn: Mr. Lawrence Colin

OTHER

ITT Electro-Physics Labs Inc.
3355- 52nd Avenue
Hyattsville, Maryland 20781
1 Attn: Mr. W.T. Whelan

Institute for Defense Analyses
400 Army-Navy Drive
Arlington, Virginia 22202
1 Attn: Dr. Louis Wetzel

MITRE Corporation
E Bldg., Room 353
Bedford, Massachusetts 01730
1 Attn: Mr. W.A. Whitcraft, Jr.
1 Attn: Mr. Bill Talley

RAND Corporation
1700 Main Street
Santa Monica, California 90406
1 Attn: Dr. Cullen Crain
1 Attn: Library

Raytheon Company
Spencer Laboratory
2 Wayside Road
Burlington, Massachusetts 01803
1 Attn: Mr. L.C. Edwards

Stanford Research Institute
Menlo Park, California 94025
1 Attn: Dr. David Johnson

Sylvania Electronics Systems
Electronics Defense Laboratory
P.O. Box 205
Mt. View, California
1 Attn: Mr. John DonCarlos

Mr. Thurston B. Poisson
Box 8164 SW Station
1 Washington, D.C. 20024

Astrophysics Research Corporation
10889 Wilshire Blvd.
Los Angeles, California 90024
1 Attn: Dr. Alfred Reifman

Institute of Science & Technology
The University of Michigan
P.O. Box 618
Ann Arbor, Michigan 48105
1 Attn: BAMIRAC Library

Bendix Corporation
Bendix Radio Division
Baltimore, Maryland 21204
1 Attn: Mr. John Martin

AVCO Systems Division
Lowell Industrial Park
Lowell, Massachusetts 01851
1 Attn: Mr. Sidney M. Bennett

U.S. Department of Commerce
ITSA - ESSA
Boulder, Colorado 80302
1 Attn: Mr. William Utlaut
1 Attn: Mr. L. H. Tveten
1 Attn: Mr. W.A. Klemperer,
Div. 530, ESSA

Page Communications, Inc.
3300 Whitehaven St., NW
Washington, D.C. 20008
1 Attn: Mr. David Fales, III

Massachusetts Institute of
Technology
Lincoln Laboratory
P.O. Box 73
Lexington, Massachusetts 02173
1 Attn: Dr. J.H. Chisholm

Massachusetts Institute
of Technology
Center for Space Research
Reading Room 37-582
1 Cambridge, Massachusetts 02138

Institute for Defense Analyses
100 Prospect Avenue
Princeton, New Jersey 08540
1 Attn: Dr. Edward Frieman

University of California
Mathematics Department
Berkeley, California 94720
1 Attn: Dr. E.J. Pinney

Electronics Research Laboratory
University of California
Berkeley, California 94720
1 Attn: Prof. D.J. Angelakos

Battelle-Defender
Battelle Memorial Institute
505 King Avenue
1 Columbus, Ohio 43201

HRB-Singer, Inc.
Science Park
P.O. Box 60
State College, Pennsylvania 16801
1 Attn: Library

Pickard & Burns,
Research Department
103 Fourth Avenue
Waltham, Massachusetts 02154
1 Attn: Dr. J.C. Williams

Sylvania Electronic Systems
Applied Research Laboratory
40 Sylvan Road
Waltham, Massachusetts 02154
1 Attn: Library

Department of Electrical
Engineering
Radiolocation Research Laboratory
University of Illinois
Urbana, Illinois 61803
1 Attn: 311 EERL (Mr. D.G. Detert)

Arecibo Ionospheric Observatory
Box 995
Arecibo, Puerto Rico 00613
1 Attn: Librarian

The University of Texas
Electrical Engineering Research
Laboratory
Route 4, Box 189
Austin, Texas 78756
1 Attn: Mr. C.W. Tolbert

Rice University
Fondren Library
P.O. Box 1892
1 Houston, Texas 77001

Purdue University
Library
1 West Lafayette, Indiana

Telcom, Incorporated
5801 Lee Highway
Arlington, Virginia 22207
1 Attn: Mr. J.D. Ahlgren,
Vice President

IBM
Armonk, N.Y. 10504
1 Attn: S.W. Woolven
Info. Retrieval Specialist

General Telephone & Electronics
Laboratories
208-20 Willets Pt. Blvd.
1 Bayside, New York 11360

UNCLASSIFIED

Security Classification

DOCUMENT CONTROL DATA · R & D

(Security classification of title, body of abstract and indexing annotation must be entered when the overall report is classified)

1. ORIGINATING ACTIVITY (Corporate author)
Stanford Electronics Laboratories
Stanford University, Stanford, California

2a. REPORT SECURITY CLASSIFICATION
UNCLASSIFIED

2b. GROUP

3. REPORT TITLE
MIXED-MODE OBLIQUE IONOGRAMS A COMPUTER RAY-TRACING INTERPRETATION

4. DESCRIPTIVE NOTES (Type of report and inclusive dates)
Technical Report and E.E. Thesis

5. AUTHOR(S) (First name, middle initial, last name)
James Robert Barnum

6. REPORT DATE
December 1968

7a. TOTAL NO. OF PAGES
89

7b. NO. OF REFS
28

8a. CONTRACT OR GRANT NO.
Nonr-225, NR 088 019

b. PROJECT NO.

c.

d.

9a. ORIGINATOR'S REPORT NUMBER(S)
SEL-68-095
TR No. 148

9b. OTHER REPORT NO(S) (Any other numbers that may be assigned this report)

10. DISTRIBUTION STATEMENT This document is subject to special export controls and each transmittal to foreign governments or foreign nationals may be made only with prior approval of the Office of Naval Research, Field Projects Programs, Washington, D.C. 20360.

11. SUPPLEMENTARY NOTES

12. SPONSORING MILITARY ACTIVITY
Office of Naval Research

13. ABSTRACT Twenty-four hour high-resolution FMCW soundings taken over an East-West 1900-km forward-propagation path show unexpectedly complex mode structure near sunset. Because of the presence of 1- and 2-hop sporadic-E modes, it was suggested that multiple reflections from sporadic-E and F-layers--such as "M" and "N" modes--accounted for much of the unexplained structure.

This work represents an attempt to see how well these "mixed" modes can be understood by employing computer ray-tracing procedures developed by Dr. T. A. Croft at Stanford Electronics Laboratories.

A simple β-Chapman layer, with its parameters adjusted to give synthetic ionograms that matched the experimental 1- and 2-hop F-layer modes, proved to be an adequate model for the F-layer profile over the path. Reference to the calibrated experimental ionograms yielded values for the sporadic-E reflection heights for each time of day. Assuming no horizontal tilts in layer density and ignoring the earth's magnetic field, synthetic ionograms involving multiple F-layer and sporadic-E reflections were then computed.

The model-experiment comparisons show that surprisingly accurate estimations of both 1- and 2-hop and mixed modes are possible, using only relatively simple computational procedures. Although similar work has been done in this area, the present study is novel in its use of calibrated oblique ionograms for model derivation. The work should lead to a better understanding of both HF forward and backscatter propagation studies which are plagued with multiple, interlayer propagation modes.

DD FORM 1 NOV 65 1473

UNCLASSIFIED

Security Classification

14. KEY WORDS	LINK A		LINK B		LINK C	
	ROLE	WT	ROLE	WT	ROLE	WT
OBLIQUE IONOGRAMS SPORADIC-E COMPLEX MODES IONOSPHERIC MODELS COMPUTER RAY-TRACING SYNTHESIZED IONOGRAMS HORIZONTAL TILTS COMMUNICATION DATA-RATE						

(Abstract Cont)

A further extension of the modeling technique would include the insertion of additional electrons in the ionospheric profile--E-, F_1-, and F_2-layers--as becomes necessary. Horizontal tilts in electron density could also be modeled by use of a slowly-varying profile or by insertion of two or more different discrete models along the propagation path.